[a]División de Ciencias e Ingenierías, Universidad de Guanajuato,
Loma del Bosque # 103, León, Gto., México

Molecular Thermodynamics of N_2O in Biochar

Bachelor's Degree Thesis

Presented by

Ortiz Villanueva Jordan de Jesús[a]

in order to obtain the degree of

Physic's Engineer

Thesis advisor: Dr. Alejandro Gil Villegas Montiel[a]

Thesis co-advisor: Dr. Flor R. Siperstein[b]

[b] School of Chemical Engineering and Analytical Science, University of Manchester,
Manchester M13 9PL, UK

León, Gto. a 9 de Agosto de 2017

"It seems to be one of the fundamental features of nature that fundamental physical laws are described in terms of a mathematical theory of great beauty and power, needing quite a high standard of mathematics for one to understand it. You may wonder: Why is nature constructed along these lines? One can only answer that our present knowledge seems to show that nature is so constructed. We simply have to accept it. One could perhaps describe the situation by saying that God is a mathematician of a very high order, and He used very advanced mathematics in constructing the universe. Our feeble attempts at mathematics enable us to understand a bit of the universe, and as we proceed to develop higher and higher mathematics we can hope to understand the universe better."

Paul Dirac

Acknowledgments

Dedicated to my family, to the lost love and in memory of my godmother, a beautiful soul, Ma. de Lourdes Villanueva

Contents

List of Figures

7

List of Tables

Chapter 1

Abstract

In this work is presented a theoretical model to predict adsorption isotherms and isosteric heats of adsorption of nitrous oxide on biochar. By the expression in the canonical ensemble of the Helmholtz free energy, results were obtained in the SAFT-VR approximation; these latter were compared with experimental results given in reference [11]. Several direct social and environmental benefits that can be obtained from the application of this model are the reduction of N_2O (a greenhouse gas) emissions to the atmosphere, the improvement in biochar's performance on soil ammendments, and give rise to a more complete description of this process (not very well understood nowadays) as well as the generation of more research in México relative to sorption of greenhouse gases on biochar or other activated carbons.

Also, a comparison between values for the compressiblity factor of the SW bulk fluid obtained with related theories against Monte Carlo simulations has been made. Plots of the critical parameters like pressure, density, temperature and compressibility factor for the bulk fluid are presented using the SAFT-VR [1] equation of state and compared with Boublik's theory, Augmented van der Waals and Gibbs Ensamble Monte Carlo (GEMC) simulation results. SAFT-VR theory allows the incorporation of the dipolar contribution term of this molecule, so it will also be discussed.

Chapter 2

Introduction

N_2O is a chemical compound consisting of a Nitrogen molecule bonded to an Oxygen atom. Its scientific name is *Dinitrogen monoxide*, but is popularly known as *laughing gas* or *nitrous oxide*. At room temperature, N_2O is a colorless, non-flammable, non-toxic gas. Nitrous is commonly used in dentistry due to its anaesthetic (painkilling) properties. At higher concentrations, nitrous acts as a dissociative drug which causes a sense of euphoria and both visual and auditory hallucinations. At high temperature, nitrous oxide decomposes into its component atoms allowing use as an oxidizer or conversion into breathable air. Nitrous oxide is also a greenhouse gas naturally emitted by fertilizer and implicated in global warming.[3]

In 2015, the percentage of nitrous oxide in the total global greenhouse emissions was about 6%, compared with te 76% of carbon dioxide; nevertheless, the Global Warming Potential (GWP) of nitrous oxide is 298, meaning that it warms more the Earth than carbon dioxide (See Fig. 2.1).[38]
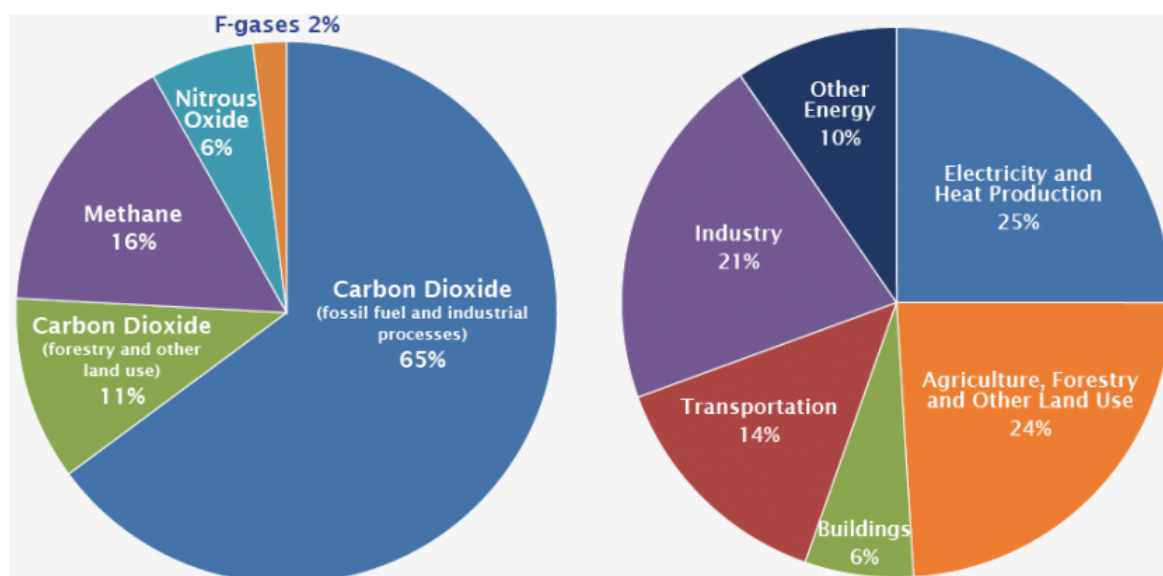
Figure 2.1: *Global Greenhouse Gas Emissions by Gas (left) and by Economic Sector (right). (Taken from reference [38]).*

It is this last characteristic of nitrous oxide that was investigated in the present thesis; nowadays, there are many projects whose interest is the use of renewable energies to fight

the global warming and take care of the environment spending the smallest quantity of materials and investments. In particular, the present work is based on a project of the University of Guanajuato in collaboration with the University of Manchester, which aims at understanding and describing the adsorption mechanisms of this greenhouse gas on an special type of activated carbon called biochar. The University of Guanajuato has the task of developing a theoretical model, whereas the University of Manchester has the task of realizing the corresponding experiments; the relevance of biochar will be discussed further in this section.

The fundamentals presented in this work, based on the SAFT-VR theory, have been used in many cases, like the modeling and description of adsorption isotherms of asphaltenes and biodiesels.[36] It is shown that with this theory was also possible to make good predictions of adsorption isotherms of nitrous oxide on biochar; the results are presented in the last part of the document.

Another motivation, was the possible inclusion of the dipolar contribution of the nitrous oxide to the model and a possible comparison of the results with the experiments to determine if this contribution is important or not, and under wich circumstances it can be.
In this second chapter the activated carbon and the biochar theories are discussed in order to understand the importance and relevance of the use of these materials and how they can help to preserve the environment. In the third chapter the fundmentals of adsorption are discussed, as well as distribution functions in statistical mechanics, adsorption isotherms and some important theoretical models to describe them.

Afterward, details of the the development of the specific model applied to adsorption of nitrous oxide on biochar, using the SAFT-VR theory, are given.

Then, the results obtained and the discussion of them are presented to give, in the final section, the conclusions and perspectives of the work.

2.1   Activated carbon adsorption

The adsorption behavior of an activated carbon cannot be interpreted on the basis of surface area and pore size distribution alone. The determination of a correct model for adsorption on activated carbon adsorbents with complex chemical structure is therefore, a complicated problem. A proper model must take in account both the chemical and the porous structure of the carbon, which includes the nature and concentration of the surface chemical groups, the polarity of the surface, the surface area, and the pore size distribution, as well as the physical and chemical characteristics of the adsorbate, such as its chemical structure, polarity, and molecular dimensions. In the case of adsorption from solutions, the concentration of the solution and its pH are also important additional factors.

Thus, activated carbons are excellent and versatile adsorbents. Their important applications are the adsorptive removal of color, smell and taste, and other undesirable organic and inorganic pollutants from drinking water, in the treatment of industrial waste water; air purification in inhabited spaces, such as in restaurants, food processing, and chemical industries; for the purification of many chemical, food, and pharmaceutical products; in respirators for work under hostile environments; and in a variety of gas-phase applications.

Their use in medicine and health applications to fight certain types of bacterial aliments and for the adsorptive removal of certain toxins and poisons, and for the purifications of blood, is being fast developed. (See Fig. 2.2)

Activated carbons can be used in various forms: the powdered form, the granulated form, and now the fibrous form. Powdered activated carbons (PAC) generally have a finer particle size of about 44 μm, which permits faster adsorption. The granulated activated carbon (GAC) have granules 0.6 to 4.0 mm in size and are hard, abrasion resistant, and relatively dense to withstand operating conditions. The fibrous activated carbon fibers (ACF) are expensive materials for waste water treatment, but they have the advantage of being easy to model into the shape of the adsorption system and produce low hydro-dynamic resistance to flow.

Figure 2.2: *Applications of pelletized activated carbon (Taken from reference [4]).*

2.2 Activated carbons

Activated carbons posses a microcrystalline structure, a highly developed porosity and an extended interparticulate surface area. Its preparation involves two main steps: the carbonization of the carbonaceous raw material (this is made at temperatures below 800 °C in an inert atmosphere) and the activation of the carbonized product. The properties of the final product will be different, depending on the nature of the activating agent, the conditions of the carbonization and activation process.

During the carbonization process, most of the noncarbon elements such as oxygen, hydrogen, and nitrogen are eliminated by the pirolytic decomposition of the starting material. The residual elementary carbon atoms group themselves into stacks of flat, aromatic sheets cross-linked in a random manner. These aromatic sheets are irregularly arranged, which leaves free interstices. These interstices give rise to pores, which make activated carbons excellent adsorbents. During carbonization these pores are filled with the tarry matter or the products of decomposition or at least blocked partially by disorganized carbon.

The pore structure in carbonized char is further developed and enhanced during the activation process, which converts the carbonized raw material into a form that contains the greatest possible number of randomly distributed pores of various sizes and shapes, giving rise to an extended and extremely high surface area of the product.

Activation of the char is usually carried out in an atmosphere of air, CO_2, or steam in the temperature range of 800°C to 900°C. This results in the oxidation of only prefered regions within the char, so that as combustion proceeds, a preferential etching takes place. This results in the development of a large internal surface, which in some cases may be as high as 2500 m^2/g. Electron Spin Resonance (ESR) studies have shown that the aromatic sheets in activated carbons contain free radical structure or structure with unpaired electrons. These unpaired electrons are resonance stabilized and trapped during the carbonization process, due to the breaking of bonds at the edges of the aromatic sheets, and thus, they create edge carbon atoms. These edge carbon atoms have unsaturated valencies and can interact with heteroatoms such as oxygen, hydrogen, nitrogen and sulfur, giving rise to different types of surface groups.

The composition of a typical activated carbon has been found to be 88% C, 0.5% H, 0.5% N, 1.0% S, and 6 to 7% O, with the balance representing inorganic ash constituents. Oxygen content may vary, depending on the source raw material and conditions of activation process. Activated carbons in general have a strongly developed internal surface and are usually characterized by a polydisperse porus structure consisting of pores of different sizes and shapes. It has been difficult to obtain accurate information on the actual shape of the pores. It is now well accepted that activated carbons contain pores from less than a nanometer to several thousand nanometers.

The classification of pores suggested by Dubinin[45] and accepted by the International Union of Pure and Applied Chemistry (IUPAC) is based on their width, which represents the distance between the walls of a slit-shaped pore or the radius of a cylindrical pore. The pores are divided into three groups: micropores with diameters less than 2 nm, mesopores with diameters between 2 and 50 nm, and macropores with diameters greater than 50 nm.(See Fig. 2.3)

Micropores constitute about 95% of the total surface area of the activated carbon and, therefore, determine to a considerable extent the adsorption capacity of a given activated carbon, provided that the molecular dimensions of the adsorbate are not too large to enter the micropores. Micropores are filled at low relative vapor pressure before the commencement of capillary condensation.
Mesopores contribute to about 5% of the total surface area of the carbon and are filled at higher relative pressure with the occurrence of capillary condensation.
Macropores are not of considerable importance to the process of adsorption in activated carbons, as their contribution to surface area does not exceed 0.5 m^2/g. They act as conduits for the passage of adsorbate molecules into the micro and mesopores.

Because all the pores have walls, they will comprise two types of surfaces: the internal or microporous surface and the external surface. The former represents the walls of the pores and has a high surface area, and the latter constitutes the walls of the meso and macropores as well as the edges of the outward facing aromatic sheets and is comparatively much smaller.
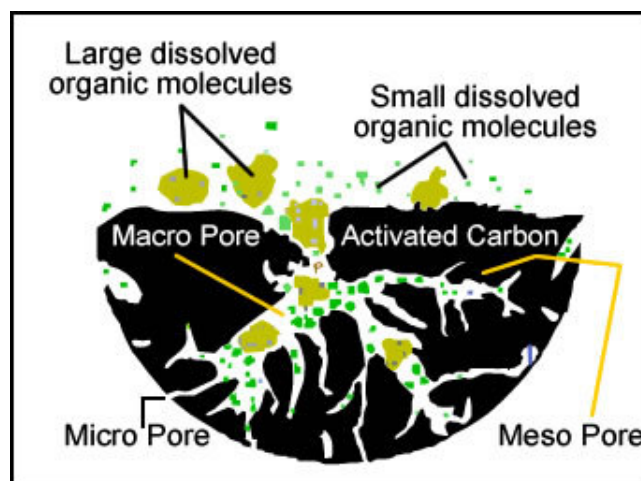
Figure 2.3: *Internal structure of activated carbon (Taken from reference [41]).*

Besides crystalline and porous structure, an activated carbon surface has a chemical structure. The adsorption capacity of an activated carbon is determined by the physical or porous structure but strongly influenced by the chemical structure of the carbon surface. In graphites that have a highly ordered crystalline structure, the adsorption capacity is determined mainly by the dispersion component of the van der Walls forces. But in activated carbons, the random ordering of the aromatic sheets causes several variations in the arrangement of electron clouds, afecting the adsorption properties. Activated carbons are associated with certains amounts of oxygen and hydrogen. In addition, they may contain small amounts of nitrogen.

Carbon-oxygen surface groups are by far the most important surface groups that influence the surface characteristics such as the wettability, polarity, acidity and the physico-chemical properties such as catalyic, electrical and chemical reactivity of these materials. In fact, the combined oxygen has often been found to be the source of the property by which a carbon becomes useful and effective in certain respects. Neverthless, the activated carbon surface groups can not be treated as ordinary organic compounds because they interact differently in different environments. There are several uses and applications that these materials can have, depending on the compound existing on their surface.

2.3   The biochar

What is biochar?

Biochar is a solid material obtained from the carbonization (thermochemical conversion) of biomass in an oxygen-limited environments. In more technical terms, biochar is produced by thermal decomposition of organic material (biomass such as wood, manure or leaves) under limited supply of oxygen (O_2), and at relatively low temperatures ($<700°C$). This process mirrors the production of charcoal, which is perhaps the most ancient industrial technology developed by humankind. Biochar can be distinguished from charcoal -used mainly as a fuel- in that a primary application is used as a soil amendment with the intention to improve soil functions and to reduce emissions from biomass that would

otherwise naturally degrade to greenhouse gases.[6]

Sustainable biochar is a powerfully simple tool that can 1) fight global warming; 2) produce a soil enhancer that holds carbon and makes soil more fertile; 3) reduce agricultural waste; and 4) produce clean, renewable energy (See Fig. 2.4). In some biochar systems all four objectives can be met, while in others a combination of two or more objectives will be obtained.[6]

Carbonization is the process of converting a feedstock into biochar through reductive thermal processing. The process involves a combination of time, heat and pressure exposure factors that can vary between processors, equipment, and feedstocks. There are two main processes: pyrolysis or gasification. Energy products in the form of gas or oil are produced along with the biochar. These energy products may be recoverable for another use, or may simply be burned and released as heat. In addition, biochar can be made from a wide variety of biomass feedstocks. As a result, different biochar systems emerge on different scales. These systems may use production technologies that do or do not produce recoverable energy as well as biochar, and range from small household units to large bioenergy power plants.[6]

A valuable soil ammendment

This 2,000 year-old practice converts agricultural waste into a soil enhancer that can hold carbon, boost food security, and increase soil biodiversity, and discourage deforestation. The process creates a fine-grained, highly porous charcoal that helps soils retain nutrients and water.

Biochar is found in soils around the world as a result of vegetation fires and historic soil management practices. Intensive study of biochar-rich dark earths in the Amazon (terra preta), has led to a wider appreciation of biochar's unique properties as a soil enhancer.

Biochar can be an important tool to increase food security and cropland diversity in areas with severely depleted soils, scarce organic resources, and inadequate water and chemical fertilizer supplies.

Biochar also improves water quality and quantity by increasing soil retention of nutrients and agrochemicals for plant and crop utilization. More nutrients stay in the soil instead of leaching into groundwater and causing pollution.

Research is now confirming benefits that include[6]:

- Reduced leaching of nitrogen into ground water

- Possible reduced emissions of nitrous oxide

- Increased cation-exchange capacity resulting in improved soil fertility

- Moderating of soil acidity

- Increased water retention

- Increased number of beneficial soil microbes

Biochar can improve almost any soil. Areas with low rainfall or nutrient-poor soils will most likely see the largest impact from addition of biochar.

A Powerfully Simple Tool to Combate Climate Change

The carbon in biochar resists degradation and can hold carbon in soils for hundreds to thousands of years (See Fig.2.5). Biochar is produced through pyrolysis or gasification-processes that heat biomass in the absence (or under reduction) of oxygen.

In addition to creating a soil enhancer, sustainable biochar practices can produce oil and gas byproducts that can be used as fuel, providing clean, renewable energy. When the biochar is buried in the ground as a soil enhancer, the system can become "carbon negative".

Biochar and bioenergy co-production can help combat global climate change by displacing fossil fuel use and by sequestering carbon in stable soil carbon pools. It may also reduce emissions of nitrous oxide.[6]
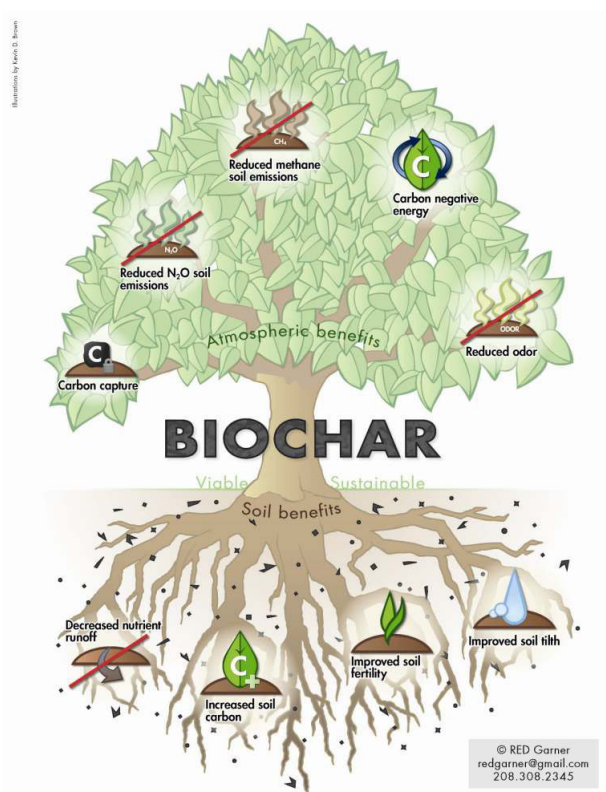
Figure 2.4: *The benefits of biochar (Image taken from reference [6]).*

Biochar and Terra Preta Soils

Biochar production is modeled after a process begun thousands of years ago in the Amazon Basin, where islands of rich, fertile soils called terra preta ("dark earth") were created by indigenous people. Anthropologists speculate that cooking fires and kitchen middens along with deliberate placing of charcoal in soil resulted in soils with high fertility and carbon content, often containing shards of broken pottery. These soils continue to "hold" carbon today and remain so nutrient rich that they have been dug up and sold as potting soil in Brazilian markets.

Rural and Developing Country Applications of Biochar Systems

Biochar systems can reverse soil degradation and create sustainable food and fuel production in areas with severely depleted soils, scarce organic resources, and inadequate water and chemical fertilizer supplies. By making croplands more fertile for longer periods of time, biochar discourages deforestation. Low-cost, small-scale biochar production units can produce biochar to build garden, agricultural and forest productivity, and provide thermal energy for cooking and drying grain. With the addition of an engine or turbine, these systems can produce kinetic energy for grinding grain or making electricity.[6]
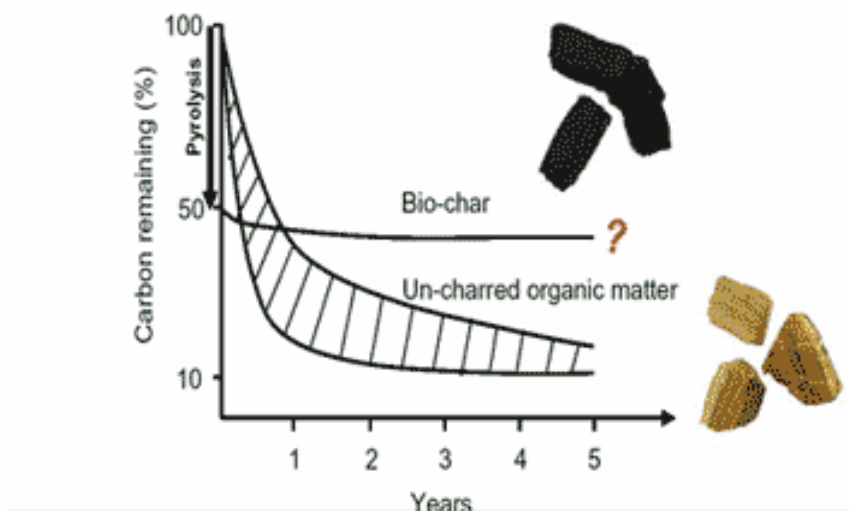
Figure 2.5: *Plot of percentage of remaining carbon in biochar and un-charred organic matter throuhgout the years.(Image taken from reference [6])*
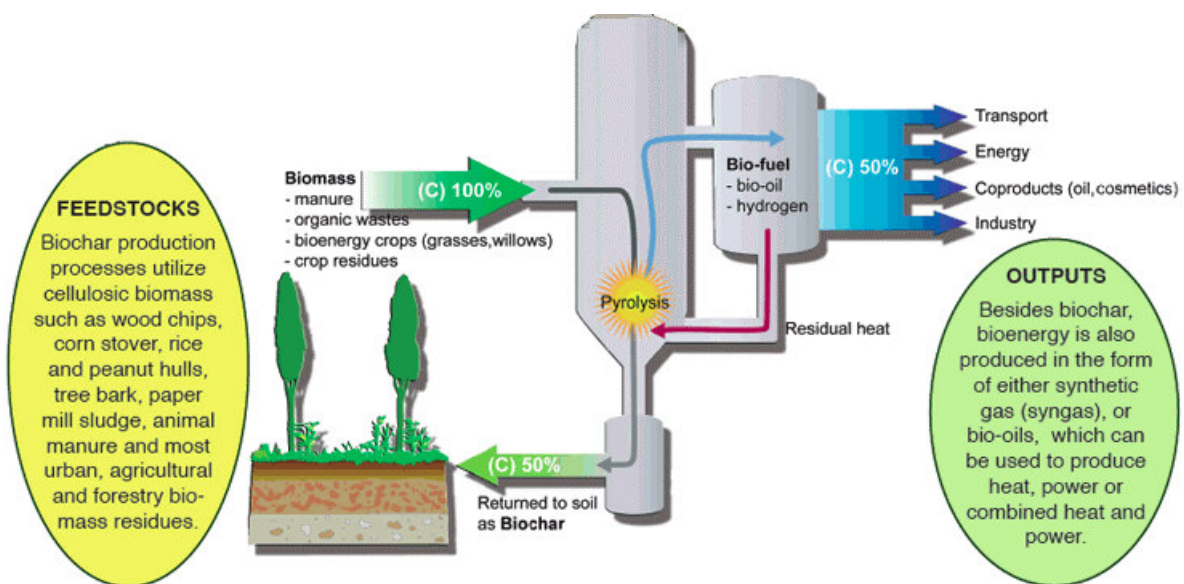
Figure 2.6: *Biochar production diagram (Image taken from reference [39])*

Biochar Technology

There are many different ways to make biochar, but all of them involve heating biomass with little or no oxygen to drive off volatile gasses, leaving carbon behind. This simple process is called thermal decomposition usually from pyrolisis or gasification. These methods can produce clean energy in the form of gas or oil along with the biochar. This energy may be recoverable for another use, or it may simply be burned and released as heat. It's one of the few technologies that is relatively inexpensive, widely applicable and quickly scalable.[6]

But biochar technology is more than just the equipment needed to produce biochar. Biochar technology necessarily includes entire integrated systems that can contain various components that may or may not be part of any particular system.[6]

In general, however, biochar systems should include the following elements:[6]

- Collection, transport and processing of biomass feedstocks

- Characterization and testing of biochar

- Production and utilization of energy co-products: gas, oil or heat

- Biochar transport and handing for soil application

- Monitoring of biochar applications for carbon accounting

- Life Cycle Assessment and full system monitoring for sustainability assessment

Feedstocks

Biochar can and should be made from biomass waste materials. Making biochar from biomass waste materials should create no competition for land with any other land use option-such as food production or leaving the land in its pristine state.

Biomass waste materials appropiate for biochar production include crop residues (both field residues and processing residues such as nut shells, fruit pits, bagasse, etc), as well as yard, food and forestry wastes, and animal manures.

Large amounts of agricultural, municipal, and forestry biomass are currently burned or left to decompose and release CO_2 and methane back into the atmosphere. They also can pollute local ground and surface waters-a large issue for livestock wastes. Using these materials to make biochar not only removes them from a pollution cycle, but biochar can be obtained as a by-product of producing energy from this biomass. Feedstocks must not contain unacceptable levels of toxins such as heavy metals which can be found in sewage sludge and industrial or landfill waste (Figure 2.6).

It is important to study all the aspects of feedstock supply on a local community/business before setting up a biochar operation. Feedstock availability can vary year to year and within years. In developing country areas where feedstocks are often used as heating and/or cooking fuel, biochar production can be an important side benefit if done sustainably. The biochar can then be used on fields to potentially increase food production by improving soil fertility.[6]

Feedstock effects on Nutrient Properties of Biochar

The composition of biochar (the amount of carbon, nitrogen, potassium, calcium, etc)

depends on the feedstock used and the duration and temperature of pyrolysis. As an example, biochar produced from feedstocks which have greater contents of potassium (such as animal litters) often have higher potassium contents than biochar made entirely from wood (which often have higher carbon contents). However, pyrolysis conditions greatly affect nutrient properties contents and so biochar should be tested on a batch by batch basis to determine specific properties.[6]

Economic Considerations

The chioce of feedstock will be affected by the biomass resources in the immediate area and availability. Due to collection, and transport and storage costs, it often makes the most economic sense to use local feedstocks (if they are also an environmentally sustainable option). The most basic costs and benefits to consider with feedstock choices are highlighted below: [6]

- **Feedstock production and collection**: If the feedstock is a residue, such as municipal biomass waste, logging or cropping residues, or a by-product such as bagasse, then production is less an economic issue than if the feedstock is purposely grown for the production of biochar (such as switchgrass) which would include the costs and inputs needed for the growing and harvesting of the crop. Revenue in the form of tipping fees may be obtained from certain waste feedstocks.

- **Use Tradeoff**: This would include the potential nutrient value lost from using feedstock for biochar production rather than as a direct fertilizer on the field. How this trade off works will vary on the area and on the feedstock. For example, chicken litter may be valuable in some areas as a direct fertilizer while in other areas it may be treated as a waste and represent a disposal cost.

- **Feedstock transport**: When waste biomass is found far from the place where it will be used, transportation costs can be very high. In some situations it may make sense to densify the biomass by chipping or pelletizing before transport.

- **Feedstock storage and pre-processing**: Many feedstocks will need to be dried before pyrolysis. Depending on the feedstock choice, the drying process could occur passively through careful storage or may need more intervention?such as using a drier (thus requiring energy and labor). Energy for drying could in some cases be obtained from the pyrolysis of previous batches of feedstock.

Biochar Production Technologies

Biochar Production Units

Equipment for making biochar can be as simple as a primitive campfire or as complex as a modern bio-refinery. The basic process is called pyrolysis.

Pyrolysis is the breaking down (lysis) of a material by heat (pyro). As the material is broken down, it releases gas. This is the first step in the combustion or gasification of biomass.

All the processes involved in pyrolysis, gasification, and combustion can be seen in the flaming match. The flame provides heat for pyrolysis, and the resulting gases and vapors burn in the luminous zone in a process called flaming combustion, leaving behind

char. After the flame passes a given point, the char may or may not continue to burn. When the match is put out, the remaining wood continues to bake, or pyrolyze, releasing a smoke composed of condensed tar droplets as it cools (See Fig. 2.7)
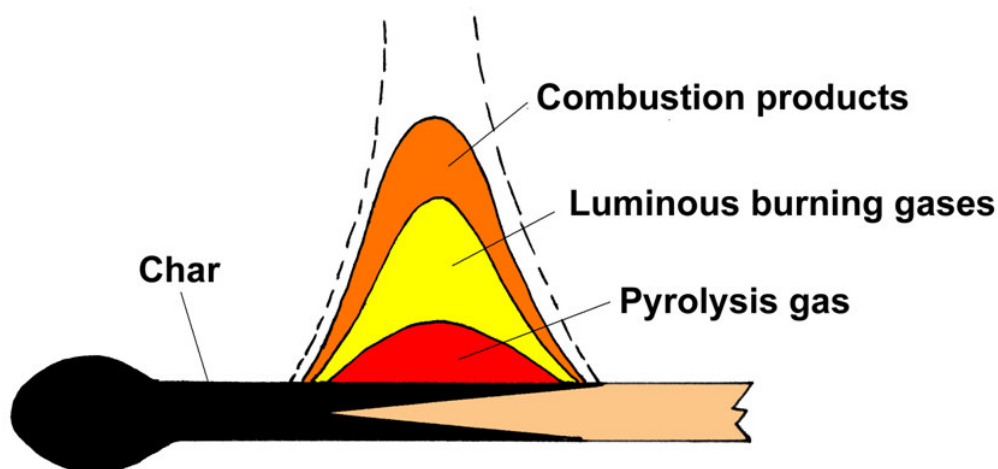
Figure 2.7: *Processes involved in pyrolisis, in a flaming match. (Image taken from reference [6])*

Biochar production systems are generally classified as either pyrolisis or gasification systems

Pyrolisis systems

Pyrolysis systems use kilns, retorts and other specialized equipment to contain the baking biomass while excluding oxygen. The reaction vessel is vented, to allow pyrolysis gases to escape. Pyrolysis gases are often called "syngas". The process becomes self-sustaining as the syngas produced is combusted, and heat is released.

There are two types of pyrolysis systems in use today: fast pyrolysis and slow pyrolysis. Fast pyrolysis tends to produce more oils and liquids while slow pyrolysis produces more syngas.

Gasification systems

Gasification systems produce smaller quantities of biochar in a directly-heated reaction vessel with introduced air.

The more oxygen a production unit can exclude, the more biochar it can produce. Biochar production is optimized in the absence of oxygen.

Scale and Variety of Units

Gasification and pyrolysis production systems can be developed as mobile or stationary units.

At the local or regional level, pyrolysis and gasification units can be operated by co-operatives or larger industries, and can process up to 4,000 kg of biomass per hour. Small

scale gasification and pyrolysis systems that can be used on farm or by small industries are commercially available with biomass inputs of 50 kg/hr to 1,000 kg/hr.

Biochar ovens are low tech biochar production units with a primary design function of producing biochar. This category of biochar production unit can be suitable for clean, healthy, distributed low tech biochar production (DLT) by developing country smallhold-ers and micro-entrepreneurs; "backyard" producers utilizing yard waste; small and urban farmers; nurseries; communal gardens; etc to convert the thinly distributed feedstock (TDF) available to them. The feedstock 'chamber' of these units will usually be in the range of very small to 4-500 liters. The primary functional design of these units is to produce biochar. To date, the primary technologies used in units that fall within this category are retorts; Top Lit Up Draft (TLUD) units and TLUD/retort hybrids; and Top Fed Open Draft (TFOD) units such as cones and pyramids (metal & pit) and rings. Other functional designs may fall within this category (based on size, primary design function, and technology level) as they are developed. The name of this category is based on the metaphor that, as a bread oven is a unit used to bake dough to produce bread, a biochar oven is unit used to bake feedstock to produce biochar.

Charcoal-making stoves show promise of bringing low-cost biochar to rural areas. Biochar production can help build soils and provide households with new opportunities to earn income.

There is also potential to develop stoves and furnaces for urban and suburban use that gasify biomass and leave behind charcoal. Such stoves could cook food and heat water while they make biochar for gardens and landscaping.
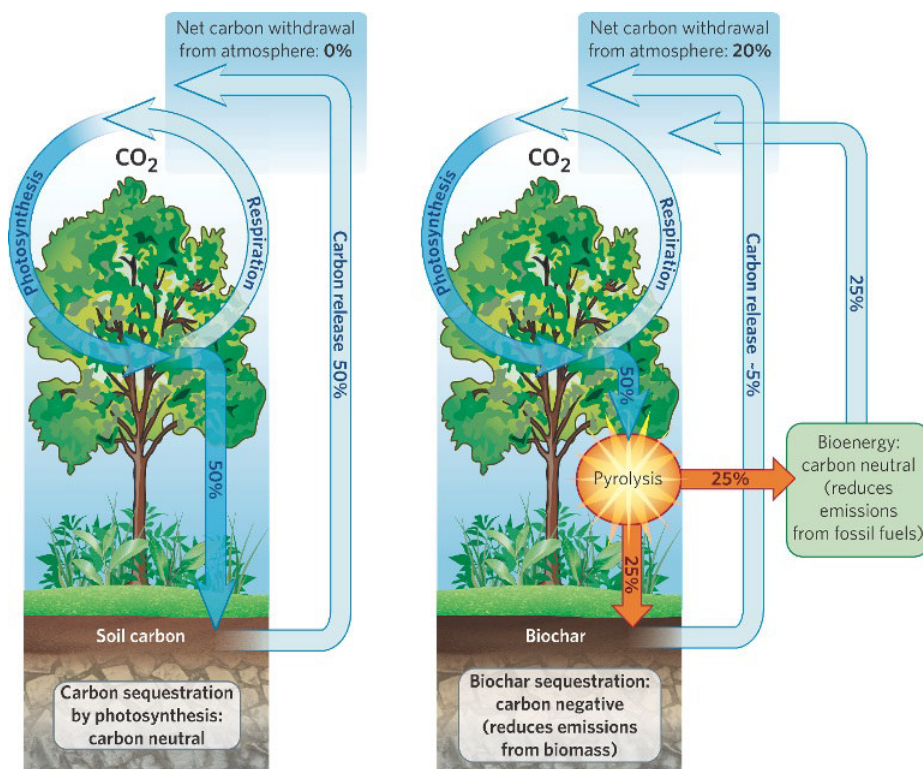
Figure 2.8: *A carbon negative diagram. (Image taken from reference [6])*

Climate Change and Biochar

How can Biochar Be Carbon Negative

Fossil fuels are carbon positive; they add more carbon dioxide (CO_2) and other greenhouse gasses to the air and thus exacerbate global warming. Ordinary biomass fuels are carbon neutral; the carbon captured in the biomass by photosynthesis would have eventually returned to the atmosphere through natural processes like decomposition. Sustainable biochar systems can be carbon negative by transforming the carbon in biomass into stable carbon structures in biochar which can remain sequestered in soils for hundreds and even thousands of years. The result is a net reduction of CO_2 in the atmosphere, as illustrated in Figure 2.9.

Climate Smart Benefits of Biochar

Carbon in biochar can persist in soils over long time scales. Beyond the carbon sequestered in the biochar itself, biochar incorporated in soils also offers numerous other potential climate benefits.

1. **Soil Fertility**: Biochar can improve soil fertility, stimulating plant growth, which then consumes more CO_2 in a positive feedback effect.

2. **Reduced fertilizer inputs**: Biochar can reduce the need for chemical fertilizers, resulting in reduced emissions of greenhouse gases from fertilizer manufacture.

3. **Reduced N_2O and CH_4 emissions**: Biochar can reduce emissions of nitrous oxide (N_2O) and methane (CH_4) (two potent greenhouse gases) from agricultural soils.

4. **Enhanced soil microbial life**: Biochar can increase soil microbial life, resulting in more carbon storage in soil.

5. **Reduced emissions from feedstocks**: Converting agricultural and forestry waste into biochar can avoid CO_2 and CH_4 emissions otherwise generated by the natural decomposition or burning of the waste.

6. **Energy generation**: The heat energy (and also the bio-oils and synthesis gases) generated during biochar production can be used to displace carbon positive energy from fossil fuels.
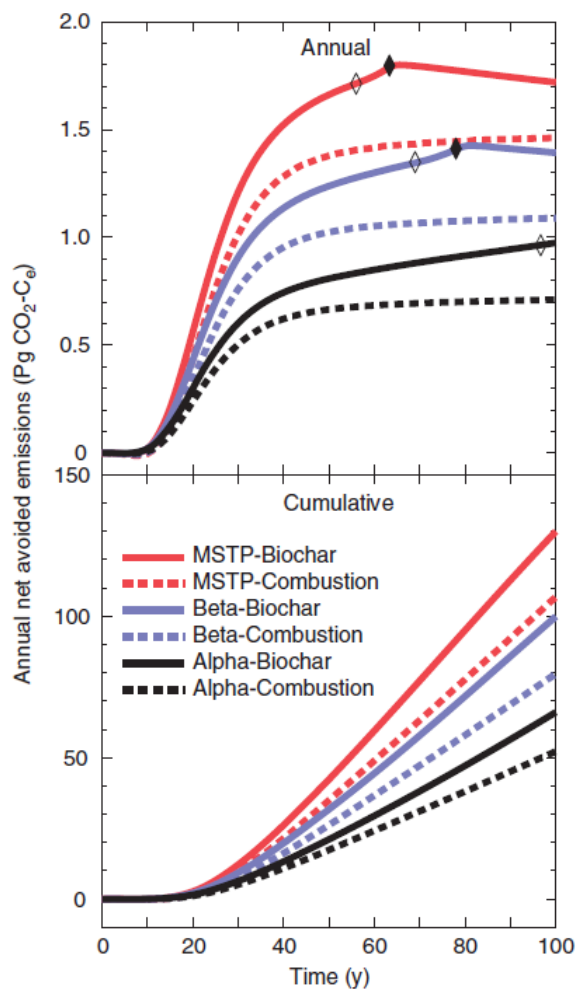
Figure 2.9:   *Results of the study (Woolf et al, 2010)[43]. Three scenarios are modelled showing different degrees of demands on global biomass resources (red=maximum sustainable technical potential (MSTP); blue=medium; black=low). Sustainable biochar is represented by solid lines; biomass combustion by dashed lines. The top panel shows annual avoided emissions; the bottom panel, cumulative avoided emissions over 100 years. In all three scenarios sustainable biochar trumps biomass combustion in terms of avoided emissions. (Taken from reference [6]).*

How Much Carbon Can Biochar Remove from the Atmosphere?

According to one prominent study [43], sustainable biochar implementation could offset a maximum of 12% of anthropogenic GHG emissions on an annual basis. Over the course of 100 years, this amounts to a total of roughly 130 petagrams (106 metric tons) of CO_2-equivalents. The study assessed the maximum sustainable technical potential utilizing globally available biomass from agriculture and forestry. The study assumed no land clearance or conversion from food to biomass-crops (though some dedicated biomass-crop production on degraded, abandoned agricultural soils was included), no utilization of industrially treated waste biomass, and biomass extraction rates that would not result in soil erosion.

Figure 2.9 [43] shows avoided emissions attributable to sustainable biochar production or biomass combustion over 100 years, relative to the current use of biomass. Three scenarios are modelled showing different degrees of demands on global biomass resources (red=maximum sustainable technical potential (MSTP); blue=medium; black=low). Sustainable biochar is represented by solid lines; biomass combustion by dashed lines. The top panel shows annual avoided emissions; the bottom panel, cumulative avoided emissions over 100 years. In all three scenarios sustainable biochar trumps biomass combustion in terms of avoided emissions.

Biochar in Carbon Trading Markets

One of the most critical characteristics of biochar as a climate change mitigation technology is its long-term persistence in soil. Quantification of the persistent carbon component of biochar can facilitate the participation of biochar projects in carbon markets, providing an additional revenue stream to projects delivering greenhouse gas emissions reductions through soil carbon sequestration.

Several attempts have been made to create biochar carbon offset methodologies in existing voluntary carbon market registries but to date none have been approved for use. Most prominently, IBI along with partners The Climate Trust and The Prasino Group, submitted a proposed biochar carbon offset methodology to the American Carbon Registry (ACR)-a leading voluntary carbon offset registry. In March 2015, after three years of review, this draft methodology was listed as inactive by ACR due to concerns around the embedded test method to estimate biochar carbon persistence (known as BC+100)-used to estimate the quantity of biochar carbon remaining in the soil after 100 years. Future efforts to revive the methodology in the ACR process-and indeed other carbon offset registries-should focus on bolstering the evidence for BC+100, or identifying novel methods to measure, monitor and verify biochar carbon persistence under field conditions.

Chapter 3

Fundamentals

3.1 Adsorption

Absorption occurs when atoms pass through or enter a bulky material (the molecules are entirely dissolved or diffused in the absorbent to form a solution) and once dissolved, the molecules cannot be separated easily from the absorbent. On the other hand, adsorption occurs when the molecules are held loosely on the surface of the adsorbent and can be easily removed; it is generally classified into physisorption (weak van der Waals forces) and chemisorption (covalent bonding), and it can also be caused by electrostatic attraction. Figure 3.1 illustrates this difference between absorption and adsorption.[46]
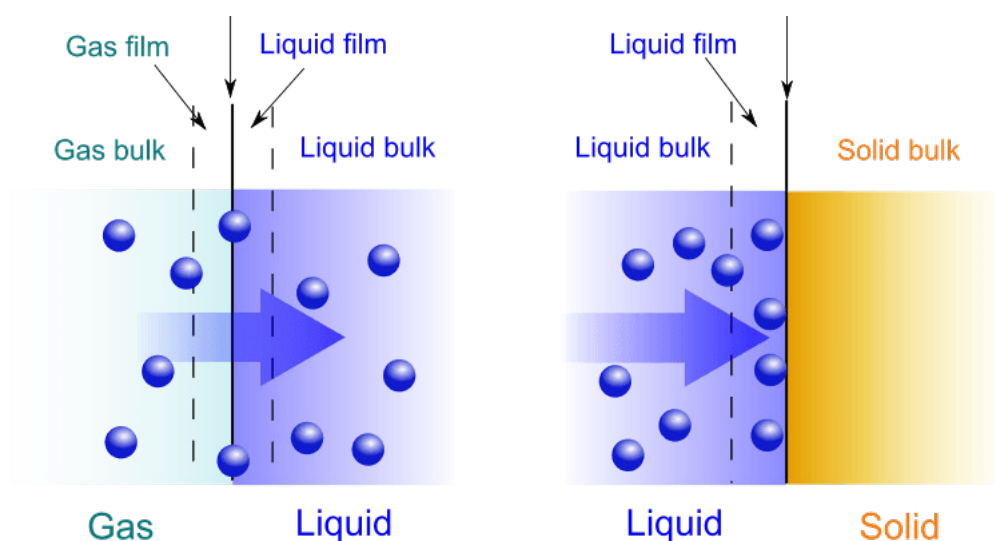
Figure 3.1: *Gas-liquid absorption (a) and liquid-solid adsorption (b) mechanism. Blue spheres are solute molecules (Taken from reference [46]).*

Adsorption arises as a result of the unsaturated and unbalanced molecular forces that are present on every solid surface. When a solid is brought into contact with a liquid or gas, there is an interaction between the fields of forces of the surface and that of the liquid or the gas. The solid tends to satisfy these residual forces by attracting and retaining on its surface the molecules, atoms, or ions of the gas or liquid. This results in a greater concentration of the gas or vapor phase. The process by which this surface excess is caused is called adsorption. The substance attached to the surface is called adsorbate,

and the substance to which it is attached is known as the adsorbent. Adsorption of a gas on a solid or liquid surface is a spontaneous process. It is, therefore, accompanied by a decrease in free energy of the system. Furthermore, the gaseous molecules in the adsorbed state have fewer degrees of freedom than in the gaseous state. This results in a decrease in entropy during adsorption. Using the thermodynamic relationship:[5]

$$\Delta G = \Delta H - T\Delta S \quad ,$$

it follows that the term ΔH, which is the heat of adsorption, must be negative indicating that adsorption is always an exothermic process, respective of the nature of the forces involved in the adsorption process. However, a few adsorption cases have been reported to be endothermic.[5]

The adsorption involves two types of forces: **physical forces** that may be dipole moments, polarization forces, dispersive forces, or short range repulsive interactions and **chemical forces** arising out of the redistribution of the electrons between the solid surface and the adsorbed atoms. Depending upon the nature of the forces involved, the adsorption is of two types: *physical adsorption* and *chemisorption.* [5]

In physical adsorption, the adsorbate is bound to the surface by relatively weak van der Walls forces, which are similar to the molecular forces of cohesion and are involved in the condensation of vapors into liquids.

Chemisorption involves exchange or sharing of electrons between the adsorbate molecules and the surface of the adsorbent resulting in a chemical reaction. The bond formed between the adsorbate and the adsorbent is essentially a chemical bond and is thus much stronger than in the physisorption. The most important difference between the two kinds of adsorption is the magnitude of the enthalpy of adsorption. In physical adsorption the enthalpy of adsorption is of the same order as the heat of liquefaction and does not usually exceed 10 to 20 kJ per mol, whereas in chemisorption the enthalpy change is generally of the order of 40 to 400 kJ per mol. Figure 3.2 clarifies this energy ranges
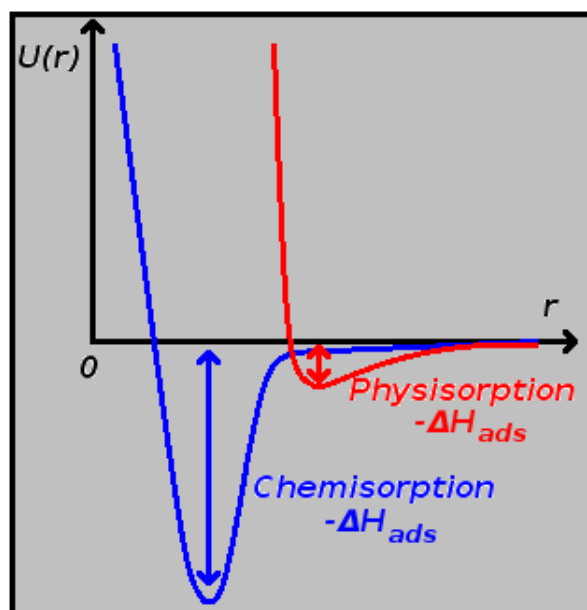
Figure 3.2: *Differences in adsorption enthalpies for physisorption and chemisorption. U(r) is the intermolecular potential.*

Physical adsorption is nonspecific and occurs between any adsorbate-adsorbent systems, but chemisorption is specific. Another important point of difference between physisorption and chemisorption is the thickness of the adsorbed phase. Although it is multimolecular in physisorption, the thickness is unimolecular in chemisorption. When it is not certain that the process of adsorption is either physisorption or chemisorption or when both are occuring in appreciable proportions, then it is preferable to use a less commital term: *sorption.*[5]

3.1.1 Adsorption equilibrium

When a solid surface is exposed to a gas, the molecules of the gas strike the surface of the solid when some of these striking molecules stick to the solid surface and become adsorbed, while some others rebound back.

Initially the rate of adsorption is large because the whole surface is bare, but the rate of adsorption continues to decrease, while the rate of desorption continues to increase, until an equilibrium is reached, where the rate of adsorption is equal to the rate of desorption. At this point the solid is in adsorption equilibrium with the gas. It is a dynamical equilibrium because the number of molecules sticking to the surface is equal to the number of molecules rebounding from it.

As the amount adsorbed at the equilibrium for a given adsorbate-adsorbent system depends upon the pressure of the gas and the temperature of adsorption, the adsorption equilibrium can be represented as an adsorption isotherm at constant temperature, the adsorption bar at constant pressure, and the adsorption isostere for a constant equilibrium adsorption.

In actual practice the determination of adsorption at constant temperature is most convenient and the adsorption isotherm is the most extensively employed method for representing the equilibrium states of an adsorption system. The adsorption isotherm gives useful information regarding the adsorbate, the adsorbent, and the adsorption process. It helps in the determination of the surface area of the adsorbent, the volume of the pores, and their size distribution. It also provides important information regarding the magnitude of the enthalpy of adsorption and the relative adsorbility of a gas or a vapor on a given adsorbent with respect to chosen standards.[5]

The adsorption data can be represented by several isotherm equations, the most important being the Langmuir, the Freundlich, the Brunauer-Emmett-Teller (BET), and Dubinin equations.[5] The first two isotherm equations apply equally to physisorption as well as to chemisorption. The BET and Dubinin equations are most important for the analysis of physical adsorption of gases and vapors on porous carbons.

For a given adsorbate-adsorbent system, the equilibrium amount adsorbed x/m is a function of pressure and temperature; i.e.,

$$\frac{x}{m} = f(p, T) \quad ,$$

where x/m is the amount adsorbed per unit mass of the adsorbent at the equilibrium pressure p, and T is the temperature of adsorption. The adsorption equilibrium can be approached in three different ways.[5]

Adsorption isobar

When pressure is kept constant and T is varied, an isobar is obtained [5]

$$\frac{x}{m} = f(T) \ \ [p = constant] \quad .$$

Adsorption isostere

An isostere is obtained when, for a constant equilibrium amount adsorbed, the temperature is varied and the pressure (essentially to keep x/m constant) is a function of the temperature [5]

$$p = f(T) \ \ [\tfrac{x}{m} = constant] \quad .$$

Adsorption isotherm

If the temperature is kept constant, then for a given adsorbent-adsorbate system x/m depends on the equilibrium pressure, and the equilibrium can be represented as:

$$\frac{x}{m} = f(p) \ \ [T = constant] \quad .$$

Such an equilibrium is called adsorption isotherm.[5]

3.2   Ensembles

The goal to define an ensemble, is to calculate thermodynamic properties in terms of molecular properties. Given the structure of the individual molecules of a given system and the form of the intermolecular potential, it is posible to calculate quantities like entropy and free energy.

The concept of *ensemble* was first introduced by Gibbs in 1879. An ensamble is a collection of a very large number of systems, each constructed to be a replica on a thermodynamic (or macroscopic) level of the particular thermodynamic system of interest; it is equivalent to say that an ensemble is a set of objects with exactly the same thermodynamic information (with the same values of macroscopic variables needed to completely specify a state of the system). Even when the systems are consistent with the macroscopic information, this is not true for the microscopic level, because the systems may be in different quantum states, including the degeneracy of each one.

In order to work with the several ensembles that can be used (See Table 3.1), the system must obey the *Principle of equal a priori probabilities*; that is to say, it is necessary that each and every one of the quantum states is represented an equal number of times in the ensemble. Since there are no information to consider any one of the quantum states to be more important than any other, each one must be treated equally. All of the quantum states are consistent with the given values of the macroscopic parameters of the system.

Thus, an ensemble average of a mechanical property can be defined as the average value of this property over all the members of the ensemble, utilizing the principle of equal a priori probabilities. And also, it is postulated that the ensemble average of a mechanical property can be equated to its corresponding thermodynamic property.

Ensemble	Fixed Variables	Partition Function	Thermodynamic expressions
Microcanonical	N, V, E	Ω (Number of quantum states)	$S = k\, ln\Omega$ $dS = \frac{1}{T}dE + \frac{p}{T}dV - \frac{\mu}{T}dN$ $\frac{1}{kT} = \left(\frac{\partial ln\,\Omega}{\partial E}\right)_{N,V}$ $\frac{p}{kT} = \left(\frac{\partial ln\,\Omega}{\partial V}\right)_{N,E}$ $\frac{\mu}{kT} = -\left(\frac{\partial ln\,\Omega}{\partial N}\right)_{V,E}$
Canonical	N, V, T	$Q(N,V,T) = \sum_j e^{-E_j(N,V)/kT}$	$A = -kT\, lnQ$ $dA = -SdT - pdV + \mu dN$ $S = k\, lnQ + kT\left(\frac{\partial\, lnQ}{\partial T}\right)_{N,V}$ $p = kT\left(\frac{\partial\, lnQ}{\partial V}\right)_{N,T}$ $\mu = -kT\left(\frac{\partial\, lnQ}{\partial N}\right)_{V,T}$ $E = kT^2\left(\frac{\partial\, lnQ}{\partial T}\right)_{N,V}$
Grand canonical	V, T, μ	$\Xi(V,T,\mu) = \sum_N Q(N,V,T)e^{\mu N/kT}$	$pV = kT\, ln\Xi$ $d(pV) = SdT + Nd\mu + pdV$ $S = k\, ln\Xi + kT\left(\frac{\partial\, ln\Xi}{\partial T}\right)_{V,\mu}$ $N = kT\left(\frac{\partial\, ln\Xi}{\partial \mu}\right)_{V,T}$ $p = kT\left(\frac{\partial\, ln\Xi}{\partial V}\right)_{\mu,T} = kT\frac{ln\Xi}{V}$
Isothermal-isobaric	N, T, p	$\Delta(N,T,p) = \sum_E \sum_V \Omega(N,V,E)e^{-E/kT}e^{-pV/kT}$	$G = -kT\, ln\Delta$ $dG = -SdT + Vdp + \mu dN$ $S = k\, ln\Delta + kT\left(\frac{\partial\, ln\Delta}{\partial T}\right)_{N},p$ $V = -kT\left(\frac{\partial\, ln\Delta}{\partial p}\right)_{N,T}$ $\mu = -kT\left(\frac{\partial\, ln\Delta}{\partial N}\right)_{T,p}$

Table 3.1: *Sumarizing table of several ensembles used in statistical mechanics*

3.3   Distribution functions in classical monoatomic fluids

It is well known that the ideal gas equation of state does not reproduce the results from observations and experiments with gases at high densities. Then, many equations have been developed to study deviations from ideal gas behavior, being the virial expansion one of the most sounded methods due to its theoretical foundations; the virial equation of state is represented by an infinite power series in density:[7]

$$\frac{p}{kT} = \rho + B_2(T)\rho^2 + B_3(T)\rho^3 + ... + B_j(T)\rho^j \tag{3.1}$$

where k is the Boltzmann's constant and $B_2(T), B_3(T), ..., B_j(T)$ are called the second, third, jth virial coefficients, respectively, and depend on the temperature and on the particular gas under consideration, but are independent of density or pressure. Another important observation is that the jth virial coefficient can be calculated in terms of the interactions of j molecules in a volume V. Thus, the N-body problem of an imperfect gas can be reduced to a series of one-body, two-body, three-body problem and so on.

Nevertheless, the virial expansion has a radius of convergence beyond wich the series no longer represents the pressure. This point possibly has something to do with the onset of the liquid state in which the interactions can no longer be treated as a sequence of two-body, three-body intereactions, etc.[7]

A theoretical treatment of liquids, therefore, requires to seek new methods that are more directed to the many-body nature of liquids.[7]

The question is: To what extent it is possible to reproduce pressure-volume isotherms (See Fig. 3.3), both above and below the critical temperature, using only a few virial coefficients? The study of this question has lead to several equations of state, which are compared with "experimental data" on hard sphere fluids. These "data" are actually the results of solving the equations of motion of several hundred hard spheres numerically on a large computer and then calculating observable macroscopic quantities by time averaging the appropiate microscopic equations. Such calculations are called *molecular dynamics* calculations.[7]

It is interesting to note that the molecular dynamics calculations seem to indicate that a system of hard spheres exhibits both a fluid and a solid branch, with the transition occurring at around a volume $\upsilon = 1.6\upsilon_0$, where υ_0, the closest-packed volume of a system of hard spheres, is equal to $N\sigma^3/\sqrt{2}$. The agreement of these truncated virial expansions is satisfactory up to a reduced density of about 0.5.

It is well recognized in numerical analysis, however, that taking just the truncated power series of a function is an unsatisfactory method of approximating it and more sophisticated techniques are required. One such method is that of Padé approximants, which simply represents the function by a ratio of polynomials, whose coefficients are found by expanding this ratio in a power series and then requiring the first n terms to correctly give the first n Taylor expansion coefficients of the function itself. For example, suppose that are known the first n terms in the expansion of some function $f(x)$, i.e., it is given:

$$f(x) = a_0 + a_1 x + ... + a_n x^n + O(x^{n+1}) \quad , \tag{3.2}$$
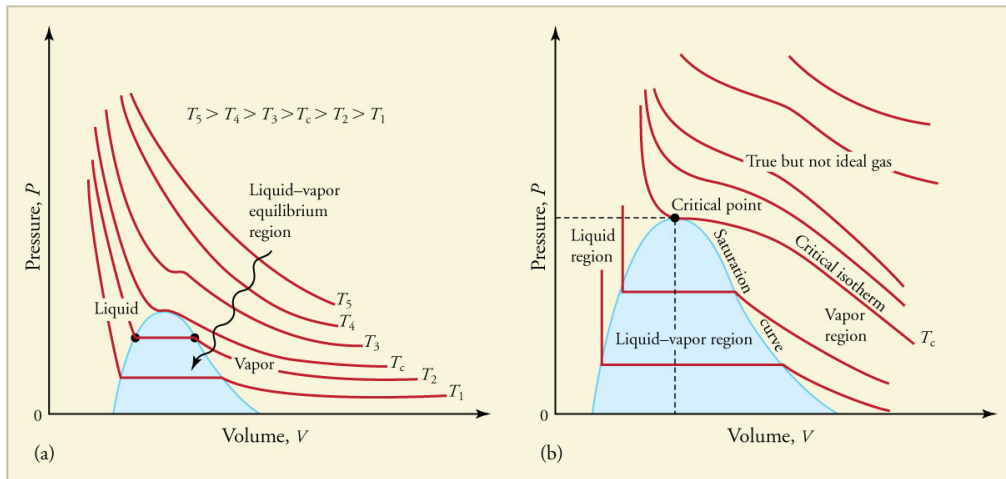
Figure 3.3: *PV diagrams. (a) Each curve (isotherm) represents the relationship between P and V at a fixed temperature; the upper curves are at higher temperatures. The lower curves are not hyperbolas, because the gas is no longer an ideal gas. (b) An expanded portion of the PV diagram for low temperatures, where the phase can change from a gas to a liquid. The term "vapor" refers to the gas phase when it exists at a temperature below the boiling temperature. (Image and text taken from: https://cnx.org/contents/oSrOCkyf@4/Phase-Changes)*

where $a_0, a_1, ..., a_n$ are complex or real coefficients. Now, it is constructed the so-called N,M Padé approximant to this function by writing

$$f(x) \approx \frac{c_0 + c_1 x + ... + c_{N-1} x^{N-1}}{1 + d_1 x + ... + d_{N-1} x^{M-1}} \quad , \tag{3.3}$$

and then finding the c's and d's by expanding this in x and requiring the first n+1 terms to be the same as those in Eq. (3.2). Clearly, the number of Padé coefficients to be determined, M + N - 1, must equal the number of known Taylor expansion coefficients, n + 1. This direct expansion of the denominator in Eq. (3.3) can become quite laborious, and fortunately the evaluation of the c's and d's can be written as a matrix problem.

Nevertheless. such approximations are not enough because they really avoid the true nature of liquids, namely, that each molecule is in constant interaction with all of its neighbors. This makes the virial expansion technique not applicable, and we must abandon it and treat the problem by methods that are more suitable for dense systems.[7]

3.3.1 Distribution functions

Consider a system of N particles in a volume V and at a temperature T. The probability that a molecule 1 is in dr_1 at r_1, molecule 2 in dr_2 at r_2, etc., is given by[7]

$$P^{(N)}(r_1, ..., r_N) dr_1 ... dr_N = \frac{e^{-\beta U_N} dr_1 ... dr_N}{Z_N} \quad , \tag{3.4}$$

with Z_N as the configuration integral:

$$Z_N = \int \cdots \int e^{-\beta [U_N^{(0)} + U_N^{(1)}]} dr_1 \cdots dr_N \quad , \tag{3.5}$$

where $\beta = 1/kT$, k is the Boltzmann's constant, U_N is the total potential energy of the system and r_i, and dr_i are the position and volume element for the i-th molecule, respectively . The probability that molecule 1 is in dr_1 at r_1,..., molecule n in dr_n at r_n, irrespective of the configuration of the remaining $N - n$ molecules is obtained by integrating Eq. (3.4) over the coordinates of molecules $n + 1$ through N: [7]

$$P^{(n)}(r_1, ..., r_n) = \frac{\int ... \int e^{-\beta U_N} dr_{n+1}...dr_N}{Z_N} \quad . \tag{3.6}$$

Now, the probability that *any* molecule is in dr_1 at r_1,...,and *any* molecule is in dr_n at r_n, irrespective of the configuration of the rest of the molecules, is: [7]

$$\rho^{(n)}(r_1, ..., r_n) = \frac{N!}{(N - n)!} \cdot P^{(n)}(r_1, ..., r_n) \quad . \tag{3.7}$$

This comes about since there are N choices for the first molecule, $N-1$ for the second, etc.

The simplest distribution function is $\rho^{(1)}(r_1)$. The quantity $\rho^{(1)}(r_1)dr_1$ is the probability that any one molecule will be found in dr_1. For a crystal this is a periodic function of r_1 with sharp maxima at the lattice sites, but in a fluid all points within the volume V are equivalent and so $\rho^{(1)}(r_1)$ is independent of r_1. For a fluid, therefore, one can write: [7]

$$\frac{1}{V} \int \rho^{(1)}(r_1)dr_1 = \rho(1) = \frac{N}{V} = \rho \quad (fluid) \quad , \tag{3.8}$$

where Eqs. (3.4) and (3.7) are used to equate the integral of $\rho^1(r_1)$ to N.

It is defined a correlation function $g^{(n)}(r_1, ..., r_n)$ by: [7]

$$\rho^{(n)}(r_1, ..., r_n) = \rho^n g^{(n)}(r_1, ..., r_n) \quad , \tag{3.9}$$

where $g^{(n)}$ is called a correlation function since if the molecules were independent of each other ($g^{(n)} = 1$), $\rho^{(n)}$ would equal simply ρ^n, and so the factor $g^{(n)}$ in Eq. (3.9) corrects for the "nonindependence" or, i.e., the correlation between the molecules.

Using Eq. (3.7) can be seen that: [7]

$$g^{(n)}(r_1, ..., r_n) = \frac{V^n N!}{N^n (N-n)!} \cdot \frac{\int \cdots \int e^{-\beta U_N} dr_{n+1}\cdots dr_N}{Z_N}$$

$$= V^n (1 + O(N^{-1})) \frac{\int \cdots \int e^{-\beta U_N} dr_{n+1} \cdots dr_N}{Z_N} \quad . \tag{3.10}$$

$g^{(2)}(r_1, r_2)$ is called the radial distribution function and it's particularly important since it can be determined experimentally. In a liquid of spherically symmetric molecules, $g^{(2)}(r_1, r_2)$ depends only upon the relative distance between molecules 1 and 2, i.e., upon r_{12}. Usually, it is denoted r_{12} simply by r; therefore, a standard notation is $g^{(2)}(r_{12}) = g(r)$.

Now $\rho g(r)dr$ is the "probability" of observing a second molecule in dr given that there is a molecule at the origin of r. This "probability" is not normalized to unity, but

$$\int_0^\infty \rho g(r) 4\pi r^2 dr = N - 1 \approx N \quad . \tag{3.11}$$
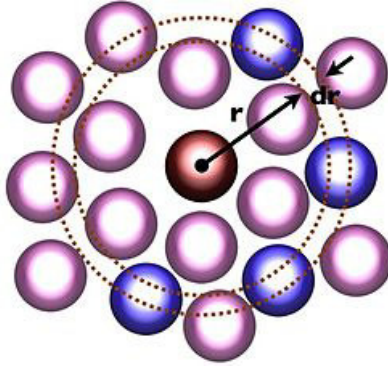
Figure 3.4: *Graphic interpretation of the radial distribution function (Image taken from reference [8])*

Eq. (3.11) show that $\rho g(r) 4\pi r^2$ is really the number of molecules between r and r + dr about a central molecule. The function g(r) can also be thought of as the factor that multiplies the bulk density ρ to give a local density $\rho(r) = \rho g(r)$ about some fixed molecule. Clearly $g \to 0$ as $r \longrightarrow 0$ since molecules become effectively "hard" as $r \to 0$. Also since the influence of the molecule at the origin diminishes as r becomes large, $g \to 1$ as $r \to \infty$. $g(r)$ is called the *radial distribution function* of the fluid. Figure 3.4 show the graphic interpretation of the radial distribution for a fluid.

The radial distrubtion function turns out to be of central importance in the theory of liquids for two reasons. First, if it is assumed that the total potential energy of the N-body system is pair-wise additive, i.e., it can be written as: [7]

$$U_N(r_1, ..., r_N) = \sum_{i<j} u(r_{ij}) \quad , \quad (3.12)$$

where the summation goes over all pair of molecules. Then, all the thermodynamic functions of the system can be written in terms of $g(r)$. In addition, the radial distribution function can be determined from the structure factor (which is defined as the Fourier Transform of g(r)) by X-ray diffraction studies on liquids. In a solid, the molecules are arranged in a regular repeating order, and this leads to a sharp X-ray diffraction pattern from which the order of the molecules in the solid can be obtained. The X-ray diffraction pattern of a liquid is more diffuse, but nevertheless can be used to determine the local short-range order in a fluid.

The peaks in the curve represent smeared-out shells of first nearest neighbors, second nearest neighbors, etc., which in a sense are remnants of the ordering found in the solid. [7]

3.3.2 Relation of thermodynamic functions to g(r)

The canonical partition function, in the classical limit (high temperatures), of a system of N atoms or molecules can be written as: [7]

$$Q_N = \frac{1}{h^{3N}} \int \int e^{-\beta H} d\vec{p}^N d\vec{r}^N \quad ,$$

being h the Planck's constant, H the Hamiltonian of the system, $\vec{p}$ the vector of momentum of the molecule, and $\vec{r}$ its vector position. Taking into account only the interaction

potential and the translational term in the kinetic energy , the momentumś integration
of the previous equation gives: [7]

$$Q_N = \frac{Z_N}{N!\Lambda^{3N}} \quad , \tag{3.13}$$

where Λ is the De Broglié's wavelenght:

$$Z_N = \int e^{-\beta U(r_1, r_2, \ldots, r_N)} dr_1 dr_2 \ldots dr_N, \qquad \Lambda = \sqrt{\frac{h^2}{2\pi mkT}} \quad ,$$

being m the mass of a molecule.

Then, using the relationship $E = kT^2(\frac{\partial ln Q_N}{\partial T})$, the energy can be expressed as:

$$E = \tfrac{3}{2}NkT + kT^2(\tfrac{\partial ln Z_N}{\partial T})$$
$$= \frac{3}{2}NkT + \bar{U} \quad , \tag{3.14}$$

with

$$\bar{U} = \frac{\int \cdots \int U e^{-\beta U} dr_1 \cdots dr_N}{Z_N} \quad .$$

This latter result, with equations 3.12, 3.7 and 3.9, becomes: [7]

$$\bar{U} = \frac{N^2}{2V} \int_0^\infty u(r)g(r)4\pi r^2 dr \quad , \tag{3.15}$$

then, the total energy, E, is

$$\frac{E}{NkT} = \frac{3}{2} + \frac{\rho}{2kT} \int_0^\infty u(r)g(r, \rho, T)4\pi r^2 dr \quad . \tag{3.16}$$

For the pressure equation, it is assumed that this variable is independet of the shape
of the container for large volumes, so a cube is the simplest choice. Using equation 3.9
and the change of variables $x_k = V^{1/3}x'_k$ it is possible to rearrenge the expression for Z_N
and its derivative to use it in the thermodynamic relation $p = kT(\frac{\partial ln Q}{\partial V})_{N,T}$: [7]

$$\frac{p}{kT} = \rho - \frac{\rho^2}{6kT} \int_0^\infty r u'(r)g(r)4\pi r^2 dr \quad . \tag{3.17}$$

To obtain the chemical potential by one of the best known methods, it is necessary to
introduce a "coupling parameter", ξ, from zero to one in order to replace the interaction
of some central molecule with the jth molecule of the system by $\xi u(r_{1j})$. This is expressed
by using equation 3.12: [7]

$$U(r_1, \ldots, r_N, \xi) = \sum_{j=2}^N \xi u(r_{1j}) + \sum_{2 \le i < j \le N} u(r_{ij}) \quad . \tag{3.18}$$

With the definition for the chemical potential μ and with N large:

$$\mu = \left(\frac{\partial A}{\partial N}\right)_{V,T} = A(N, V, T) - A(N - 1, V, T) \quad . \tag{3.19}$$

It is possible to use this latter equation in the definition for the Helmholtz free energy,
represented by A, using the canonical ensamble (See Table 3.1) to have Z_N and its
derivative as a function of ξ to obtain: [7]

$$\frac{\mu}{kT} = ln\ \rho\Lambda^3 + \frac{\rho}{kT} \int_0^1 \int_0^\infty u(r)g(r; \xi)4\pi r^2 dr d\xi \quad . \tag{3.20}$$

3.4 Perturbation Theories of liquids

Much evidence points to the fact that the structure of a liquid is primarily determined by the short-range repulsive forces and that the relatively longer-range attractive part of the potential provides a net force that gives a somewhat uniform attractive potential. Thus, in a sense it is pictured the repulsive part of the potential as determining the structure of the liquid and the attractive part as holding the molecules together at some specified density.

This physical picture suggests an attempt to treat a fluid as a system of molecules governed by a repulsive potential with an attractive potential that is treated as a small perturbation. The unperturbed system, i.e., the system of repulsive molecules, is usually taken to be a system of hard spheres since this system is fairly well understood.[7]

Statistical Mechanical perturbation theory

In this section it is described the statistical mechanical perturbation theory developed by Zwanzig in 1954. The results obtained by performing a perturbation expansion on the canonical partition function of the system and on the configuration integral in particular.

Let the total potential energy be separated into two parts,[7]

$$U_N = U_N^{(0)} + U_N^{(1)} \quad , \tag{3.21}$$

where $U_N^{(0)}$ is the potential energy of an unperturbed (reference) system and $U_n^{(1)}$ is the perturbation. The reference system is usually taken to be a hard-sphere system, but this is not necessary. The perturbation potential is usually defined by the difference between the potential of the real system and the potential of the reference system, i.e., by $U_N^{(1)} = U_N - U_N^{(0)}$.

The configuration integral for this potential is

$$Z_N = \int \cdots \int e^{-\beta[U_N^{(0)} + U_N^{(1)}]} dr_1 \cdots dr_N \quad , \tag{3.22}$$

now it is possible to multiply and divide by

$$\int \cdots \int e^{(-\beta U_N^{(0)})} dr_1 dr_2 \cdots dr_N \quad , \tag{3.23}$$

to get: [7]

$$Z_N = \int \cdots \int e^{-\beta U_N^{(0)}} dr_1 \cdots dr_N \frac{\int \cdots \int e^{-\beta[U_N^{(0)} + U_N^{(1)}]} dr_1 \cdots dr_N}{\int \cdots \int e^{-\beta U_N^{(0)}} dr_1 \cdots dr_N} \quad . \tag{3.24}$$

The second factor here can be considered to be the average of $exp(-\beta U_N^{(1)})$ over the *unperturbed* or *reference* system. Thus: [7]

$$Z_N = Z_N^{(0)} \langle exp(-\beta U_N^{(1)}) \rangle_0 \quad , \tag{3.25}$$

where $Z_N^{(0)}$ is the configurational integral of the unperturbed system and $\langle \ \rangle_0$ indicates a canonical average in the *unperturbed* system. It assumed that $Z_N^(0)$ is known, and consider

$U_N^{(1)}$ to be small enough to expand the exponential in $U_N^{(1)}$. This gives an expansion in powers of β or $1/T$, according to: [7]

$$\langle exp(-\beta U_N^{(1)})\rangle_0 = 1 - \beta\langle U_N^{(1)}\rangle_0 + \frac{\beta^2}{2!}\langle U^{(1)2}\rangle_0 + \cdots \qquad . \qquad (3.26)$$

It is desired to express the free energy and related thermodynamic functions as a power series in β. Since $A = -kTlnQ$ and $Q = Z_N/N!\Lambda^{3N}$, it is possible to write [7]

$$-\beta A = ln\left(\frac{Z_N^{(0)}}{N!\Lambda^{3N}}\right) + ln\left\langle exp(-\beta U_N^{(1)})\right\rangle_0 = -\beta A_0 - \beta A^{(1)} \qquad , \qquad (3.27)$$

where A_0 is the free energy of the reference system and $A^{(1)}$ is the perturbation free energy [7]

$$A^{(1)} = -kTln\left\langle exp(-\beta U_N^{(1)})\right\rangle_0 \qquad . \qquad (3.28)$$

It is this last quantity that must be expressed as a power series in β. Then it is written[7]

$$A^{(1)} = \sum_{n=1}^{\infty}\frac{\omega_n}{n!}(-\beta)^{n-1} \qquad , \qquad (3.29)$$

where the ω_n coefficients are to be determined in terms of the $\left\langle (U_N^{(1)})^n\right\rangle_0$ of Eq. 3.26 by writing: [7]

$$exp(-\beta A^{(1)}) = exp\left(\sum_{n=1}^{\infty}\frac{\omega_n}{n!}(-\beta)^n\right) \qquad . \qquad (3.30)$$

Now, it is expanded the right-hand side in powers of β and compared with coefficients of β^n to give: [7]

$$exp(-\beta A^{(1)}) = \left\langle exp(-\beta U_N^{(1)})\right\rangle_0 = \sum_{k=0}^{\infty}\frac{(-\beta)^k}{k!}\left\langle (U_N^{(1)})^k\right\rangle_0 \qquad .$$

Some algebra steps give rise to the first few ω_n: [7]

$$\begin{array}{rcl}\omega_1 & = & \langle U_N^{(1)}\rangle_0 \\ \omega_2 & = & \langle (U_N^{(}1))^2\rangle_0 - \langle U_N^{(1)}\rangle_0\,^2 \\ \omega_3 & = & \langle (U_N^{(1)})^3\rangle_0 - 3\langle (U_N^{(1)})^2\rangle_0\langle U_N^{(1)}\rangle_0 + 2\langle U_N^{(1)}\rangle_0\,^3\end{array} \qquad , \qquad (3.31)$$

thus it is shown that at high temperatures, the free energy is: [7]

$$A = A_0 + \omega_1 - \frac{\omega_2}{2kT} + O(\beta^2) \qquad . \qquad (3.32)$$

The first term in the expansion, $\omega_1 = \langle U_N^{(1)}\rangle_0$, simplifies considerably when $U_N^{(1)}$ can be written as a sum of pair potentials (Eq. 3.12), so in this case

$$\left\langle U_N^{(1)}\right\rangle_0 \quad = \quad \left\langle \sum_{i<j}u^{(1)}(r_{ij})\right\rangle_0 \quad = \quad \frac{N(N-1)}{2}\left\langle u^{(1)}(r_{12})\right\rangle_0$$

$$= \quad \frac{N(N-1)/2}{Z_N^{(0)}}\int\cdots\int e^{-\beta U_N^{(0)}}u^{(1)}(r_{12})dr_1\cdots dr_N$$

$$= \quad \tfrac{1}{2}\int_V\int u^{(1)}(r_{12})dr_1 dr_2 = \frac{\rho^2 V}{2}\int u^{(1)}(r_{12})g_0^{(2)}(r_{12})dr_{12} \qquad .$$

$$(3.33)$$

The zero subscript in the las two integrals indicates that the distribution function is that of the reference system.

On the other hand, terms like $\left\langle (U_N^{(1)})^2 \right\rangle_0$ are awkward since they introduce higher-order density functions, namely, $\rho^{(3)}$ and $\rho^{(4)}$, which are due to terms like $u(r_{ij})u(r_{jk})$ and $u(r_{ij})u(r_{kl})$ which arise when $U_N^{(1)}$ is squared. [7]

3.4.1 The van der Waals equation

From the Eq. 3.25, taken as a reference system a hard-sphere fluid, it is assumed that U_N is pair-wise additive and to be of the form $u(r) = u_{HS}(r) + u^{(1)}(r)$, where $u^{(1)}(r)$ is some arbitrary attractive part (and so is negative). Then can be assumed that $\beta U_N^{(1)}$ is small enough that: [7]

$$
\begin{aligned}
\left\langle exp(-\beta U_N^{(1)}) \right\rangle_0 &\approx 1 - \beta \left\langle U_N^{(1)} \right\rangle_0 \\
&\approx exp \left\langle -\beta (U_N^{(1)}) \right\rangle_0 \quad .
\end{aligned}
\tag{3.34}
$$

Equation 3.34 follows since the assumption that terms in β^2 and higher terms can be neglected. Then, with these two equations: [7]

$$
\left\langle U_N^{(1)} \right\rangle_0 = \frac{\rho^2 V}{2} \int_0^\infty u^{(1)}(r) g_{HS}(r) 4\pi r^2 dr \quad .
$$

Certainly $g_{HS}(r)$ was not available to van der Waals, and he effectively approximated $g_{HS}(r)$ by [7]

$$
g_{HS}(r) = \begin{cases} 0 & r < \sigma \\ 1 & r > \sigma \end{cases} \quad .
\tag{3.35}
$$

This form is correct for hard spheres only in the limit $\rho \to 0$. Using this $g_{HS}(r)$, [7]

$$
\begin{aligned}
\langle U_N^{(1)} \rangle_0 &= 2\pi \rho^2 V \int_\sigma^\infty u^{(1)}(r) r^2 dr \\
&= -aN\rho \quad ,
\end{aligned}
\tag{3.36}
$$

where:

$$
a = -2\pi \int_\sigma^\infty u^{(1)}(r) r^2 dr \quad .
\tag{3.37}
$$

The minus sign in the definition of a has been included to make a a positive number ($u^{(1)}(r)$ is negative). Then, the Eq. 3.25 has been reduced to [7]

$$
Z_N = Z_N^{(0)} e^{\beta a \rho N} \quad ,
\tag{3.38}
$$

and so it is possible to write [7]

$$
\begin{aligned}
\frac{p}{kT} &= \left(\frac{\partial ln Z_N^{(0)}}{\partial V} \right)_{N,T} - \frac{a\rho^2}{kT} \\
&= \frac{p^{(0)}}{kT} - \frac{a\rho^2}{kT} \quad ,
\end{aligned}
\tag{3.39}
$$

where $p^{(0)}$ is the pressure of the unperturbed system.

The final approximation of the van der Waals theory is to assume that the hard-sphere configuration integral is of the form V_{eff}^N, where the effective volume is determined by

assuming that the volume available to a molecule in the fluid has a volume $4\pi\sigma^3/3$ excluded to it by each other molecule of the system. However, we have to divide this quantity by 2 since this factor of $4\pi\sigma^3/3$ arises from a pair of molecules interacting, and only half the effect can be assigned to a given molecule. Therefore $V_{eff} = V - 2\pi N\sigma^3/3$, and [7]

$$Z_N^{(0)} = (V - Nb)^N, \quad b = \frac{2\pi\sigma^3}{3} \quad . \tag{3.40}$$

Substituting Eq. 3.40 into 3.39, then it is obtained the famous van der Waals equation[7],

$$\frac{p}{kT} = \frac{\rho}{1 - b\rho} - \frac{a\rho^2}{kT} \quad . \tag{3.41}$$

Equation 3.41 is the van der Waals equation of state. Thus the constants a and b, defined in Eqs. 3.37 and 3.40, are the usual van der Waals constants, but here they are given in terms of the intermolecular potential function. So a and b are calculated for the square-well potential, for example, and compare the results to the empirically determined van der Waals parameters. The agreement is not particularly satisfactory, indicating that the van der Waals equation is not good quantitative equation of state. Nevertheless, it does indicate a critical point and condensation by way of a simple model.

The perturbation theoretic derivation of the van der Waals equation suggests a number of obvious improvements. The most obvious ones are:

1. Use a better form for $g(r)$.

2. Use a better expression for $Z_N^{(0)}$.

3. Use a more realistic unperturbed system.

4. Consider higher terms in β.

3.5   Intermolecular interactions and Effective Potentials

The calculation of the potential energy inevitably involves assumptions concerning the nature of attraction and repulsion between molecules. Intermolecular interaction is the result of both short- and long-range effects.

Electrostatic, induction, and dispersion effects are examples of long range interactions. In these cases, the energy of interaction is proportional to some inverse power of intermolecular separation. Electrostatic interactions result from the static charge distribution between molecules. The effect can be either attractive or repulsive and it is exclusively pairwise additive. Induction effects are always attractive, resulting from the distortions caused by the molecular fields of neighbouring molecules.

However, the most important contribution is the attractive influence of dispersion arising from instantaneous fluctuations caused by electron movement. Neither induction nor dispersion are pairwise additive.

Short-range interactions are characterised by an exponential decay in the interaction energy with respect to intermolecular separation. At small intermolecular separations, there is a significant overlap of the molecular wave functions causing either intermolecular exchange or repulsion. These interaction are not pairwise additive.

In theory, it is possible to calculate the intermolecular interactions from first principles. However, in practice the first principle or ab initio approach is confined to relatively simple systems. More commonly, the influence of intermolecular interaction is expressed by some type of intermolecular potential.[42]

Many effective potentials have been developed (Maitland et al., 1981) and applied to atoms. Historically, an empirical approach was used with the parameters of the potential being obtained from experimental data such as second virial coefficients, viscosities, molecular beam cross sections etc.

Conclusions regarding the accuracy of pair potential were made by comparing the properties predicted by the potential with experiment.[42]

In contrast, computer simulation permits the theoretical rigorous evaluation of the accuracy of intermolecular potentials. However, very few potentials have been tested extensively using molecular simulation. Notable exceptions are the hard-sphere and Lennard-Jones.

Effective potentials for atoms are often incorporated into the molecular simulation of platonic molecules and increasingly, macromolecules. Therefore, the atomic pair potential is an important starting basis for predicting molecular properties.

In view of this, the evaluation of pair potentials by molecular simulation is likely to be increasingly important for the prediction of molecular fluids.[42]

Hard-spheres potential

The simplest approximation is to treat atoms as impenetrable hard-spheres, i.e.,

$$u(r) = \begin{cases} \infty & r \leq \sigma \\ 0 & r > \sigma \end{cases}, \tag{3.42}$$

where σ is the hard-sphere diameter.

In a molecular simulation, special procedures are required to evaluate the effect of the hard-sphere potential. These problems are more easily overcome by MC than MD. The potential remains of considerably utility as a reference for the development of hard-sphere equations of state.[42]

Square-Well potential

The square-well potential is the simplest intermolecular potential that is capable of representing the properties of liquids: [42]

$$u(r) = \begin{cases} \infty & r \leq \sigma \\ -\epsilon & \sigma < r \leq \lambda\sigma \\ 0 & r > \lambda\sigma \end{cases} \tag{3.43}$$

where λ is some multiple of the hard-sphere diameter and ϵ is a measure of the attractive interaction. The square-well potential represents a mathematically idealised model of molecular interactions. The properties of the square-well fluid have been investigated widely and it remains a useful starting point for the development of fluid state theories.[42]

Yukawa potential

The square-well potential can be made more realistic by changing the variation of atttractive interactions. There have been many such variations of which the Yukawa potential is an important example:[42]

$$u(r) = \begin{cases} \infty & r \leq \sigma \\ -\frac{\epsilon\sigma}{r} exp\left[-z\left(\frac{r}{\sigma}-1\right)\right] & r > \sigma \end{cases} \tag{3.44}$$

where ϵ is an attractive term, σ is the hard-sphere diameter and z is an adjustable parameter. The inverse power dependence of this potential means that it can be applied to ionic systems.[42]

Mie type potential

Real fluids have a continuous intermolecular potential, which can be approximated by the following empirical relationship:[42]

$$u(r) = \epsilon\left[\left(\frac{m}{n-m}\right)x^{-n} - \left(\frac{n}{n-m}\right)x^{-m}\right] \tag{3.45}$$

where n and m are constants, $x = r/r_m$, and r_m is the separation corresponding to minimum energy. The most common form of the Lennard-Jones potential is obtained when $n = 12$ and $m = 6$ has a valid theoretical justification (this is how dispersion forces decay).[42]
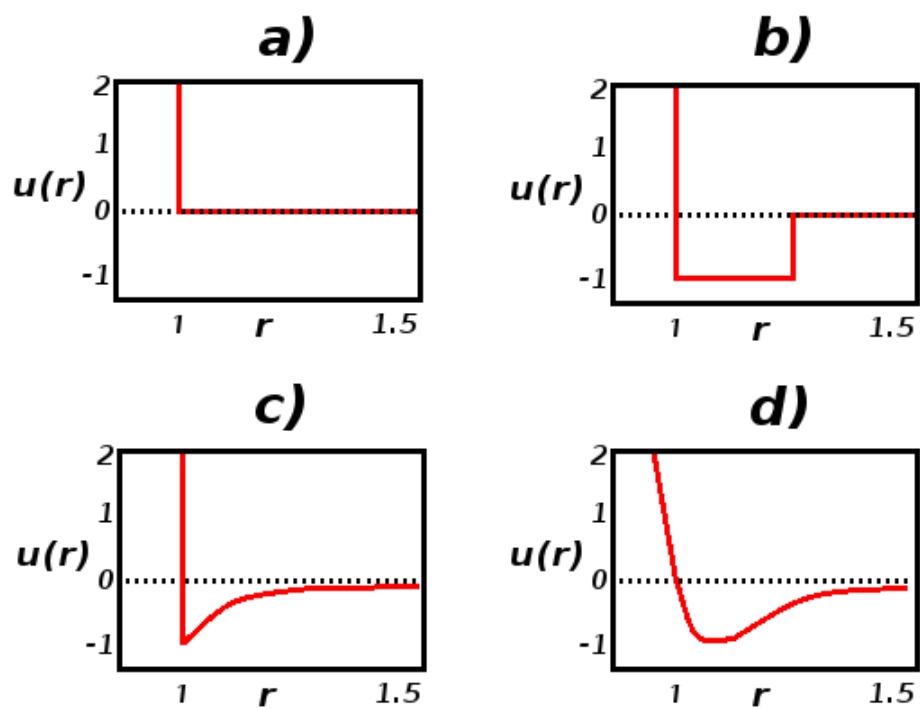
Figure 3.5: *Types of effective potentials. Hard spheres (a), Square-Well (b), Yukawa (c) and the special case of Mie: Lennard-Jones potential (d).*

3.6   Adsorption isotherm (Models and Classification)

The Langmuir equation

The Langmuir isotherm equation is the first theoretically developed adsorption isotherm that was derived using thermodynamic and statistical approaches. Many of the equations proposed later and which fit the experimental results over a wide range are either based on this equation, or these equations have been developed using the Langmuir concept. Thus, Langmuir equation still plays an important role in physisorption as well as chemisortpion theories.

Langmuir derived this equation based on certain assumptions, the more important are: [5]

- The adsorbed entities (atoms or molecules or ions) are attached to the surface at definite localized sites.

- Each site accomodates one and only one adsorbed entity.

- The energy state of each adsorbed entity is the same at all sites on the surface independent of the presence or absence of other absorbed entities at neighboring sites. Thus, this model assumes that the surface is perfectly smooth and homogeneous and that the lateral interactions between the adsorbed entities are negligible.

The equilibrium is assumed to be dynamic in that the rate of adsorption is equal to the rate of desorption. If at any pressure p of the gas the fraction of the sites occupied is Θ, and the fraction of the bare sites is Θ_0 (so that $\Theta + \Theta_0 = 1$) then the rate of condensation (adsorption) is: [5]

$$r_{ads} = akp \; \Theta_0 \quad , \tag{3.46}$$

where p is the pressure and k is a constant given by the kinetic theory of gases $K = N/(2\pi kmT)^{1/2}$; a is the condensation coefficient that is the fraction of the striking molecules that actually condense on the surface.

The evaporation (desorption) of an adsorbed molecule from the surface is essentially an activated process in which the energy of activation, E, for desorption may be identified with $-\Delta H$, the differential (isosteric) heat of adsorption. The rate of evaporation r_{des} can be written as: [5]

$$r_{des} = Z_m\Theta\nu e^{-E/RT} \quad , \tag{3.47}$$

where Z_m is the number of molecules adsorbed (occupied sites) per unit area of the surface so that $Z_m\Theta$ represents the corresponding number of adsorbed molecules, and ν is the frequency of oscillation of the molecules perpendicular to the surface and closely related to the frequency of vibration of the atoms or molecules of the adsorbent. Thus, at equilibrium, $r_{ads} = r_{des}$, thus, equations 3.46 and 3.47 give [5]

$$\Theta = \frac{bp}{1 + bp} \quad , \tag{3.48}$$

where

$$b = \frac{ak}{Z_m\nu e^{-E/RT}} \quad . \tag{3.49}$$

The fraction Θ can also be written as V/V_m the ratio of volume V of the gas or vapor adsorbed at pressure p and V_m, the volume of the adsorbate required to form a monomolecular layer. Θ can also be written as n/n_m, where n is the number of moles adsorbed per g of the adsorbent and n_m is the monolayer capacity in moles.

Simillarly, Θ can also be written in terms of the amount adsorbed in grams as x/x_m, where x in grams is the amount adsorbed per g of the adsorbent, and x_m is the monolayer capacity in grams.

With these several ways in wich Θ can be written the equation 3.48 can be re-expressed as: [5]

$$V = \frac{V_m b p}{1 + bp} \quad , \tag{3.50}$$

$$n = \frac{n_m b p}{1 + bp} \quad , \tag{3.51}$$

$$x = \frac{x_m b p}{1 + bp} \quad . \tag{3.52}$$

Using any of these equations, there are two limiting expressions to be considered: at low and high pressure. In the first case the concentration is proportional to the pressure and in the second, the concentration is a constant given by the asymptote of the function; figure 3.6 illustrate this behavior.
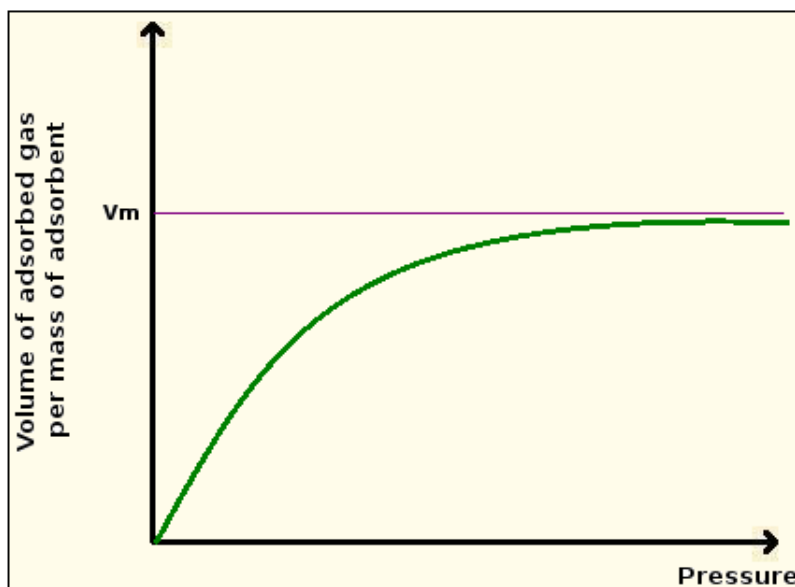
Figure 3.6: *A typical Langmuir adsorption isotherm; V_m is the monolayer capacity.*

According to equation 3.50, the plot of p/v against p should be linear from $\Theta = 0$ to $\Theta = \infty$, and it should give a reasonable value of Vm (the monolayer capacity), which should be temperature independent. However, few data conform to this criterion. Similarly, several chemisorption results are known where the Langmuir equation is valid only within a small restricted range. The assumptions that the adsorption sites on solid surfaces are energetically homogeneous and that there are no lateral interactions between the adsorbed molecules aare the weak point of this model.[5]

The BET equation

Brunauer, Emmet, and Teller derived an equation for multimolecular adsorption by a method that is the generalization of the Langmuir treatment of unimolecular adsorption. These researchers proposed that the forces acting in multimolecular adsorption are the same as those acting in the condensation of vapors. Only the first layer of adsorbed molecules, which is in direct contact with the adsorbent surface, is bound by adsorption forces originating from the interaction between the adsorbate and the adsorbent. Thus, the molecules in the second and subsequent layers have the same properties as in the liquid or gaseous phase.

The assumption that the adsorbate has liquid-like properties after the first layer is difficult to reconcile because both porous and nonporous adsorbents exposed to a saturated vapor sometimes adsorb strictly a limited amount and not the infinitely large quaintity as postulated by the BET model.

The basic assumption of the BET theory is that the Langmuir isotherm can be applied to every adsorption layer. The theory postulates that the first layer of adsorbed molecules acts as a base for the adsorption of the second layer molecules, which in turn acts as a base for the third layer, and so on, so that the concept of localization is maintained in all layers. Furthermore, the forces of interaction between the adsorbed molecules are also neglected, as in the case of Langmuir concept.[5]

With these previous assumptions, the BET equation can be written as [5]

$$\Theta = \frac{cx}{(1-x)(1+(c-1)x)} \quad , \tag{3.53}$$

with

$$x = P\frac{k_i}{k_{-i}}, \ i \neq 0,1 \quad \text{and} \quad c = \frac{Pk_1}{xk_{-1}} \quad ,$$

where P is the pressure of the gas in the bulk phase, k_i is a constant proportional to the rate of condensation to form the *ith* layer and k_{-i} is proportional to the rate of evaporation to form the *ith* layer.(More details for the deduction of this formula can be found in Ref. [14])

The BET equation can be tested, using $x = p/p_0$ (this is because an infinite number of layers of the adsorbed molecules can be built up at saturation vapor pressure p_0), by writting it in the linear form as [5]

$$\frac{p}{V(p_0-p)} = \frac{1}{V_m c} + \frac{c-1}{V_m c} \ p/p_0 \quad , \tag{3.54}$$

so that a plot of $p/[V(p_0-p)]$ against p/p_0 gives a straight line with slope equal to $\frac{c-1}{V_m c}$ and interecepts as $1/(V_m c)$. This, from the slope and intercept the two constants V_m and c can be calculated.
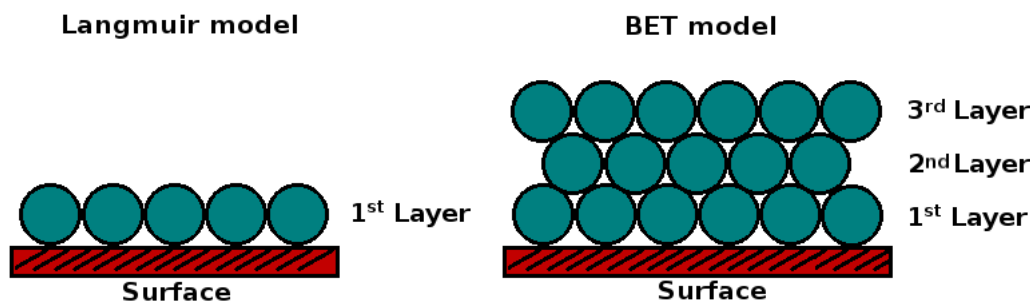
Figure 3.7: *Langmuir and BET models. The former is used in monolayer adsoprtion and the latter in multilayer adsorption.*

The BET equation has played a significant role in studies of adsorption because it represents the shapes of the actual isotherms. It also gives reasonable values for the average enthalpy of adsorption in the first layer and satisfactory values for Vm, the monolayer capacity of the adsorbate which can be used to calculate the specific surface area of the solid adsorbent.

The BET equation is applicable within the relative pressure range of 0.05 to 0.35. The failure of the equation above and below this range of relative pressures has been attributed to the faulty and simplifying assumptions of the theory. The failure below a relative pressure of 0.05 is due to the heterogeneity of the adsorbent surface. At higher relative pressures, the BET equation loses its validity because adsorption by capillary condensation along with physical adsorption also takes place.[5]

Figure 3.7 gives a general illustration for both, Langmuir and BET models.

Classification of Adsorption Isotherm

When the adsorbate is a vapor, it is preferable to express the results in terms of relative vapor pressure (p/p_0) rather than against p itself, where p_0 is the saturation vapor pressure.

Numerous attempts have been made to derive mathematical expressions to fit the adsorption isotherms, but no single adsorption isotherm equation has been found to explain all the adsorption data. The common feature of these isotherms, however, is that all isotherms tend to be linear at low pressures and correspondingly low adsorption values; i.e., the amount adsorbed x is proportional to pressure p. This low-pressure region of the adsorption isotherm is sometimes referred to as the Henry's law region, because it is in consonant with the Henrys law, according to which the solubility of a gas in a liquid is proportional to its pressure.

An examination of these isotherms has shown that most of them conform to one or the other of the five types proposed by Brunauer et al. [5]

Type I Isotherms

When a solid contains very fine micropores that have pore dimensions only a few molecular diameters, the potential field of force from the neighboring walls of the pores will overlap causing an increase in the interaction energy between the solid surface and the gas molecules. This will result in an increase in adsorption, especially at low relative

pressures. There is a possibility and considerable evidence that the interaction energy may be large enough to bring about complete filling of the pores at quite a low relative vapor pressure, giving rise to a Type I isotherm. These isotherms are thus characterized by a plateau that is almost horizontal and parallel to the pressure axis. The adsorption at higher relative pressures being small and tending to level off. Type I isotherms are generally common to chemisorption, although some physical adsorptions such as those in highly microporous active carbons and in carbon molecular sieves also conform to this Type.

The fact that the adsorption in Type I isotherms does not increase continuously as in Type II isotherms but attains a limiting value shown by the plateau is due to the pores being so narrow that they cannot accommodate more than a single molecular layer. The shape of the isotherm can be explained by the Langmuir model even though this model was derived for adsorption on an open surface or on a nonporous solid. It may, however, be mentioned that not all Type I isotherms conform to the Langmuir model. Furthermore, the Langmuir equation assumes n_m to be equal to the monolayer capacity that can be converted into surface area. The nonconformity of Type I isotherms to the Langmuir equation is due to the faulty assumption that the heat of adsorption does not vary with surface converage. In actual practice, however, the heat of adsorption varies with surface coverage in many cases.[5]
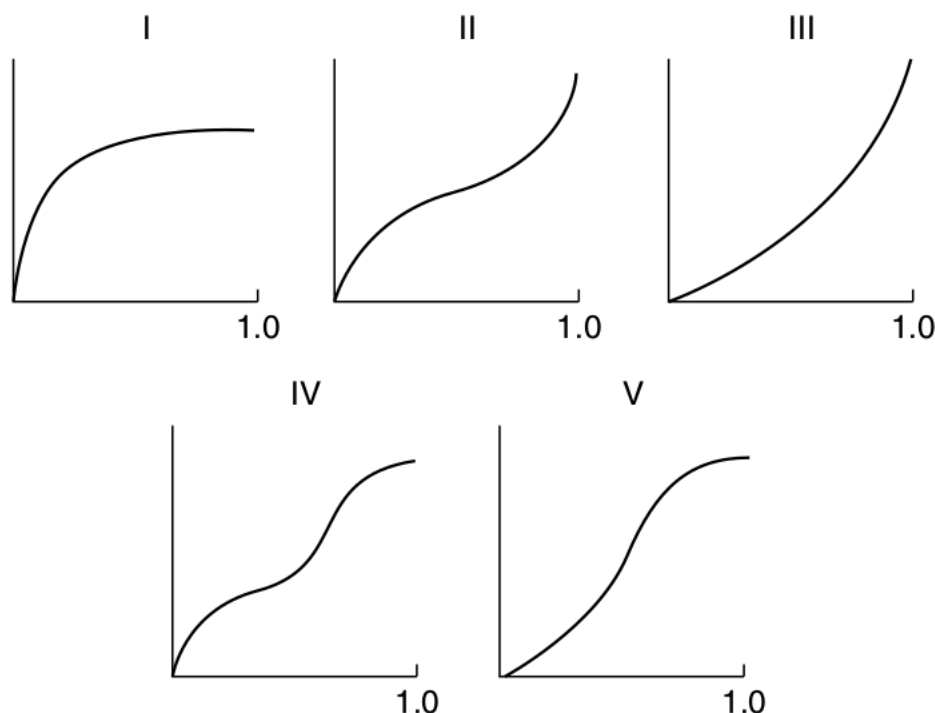
Figure 3.8: *Five many types of adsorption isotherms (Taken from reference [5]).*

Type II Isotherms

These isotherms correspond to multilayer physical adsorption. They generally show a rather long linear portion, a feature that is not strictly compatible with the requirements of the BET equation. The point at which this linear portion begins was termed *Point B*

by Emmett and Brunauer, and was taken by them as the point at which the monolayer is completed so that the adsorption at Point B should be equal to the monolayer capacity X_m. In an earlier paper, these workers had suggested that the point A (Figure 3.9), where the extrapolated linear branch cuts the adsorption axis, might represent the monolayer capacity.

However, the case of locating Point B depends upon the shape of the knee of the adsorption isotherm. If the value of c in the BET equation (the net heat of adsorption) is high, the knee is sharp and the Point B can be accurately located even when the linear branch of the isotherm is short. When c has a small value, the knee is rounded so that the location of Point B becomes difficult, and the estimated value of X_B may differ significantly from the BET monolayer capacity X_m. Thus, it is the value of c that makes the two values agree with each other. [5]
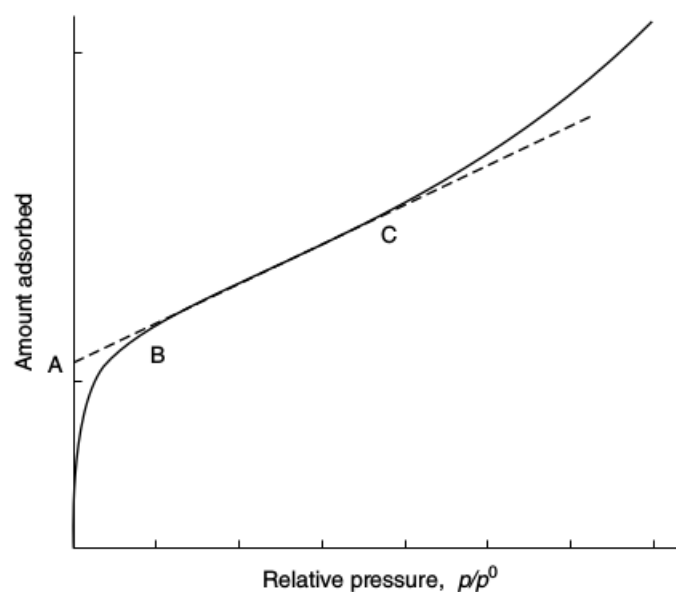
Figure 3.9: *A typical Type II isotherm showing "Point A" and "Point B". (Taken from reference [5]).*

Type III and Type V Isotherms

Type III and Type V isotherms are characterized by being convex to the pressure axis. Although in Type III isotherms the convexity continues throughout the isotherm, in Type V the isotherm reaches a plateau at fairly high relative pressures, often at p/po equal to or higher than 0.51 in the multilayer region. The convexity of the isotherms is suggestive of the cooperative adsorption, which means that the already adsorbed molecules tend to enhance the adsorption of other molecules. In other words, it implies that the adsorbate-adsorbent interactions are of less importance than the adsorbate-adsorbate interaction. The weak adsorbate-adsorbent interactions result in small adsorption at lower relative pressures. But once a molecule has been adsorbed, the adsorbate-adsorbate interactions will tend to promote the adsorption of more molecules so that the isotherm becomes convex to the pressure axis (See Fig. 3.10).

Type III isotherms are generally obtained in the case of nonporous or highly macroporous adsorbents, and type V on mesoporous or microporous adsorbents for the adsorption
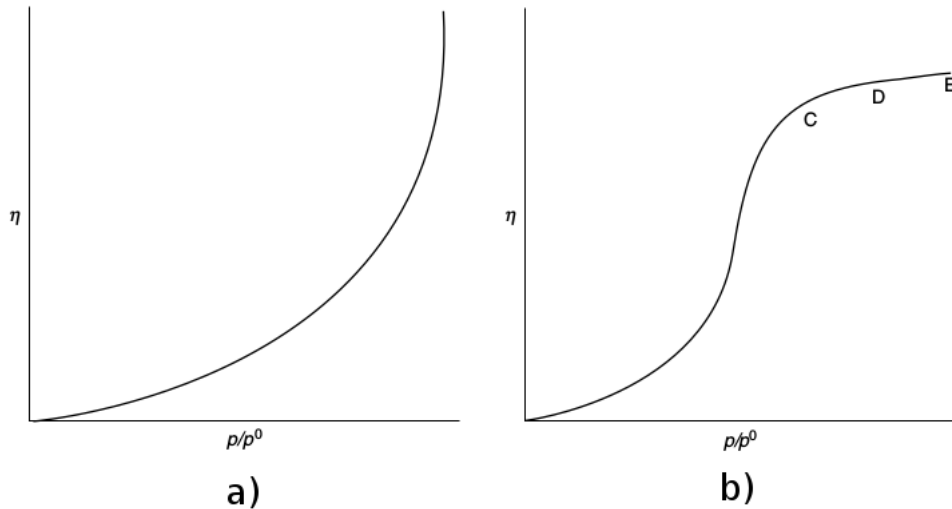
Figure 3.10: *A typical Type III (a) and Type V (b) isotherms (Taken from reference [5]).*

of both polar and nonpolar adsorbates, provided, however, that the adsorbent-adsorbate interactions are weak. Because the heat of liquefaction (or evaporation) is a measure of the adsorbate-adsorbate interaction energy, it appears that the heat of adsorption in the case of Type III isotherms is close to the heat of liquefaction, so the net heat of adsorption $(E_1 - E_L)$ is very small and close to zero. Adsorption of water vapors on charcoals, active carbons, graphitized carbon blacks, and several types of dehydrated oxide catalysts is generally Type III or Type V. This is due to the fact that the dispersion component of the interaction energy is usually small compared to the polar contribution.

The question now arises as to whether the BET equation can be used to calculate the monolayer capacity V_m or X_m from Type III isotherms in a manner similar to the one used for Type II isotherms. If the BET model is quantitatively valid for systems yielding Type III isotherms, then the value of V_m should be calculable from Equation 3.54.

Because the value of c for Type III isotherms is 1 or 2 (i.e., $c = 1$ or $c = 2$), the substitution of these values in Equation 3.54 produces two special cases. Putting $c = 1$, the simplified equation is obtained : [5]

$$\frac{p}{V(p_0 - p)} = \frac{1}{V_m} \quad , \tag{3.55}$$

so that the usual BET plot of $\frac{p}{V(p_0-p)}$ against p/p_0 will give a horizontal line parallel to the p/p_0 axis at a distance $\frac{1}{V_m}$ from it.

When $c = 2$ is substituted in the above common BET equation, it results: [5]

$$\frac{p}{V(p_0 - p)} = \frac{1}{2V_m} + \frac{1}{2V_m}p/p_0 \quad , \tag{3.56}$$

so that the slope and the intercept of the plot $\frac{p}{V(p_0-p)}$ versus p/p_0 are equal and are given by $\frac{1}{2V_m}$.

In practice, however, it is not easy to make an accurate BET plot from Type III isotherm, because the values of V are very small and of lesser accuracy, especially at lower relative pressures. This lower pressure region of the isotherm is the portion over which the BET equation is generally valid.

Furthermore, if we calculate the value of the slope from the first special case plot of $\frac{p}{V(p_0-p)}$ versus p/p_0, the value of the slope [5]

$$Slope = \frac{c-1}{V_m c} \quad , \qquad (3.57)$$

where $c = 1$ becomes very sensitive to the value of c. Therefore, the direct use of the BET equation in the conventional manner is unsuitable for Type III isotherms. A slightly modified method can, however, be used. This procedure consists in calculating p/p_0 when V becomes equal to V_m. The BET equation can then be rearranged as: [5]

$$\frac{p/p_0}{(1-p/p_0)} = \frac{V}{V_m c}[1 + (c-1)p/p_0] \quad . \qquad (3.58)$$

Substituting $V = V_m$ or $\frac{V}{V_m} = 1$ and then solving for p/p_0 gives [5]

$$\left(\frac{p}{p_0}\right)_m = \frac{-1 \pm \sqrt{c}}{c-1} \quad . \qquad (3.59)$$

Because p/p_0 is always positive, the only solution of Equation 3.59 is [5]

$$\left(\frac{p}{p_0}\right)_m = \frac{-1 + \sqrt{c}}{c-1} \quad . \qquad (3.60)$$

Now for the special case $c = 1$, the above equation becomes indeterminate. The value of p/p_0 can then be calculated directly from equation 3.54 by merely substituting $V = V_m$ and $c = 1$ and solving for p/p_0. This gives $(p/p_0)_m = 0.5$ and for $c = 2$, $(p/p_0)_m = 0.41$. Thus, as the value of c moves from $c = 2$ to $c = 1$, the value of p/p_0 changes from 0.41 to 0.50.

It is apparent that for values of c greater than unity, the value of V_m can be derived from the slope and intercept of the BET plot in the usual way. But since there are deviations at lower relative pressures, it is sometimes more convenient to locate the BET monolayer point by the relative pressure $(p/p_0)_m$ at which $V/V_m = 1$. In such cases the value of c is first determined by matching the experimental isotherm with a set of ideal BET isotherms, calculated by substituting different values of c (between 1 and 2, and even nonintegral values if necessary). This value of c can then be inserted into Equation 3.60 and the value of $(p/p_0)_m$ calculated. Then from the usual BET plot, the value of V_m can be read for a suitable value of p/p_0. However, when these values of monolayer capacity obtained from Type III isotherms were compared with V_m values obtained from independent estimates, considerable discrepancies were frequently noticed.

Type IV Isotherms

Type IV isotherms are obtained for solids containing pores in the mesopore range. The shape of the Type IV isotherm follows the same path as the Type II at lower relative pressures until its slope starts decreasing at higher pressures. At the saturation vapor pressure, the isotherm levels off to a constant value of adsorption (Figure 3.8).

This portion of the isotherm, which is parallel to the pressure axis, is attributed to filling of the larger pores by capillary condensation. The most significant characteristics of these isotherms is that they show adsorption-desorption hysteresis, which means that the amount adsorbed is always greater at any given relative pressure along the desorption
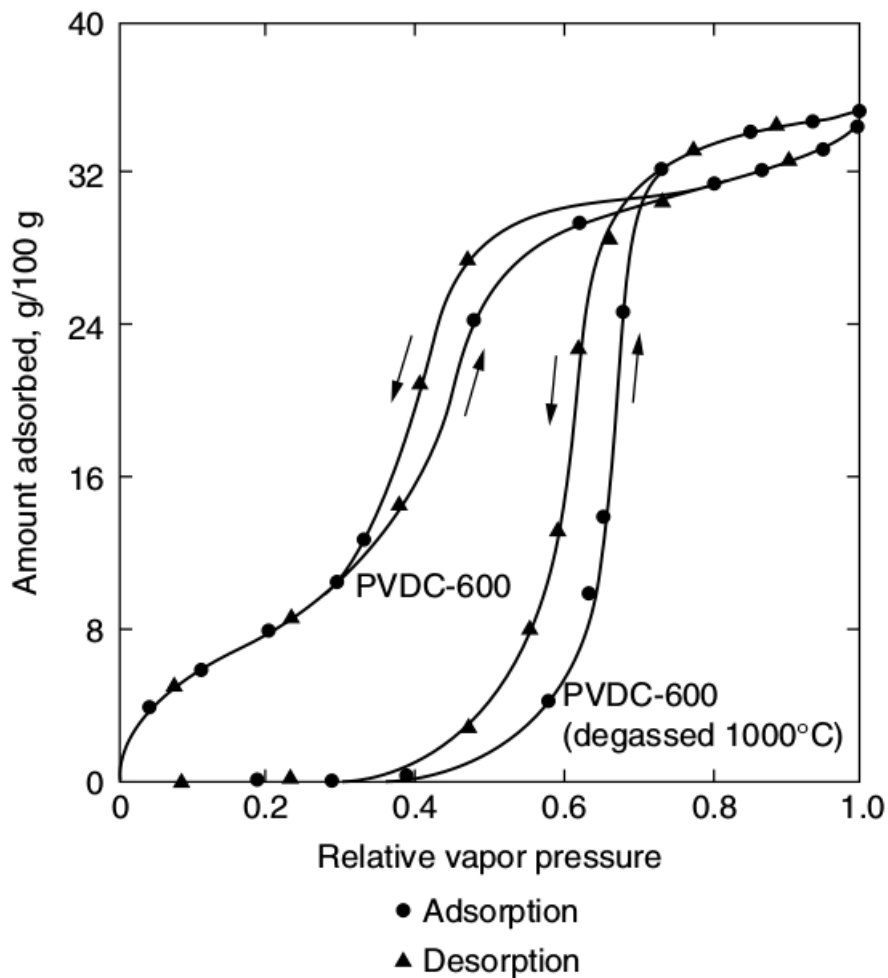
Figure 3.11: *Adsorption-desorption isotherms of water vapor on PVDC (poly-vinylidene chloride) charcoal before and after degassing at 1000° C. (Taken from reference [5]).*

branch than along the adsorption branch (Figure 3.11). This type of isotherm is generally obtained in the case of oxide gels and several porous carbon materials that have larger-sized pores. These adsoprtion isotherms have led to the development of the theory of capillary condensation.[5]

3.7 Analytic Expression for the Isosteric Heat of Adsorption using a SAFT-VR-2D equation of State

The isosteric heat of adsorption or differential enthalpy of adsorption is a valuable thermodynamic property for the design of adsorption processes that represents a measure of the adsorbate-adsorbent strength of interaction. The isosteric heat of adsorption for pure components can be obtained from calorimetric meeasurements or from adsorption isotherms measured at different temperatures. This latter approach uses a Clapeyron type relationship to determine the isosteric heat of adsorption Q_{st} [20]

$$Q_{st} = RT^2 \left(\frac{\partial ln \ p}{\partial T} \right)_n , \qquad (3.61)$$

where n represents the amount adsorbed, p and T are the pressure and temperature of the system, and R is the Universal Gas Constant. This equation is only valid for pure components and perfect gases; there is a more general concept which leads to general expressions valid even for mixtures and high pressure systems[21], and it is the differential enthalpy of adsorption:

$$\Delta \bar{h}_i^a = \left[\frac{\partial \Delta H^a}{\partial n_i^a} \right]_{T,n_j^a} = \bar{h}_i^a - h_i^o = -RT^2 \left[\frac{\partial ln \ f_i}{\partial T} \right]_{n_i^a,n_j^a} , \qquad (3.62)$$

where ΔH^a is the integral enthalpy of adsorption, $\bar{h}_i^a$ and h_i^o are the molar enthalpies of the adsorbed phase and in the perfect gas reference state; f_i is th fugacity of component i, and n_i^a is the amount adsorbed of component i.

Thus, Q_{st} and $\Delta \bar{h}_i^a$ are the same for pure components and low pressures (where the ideal gas approximation is valid).

Also, two important quantities must be introduced, in order to relate the amount of adsorbed substance; these are the absolute and Gibbs adsorption isotherms, Γ_{abs} and Γ_{Gibbs}, respectively. [48]

The surface excess concentration Γ is defined as:

$$\Gamma = \int_0^\infty dz \left[\rho(z) - \rho_b \right], \qquad (3.63)$$

where $\rho(z)$ is the density ofparticles and ρ_b is its bulk value, i.e., $\rho(z \to \infty) = \rho_b$. The surface excess amount is commonly called Gibbs surface excess concentration, denoted as Γ_{Gibbs}.

The absolute adsorption concentration, Γ_{abs}, is defined by the total concentration of adsorbed molecules,

$$\Gamma_{abs} = \rho_{ads} = \int_0^{\lambda_w \sigma} dz \rho(z), \qquad (3.64)$$

where ρ_{ads} is the density of the adsorbed fluid.

To follow up, it is convenient to summarise the way to translate between theoretical and experimental variables. If is denoted by n the number of moles of the adsorbed fluid, then it is related either to Γ_{Gibbs} or Γ_{abs} through the equation,

$$n = \frac{\Gamma A_s}{N_0}, \qquad (3.65)$$

where N_0 is the Avogadro's number and A_s is the surface area of the adsorbent. Since the specific surface area S, defined by $S = A_s/m_s$, where m_s is the mass of the asorbent solid, can be obtained by different experimental methods, the appropiate expression that connects n with Γ is:

$$n/m_s = \Gamma S/N_0, \tag{3.66}$$

and n/m_s is known as *amount of adsorbed* fluid. S is the standard value of the Brunnauer-Emmet-Teller area[49][50], normally represented by S_{BET}.

Chapter 4

Development of the model

The model consider a fluid that can be decomposed into two phases: the bulk (3D) and the adsorbed fluids. The intermolecular potential considered for both phases, is a square-well potential given in Eq. 3.43 (See Figure 4.1).

$$u(r) = \begin{cases} \infty & \text{if } r \leq \sigma \\ -\epsilon & \text{if } \sigma < r \leq \lambda\sigma \\ 0 & \text{if } r > \lambda\sigma \end{cases}$$

$$u_{pw}(z) = \begin{cases} \infty & \text{if } z \leq 0 \\ -\epsilon_w & \text{if } 0 < z \leq \lambda_w\sigma \\ 0 & \text{if } z > \lambda_w\sigma \end{cases}$$
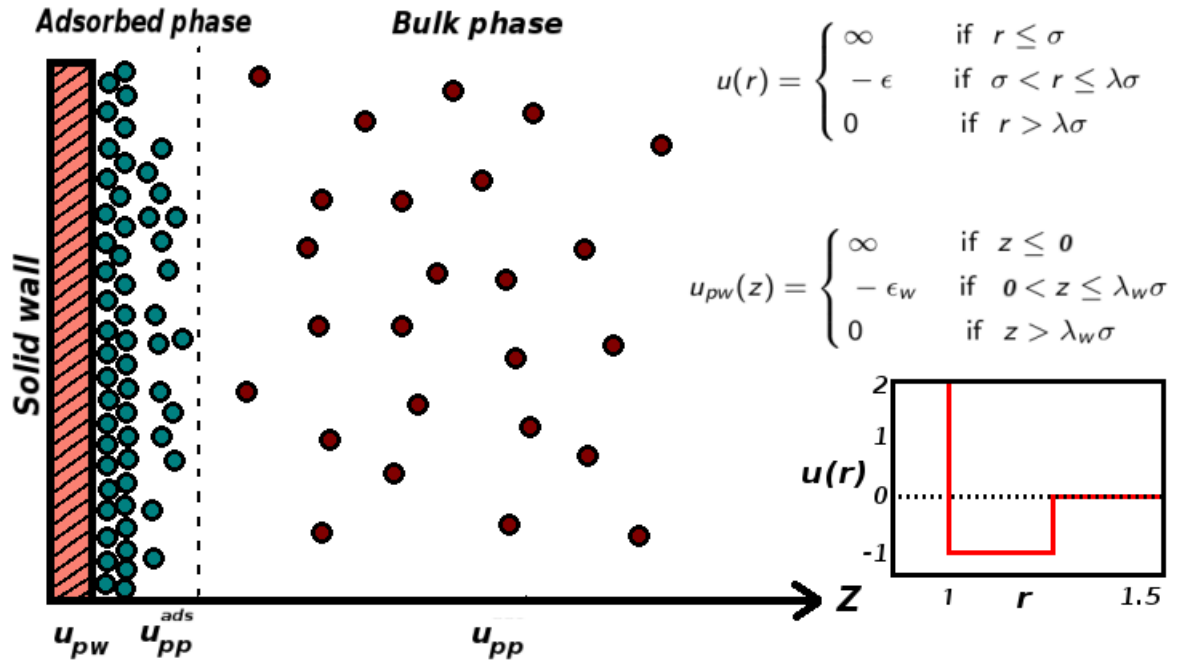
Figure 4.1: *Description of the model fluid; u_pw is the particle-wall potential, u_{pp}^{ads} is the particle-particle potential in the adsorbed phase and u_{pp} is the particle-particle potential in the bulk phase; $\lambda\sigma$ is the range of the adsorbed phase.*

Within this approximation and the framework of the Barker and Henderson perturbation theory, del Río and Gil-Villegas [23] developed a model for particles interacting via a square-well (SW) pair potential that are adsorbed onto a structureless planar surface.

The attention of researchers has been attracted by the use of two dimensional equations of state to describe adsorption in porous materials, since these avoid the concept of adsorption sites used in the development of Langmuir and BET type adsorption isotherms, mentioned in this work. Molecular-based equations of state for adsorption using a 2D approach have been widely studied and applied over the years, assuming

that the adsorbed phase can be represented by a 2D fluid in equilibrium with a 3D bulk phase[22].

The model assumes that the bulk and adsorbed particles have the same diameter σ but the attractive interaction is modified due to the effect of the substrate, and the values of the energy ϵ and attractive range λ potential parameters corresponding to the bulk and adsorbed phases are different. In this work, (ϵ, λ) and $(\epsilon_{ads}, \lambda_{ads})$ are the bulk and adsorbed particle-particle interactions, respectively. Typically, $\epsilon_{ads} \approx 0.8\epsilon$ [25] and $\lambda_{ads} < \lambda$ to allow the ratio of the critical temperatures of the adsorbed and bulk fluid phases $R_c = T_c^{ads}/T_c^{bulk} \approx 0.4.$ [10][19]

The interaction potential u_{pw} exerted on the adsorbed particles by the surface is also given by a SW potential with parameters (ϵ_w, λ_w), the energy and range of the wall, written as a function of the orthogonal coordinate distance z between the particle and the surface, fixing $z = 0$ at the position of contact of the particle with the surface:

$$u_{pw}(z) = \begin{cases} \infty & \text{if} \quad z \leq 0 \\ -\epsilon_w & \text{if} \quad 0 < z \leq \lambda_w\sigma \\ 0 & \text{if} \quad z > \lambda_w\sigma \end{cases} \qquad (4.1)$$

The expression for the classical Helmholtz free energy using the canonical ensemble can be applied to the bulk fluid (the temperature and volume can be fixed, allowing the pressure being a function of both) :

$$A = -kT \ln Q \qquad . \qquad (4.2)$$

It is necessary (in order to make molecular simulation) to define a scaled (or adimensional) free energy, using both the thermal energy (kT) and the number of particles (N) of the system:

$$a = \frac{A}{NkT} = -\frac{1}{N}\ln Q \qquad , \qquad (4.3)$$

where Q is the partition function for the system; in the classical limit (high or approximating to room temperature), this function can be written as

$$Q = \frac{1}{N!\Lambda^{3N}} \int e^{-\beta U_N(r_1, r_2, \cdots, r_N)} d\vec{r}^N \qquad . \qquad (4.4)$$

Then, according to the SAFT approach [1] (See Fig. 4.2):

$$a = \frac{A}{NkT} = \frac{A^{ideal}}{NkT} + \frac{A^{monomers}}{NkT} + \frac{A^{chain}}{NkT} + \frac{A^{assoc}}{NkT}, \qquad (4.5)$$

it is considered in this work only the ideal and the monomer contribution; chain and association terms can be included in future works.

Using Equations 4.4 and 4.3:

$$a = -\frac{1}{N}\ln Q = -\frac{1}{N}\left[\ln\left(\int e^{-\beta U_N(r_1, r_2, \cdots, r_N)} d\vec{r}^N\right) - \ln\left(N!\ \Lambda^{3N}\right)\right] \qquad .$$

To include the ideal gas contribution, the previous relation can be written as:

$$a = -\frac{1}{N}\left[\ln\left(\frac{\int e^{-\beta U_N(r_1, r_2, \cdots, r_N)} d\vec{r}^N}{V^N}\right) + \ln\left(V^N\right) - \ln\left(N!\ \Lambda^{3N}\right)\right] \qquad , \qquad (4.6)$$
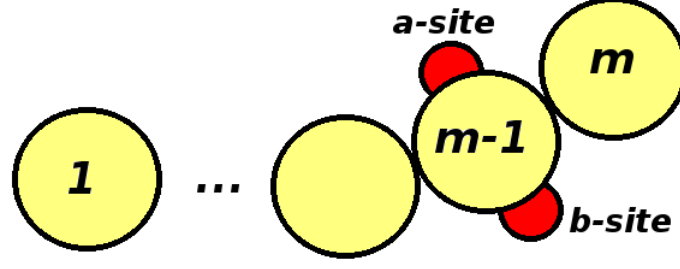
Figure 4.2: *General representation of a chain molecule with m monomers and two sites of association in SAFT approach (right).*

and then, the Stirling approximation ($ln\ N! \approx N\left[ln\ N - 1\right]$)can be used (N goes to inifinity) with the relation for the bulk density (ρ) as a function of the bulk packing fraction (η); the previous idea allows the rearrengement of Equation 4.6 to give:

$$a = ln\ 6 + ln\ \eta + ln\ \Lambda^{*3} - ln\ \pi - 1 - \frac{1}{N}ln\ M \quad , \qquad (4.7)$$

where

$$M = \frac{\int e^{-\beta U_N(r_1,r_2,\cdots,r_N)}d\vec{r}^N}{V^N}, \quad \eta = \frac{N\nu}{V} = \frac{\rho\sigma^3\pi}{6}, \quad \rho = \frac{N}{V}, \quad \Lambda^* = \frac{\Lambda}{\sigma} \quad .$$

ν is the volume per molecule, σ is the diameter of the molecule (considered as a sphere) and V is the total volume.

Now, the task is to write down the intermolecular potential using the perturbation theory of the previous chapter. This can be made using a hard spheres potential as a reference system (or the repulsion contribution), the other being attractive, polarization, magnetization or any contribution to the real potential.

The potential is given by:

$$U_N = U_N^0 + U_N^1 \quad ,$$

U_N^0 is the potential of the reference system (hard spheres, usually) and U_N^1 is the perturbation potential. Using this and averaging over the reference system in the relation for M:

$$M = \frac{\int e^{-\beta(U_N^0+U_N^1)}d\vec{r}^N}{V^N} = \frac{\int e^{-\beta U_N^0}d\vec{r}^N}{V^N}\left[\frac{\int e^{-\beta(U_N^0+U_N^1)}d\vec{r}^N}{\int e^{-\beta U_N^0}d\vec{r}^N}\right] \qquad (4.8)$$

$$= \frac{\int e^{-\beta U_N^0}d\vec{r}^N}{V^N}\left\langle exp\left(-\beta U_N^1\right)\right\rangle_0 = M_0\left\langle exp\left(-\beta U_N^1\right)\right\rangle_0 \quad ,$$

where

$$M_0 = \frac{\int e^{-\beta U_N^0}d\vec{r}^N}{V^N}, \quad \left\langle exp\left(-\beta U_N^1\right)\right\rangle_0 = \left[\frac{\int e^{-\beta(U_N^0+U_N^1)}d\vec{r}^N}{\int e^{-\beta U_N^0}d\vec{r}^N}\right] \quad .$$

Letting the perturbation be small and considering a high temperature regime, the exponential factor in brackets can be approximated by a power series in β up to the desired order (in this work, the series was truncated up to second order):

$$\left\langle exp\left(-\beta U_N^1\right)\right\rangle_0 \approx \left\langle 1 - \beta U_N^1 + \frac{\beta^2}{2}\left(U_N^1\right)^2 - \cdots + \frac{\beta^n}{n!}(U_N^1)^n\right\rangle$$

$$= 1 - \beta\left\langle U_N^1\right\rangle_0 + \frac{\beta^2}{2}\left\langle(U_N^1)^2\right\rangle_0 - \cdots + \frac{\beta^n}{n!}\left\langle(U_N^1)^n\right\rangle_0 \quad ,$$

(4.9)

and using Equations 4.8 and 4.9 in Eq. 4.7 gives:

$$
\begin{aligned}
a^{3D} &= ln\ 6 + ln\ \eta + ln\ \Lambda^{*3} - ln\ \pi - 1 - \tfrac{1}{N}ln\ M_0 - \tfrac{1}{N}ln\ \langle exp\ (-\beta U_N^1)\rangle_0 \\[6pt]
&= ln\ 6 + ln\ \eta + ln\ \Lambda^{*3} - ln\ \pi - 1 - \tfrac{1}{N}ln\ M_0 \qquad (4.10) \\[6pt]
&\quad - \tfrac{1}{N}ln\ \left(1 - \beta\langle U_N^1\rangle_0 + \tfrac{\beta^2}{2}\langle (U_N^1)^2\rangle_0 - \cdots + \tfrac{\beta^n}{n!}\langle (U_N^1)^n\rangle_0\right) \quad .
\end{aligned}
$$

Then, using the following relation:

$$
ln\ (1+x) = \sum_{n=1}^{\infty} \frac{(-1)^{n-1}}{n} x^n, \quad if \quad |x| < 1 \quad , \qquad (4.11)
$$

with

$$
x = \left| -\beta\langle U_N^1\rangle_0 + \tfrac{\beta^2}{2}\langle (U_N^1)^2\rangle_0 - \cdots + \tfrac{\beta^n}{n!}\langle (U_N^1)^n\rangle_0\right| \quad ,
$$

and taking just up to the β^2 terms in the serie, 4.10 can be rewritten as

$$
a^{3D} = a_{ideal}^{3D} + a_{HS} + \beta a_1^{3D} + \beta^2 a_2^{3D} + a_{res} \quad , \qquad (4.12)
$$

being

$$
a_{ideal}^{3D} = ln\ 6 + ln\ \eta + ln\ \Lambda^{*3} - ln\ \pi - 1, \quad a_{HS} = -\tfrac{1}{N}ln\ M_0
$$

$$
a_1^{3D} = \frac{\langle U_N^1\rangle_0}{N}, \quad a_2^{3D} = -\frac{1}{2N}\left(\langle (U_N^1)^2\rangle_0 - \langle U_N^1\rangle_0\langle U_N^1\rangle_0\right) \quad .
$$

The term a_{res} in Equation 4.12 includes the higher order contributions in β to the free energy. There are many approaches (depending on the type of fluid) that can be used to calculate the last three terms in Equation 4.12. a_1 and a_2 are the mean attractive energy and the fluctuation terms, respectively, and correspond to the perturbation for the Helmholtz free energy, containing the information of the perturbation potential. a_{HS} contains the information of the reference potential; in this work, it is used an expression derived from the compresibility factor (Θ) for non-attractive hard-spheres as a function of the bulk density obtained by Carnahan and Starling[9]

$$
\Theta_{HS} = \frac{1 + \eta + \eta^2 - \eta^3}{(1 - \eta)^3} \quad . \qquad (4.13)
$$

This latter expression combined with the following relations:

$$
P = -\left(\frac{\partial A}{\partial V}\right)\Big|_{N,T} \qquad \eta = \frac{N\nu}{V} \quad , \qquad \Theta = \frac{PV}{NkT} \quad ,
$$

gives

$$
\eta\frac{\partial a_{HS}}{\partial \eta} = \frac{1 + \eta + \eta^2 - \eta^3}{(1 - \eta)^3} \quad . \qquad (4.14)
$$

With the integration of the Equation 4.14, and knowing that $a_{ideal} = \lim_{\eta \to 0} a$, the hard-sphere term is obtained:

$$
a_{HS} = \frac{4\eta - 3\eta^2}{(1 - \eta)^2} \quad . \qquad (4.15)
$$

Then, the terms a_1 and a_2 were evaluated for a square-well fluid using two parameters (See Figure 4.2), the attractive range (λ) and the depth of the potential well (ϵ), with two different approaches; the first was to obtain the mean field term (a_1) by the theory developed by Boublík[16] and the fluctuation term (a_2) extending the information given at Benavides and del Río [17]; this approach can be found in Gil-Villegas et al [40]. The second approach uses the SAFT-VR theory [18] for both a_1 and a_2. In both approaches, the residual term (a_{res}) is given by the expression given in Gil-Villegas et al [40] (See Expressions from 4.18 to 4.20 and 4.21 to 4.23).

The expression for the compressibility factor of the bulk fluid is:

$$\Theta^{3D} = \Theta_{HS} + \beta\theta_1^{3D} + \beta\theta_2^{3D} + \theta_{res} \quad , \tag{4.16}$$

where θ_1 and θ_2 correspond to the perturbation terms for the compressibility bulk factor, given by the definition:

$$\theta_i = \eta \frac{\partial a_i^{3D}}{\partial \eta} \quad .$$

Then, equations 4.30 and 4.31 along with 4.12 and 4.16 give:

$$\frac{\mu_{bulk}}{kT} = \frac{G^{3D}}{NkT} = \frac{A^{3D}}{NkT} + \frac{PV}{NkT} = a^{3D} + \frac{1 + \eta + \eta^2 - \eta^3}{(1-\eta)^3} + \beta\theta_1 + \beta^2\theta_2 \quad . \tag{4.17}$$

For the remaining perturbation terms, the first approach[40] implemented in this work is:

$$a_1^{3D} = -4\eta\epsilon(\lambda^3 - 1)y_{HS}(x = \xi) \quad , \tag{4.18}$$

$$a_2^{3D} = -2\eta\epsilon(\lambda^3 - 1)K_{HS}^2(\eta)w_2(\beta) \quad , \tag{4.19}$$

$$a_{res} = -\eta(\lambda^3 - 1)\left[4\left(1 - 1.5s(\lambda)\eta\right)K_{HS}^2 w_3(\beta) + q(\lambda)\eta K_{HS}^3(t^3 - \beta^3)\right], \tag{4.20}$$

with

$$y_{HS} = exp\left(\mu_0 + \mu_1 x + \mu_2 x^2 + \mu_3 x^3\right),$$

$$K_{HS} = kT\left(\partial\rho/\partial P_{HS}\right)_T = \frac{(1-\eta)^4}{1+4\eta+4\eta^2-4\eta^3+\eta^4},$$

$$s(\lambda) = \frac{-49\lambda^5 - 49\lambda^4 + 293\lambda^3 + 5\lambda^2 - 211\lambda - 211}{6(\lambda^2 + \lambda + 1)},$$

$$q(\lambda) = 4.94876 + 0.097245\lambda - 12.9126\lambda^2 + 7.8632\lambda^3,$$

$$\mu_0 = -ln\left(1 - \eta\right) + \frac{42\eta - 39\eta^2 + 9\eta^3 - 2\eta^4}{6(1-\eta)^3}, \qquad \mu_1 = \frac{\eta4 + 6\eta^2 - 12\eta}{2(1-\eta)^3},$$

$$w_2(\beta) = e^\beta - 1 - \beta, \qquad w_3(\beta) = t - \beta - \tfrac{1}{2}\beta^2, \qquad t = e^\beta - 1,$$

$$\mu_2 = \frac{-3\eta^2}{8(1-\eta)^2}, \qquad \mu_3 = \frac{-\eta^4 + 3\eta^2 + 3\eta}{6(1-\eta)^3},$$

$$\xi = \xi_0 + \xi_1\eta + \xi_2\eta^2,$$

$$\xi_0 = 0.773853 - 0.157937\lambda + 0.499370\lambda^2 - 0.115220\lambda^3,$$

$$\xi_1 = (6/\pi)(2 - \lambda)e^{-5.58961 + 2.04530\lambda},$$

$$\xi_2 = 1.216473 - 2.034727\lambda + 1.238574\lambda^2 - 0.425229\lambda^3 \quad .$$

The second approach [18] is

$$a_1^{3D} = a_1^{VDW} g^{HS}(1; \eta_{eff}), \tag{4.21}$$

$$a_2^{3D} = \frac{1}{2} \epsilon K^{HS} \eta \frac{\partial a_1^{3D}}{\partial \eta}, \tag{4.22}$$

$$a_{res} = -\eta(\lambda^3 - 1) \left[4 \left(1 - 1.5 s(\lambda)\eta \right) K_{HS}^2 w_3(\beta) + q(\lambda)\eta K_{HS}^3 (t^3 - \beta^3) \right], \tag{4.23}$$

where

$$a_1^{VDW} = -4\eta\epsilon(\lambda^3 - 1),$$

$$K_{HS} = kT \left(\partial\rho/\partial P_{HS} \right)_T = \frac{(1-\eta)^4}{1+4\eta+4\eta^2-4\eta^3+\eta^4},$$

$$q(\lambda) = 4.94876 + 0.097245\lambda - 12.9126\lambda^2 + 7.8632\lambda^3,$$

$$s(\lambda) = \frac{-49\lambda^5 - 49\lambda^4 + 293\lambda^3 + 5\lambda^2 - 211\lambda - 211}{6(\lambda^2 + \lambda + 1)}, \qquad t = e^\beta - 1,$$

$$g_{HS}(1; \eta_{eff}) = \frac{1 - \eta_{eff}/2}{(1 - \eta_{eff})^3}, \qquad w_3(\beta) = t - \beta - \frac{1}{2}\beta^2,$$

$$\eta_{eff} = c_1\eta + c_2\eta^2 + c_3\eta^3,$$

$$c_1 = 2.25855 - 1.50349\lambda + 0.249434\lambda^2,$$

$$c_2 = -0.669270 + 1.40049\lambda - 0.827739\lambda^2,$$

$$c_3 = 10.1576 - 15.0427\lambda + 5.30827\lambda^2 \quad .$$

A change of representation of the variables is needed to make easier the programming codes; for this reason, all the used thermodynamic variables and parameters were made reduced quantities, using the energy of the bulk and the diameter of the molecule (ϵ and σ), given by

$$\rho\sigma^3 = \rho^*, \quad \frac{r}{\sigma} = x, \quad \frac{kT}{\epsilon} = \frac{1}{\beta^*} = T^*, \quad \frac{P_{HS}\sigma^3}{\epsilon} = P_{HS}^*,$$

$$\tag{4.24}$$

$$\epsilon_{ads}^* = \frac{\epsilon_{ads}}{\epsilon}, \quad \epsilon_w^* = \frac{\epsilon_w}{\epsilon}, \quad \epsilon^* = \frac{\epsilon}{\epsilon} = 1 \quad .$$

An analogous treatment was made for the adsorbed fluid, using only the SAFT-VR approach; when the density of the bulk is low, it is possible to neglect the interaction of

adsorbed and bulk particles. And if λ_w is small the resulting adsorbed system will be confined to a shallow monolayer. In that case, it is well-known that the potential energy of the adsorbed system can be separated according to:

$$U(x, y, z) = \sum_{i<j} \sum_j \phi_{ji}(x, y) + \sum_i U_i^{pw}(z) \quad , \tag{4.25}$$

where x, y & z are cartesian coordinates, ϕ is the particle-particle interaction via square-well potential between molecule i and j and U_i^{pw} is the square-well interaction between the i_{th} particle and the wall, depending only of the distance orthogonal to the surface, z. This form allows a separation in the free energy with a two-dimensional term using the parameters for the adsorbed fluid (the attractive range, λ_{ads}, and the depth of the square-well, ϵ_{ads}) and a one dimensional potential with the parameters of the wall (the attractive range, λ_w, and the depth of the square-well, ϵ_w); this latter parameters can be interpreted as the mean amplitud and energy of vibration. Also, $\lambda_w < (2/3)^{1/2}$ to prevent the formation of a second layer within the wall's well. [23]

With this information, and a similar procedure as in the 3D case, the expression for the Helmholtz free energy of the adsorbed fluid is obtained:

$$a^{ads} = a_{ideal}^{ads} + a_{HD} + \beta a_1^{2D} + \beta^2 a_2^{2D} - \beta \epsilon_w - ln\,(\lambda_w) \quad , \tag{4.26}$$

with

$$a_{ideal}^{ads} = ln\,\gamma - ln\,4 - ln\,\pi + ln\,\Lambda^{*2} - 1, \quad a_{HD} = \frac{9}{8}\frac{\gamma}{1-\gamma} - \frac{7}{8}ln\,(1-\gamma),$$

$$a_1^{2D} = -2\gamma\epsilon_{ads}\left(\lambda_{ads}^2 - 1\right)g_{HD}\,(\sigma, \gamma_{eff}), \quad a_2^{2D} = \frac{1}{2}\epsilon_{ads}K_{HD}\gamma\frac{\partial a_1^{2D}}{\partial \gamma},$$

$$K_{HD} = \frac{(1-\gamma)^3}{1+\gamma+0.375\gamma^2-0.125\gamma^3} \quad , \qquad g_{HD}(\sigma) = \frac{1-7\gamma_{eff}/16}{(1-\gamma_{eff})^2} \quad ,$$

$$\gamma_{eff} = d_1\gamma + d_2\gamma^2 \quad ,$$

$$d_1 = 1.4215 - 0.405625\lambda_{ads} - 0.386981\lambda_{ads}^2 \quad ,$$

$$d_2 = 1.5582 - 1.89768\lambda_{ads} + 0.405215\lambda_{ads}^2.$$

γ is the two-dimensional packing fraction of the adsorbed fluid, a_{HD} is the Helmholtz free energy obtained from the Henderson equation [15], a_1 and a_2 are the perturbation terms and g^{HD} is the contact value of the hard-disks radial distribution function given in terms on an effective packing fraction, γ_{eff}, for a square-well fluid[10][19]. Again, it is possible to write the expression for the chemical potential of the adsorbed fluid including the second order perturbation terms for the free energy and the compressibility factor

$$\frac{\mu_{ads}}{kT} = a_{ideal}^{ads} + a_{HD} + \beta a_1^{2D} + \beta^2 a_2^{2D} - \beta \epsilon_w - ln\,(\lambda_w) + \Theta^{HD} + \beta \theta_1^{2D} + \beta^2 \theta_2^{2D} \quad , \tag{4.27}$$

where the hard disks compressibility factor is obtained, again, from the definition $\theta^{2D} = \gamma\frac{\partial a}{\partial \gamma}$, and using the expression for a_{HD}:

$$\Theta^{HD} = \frac{1+\gamma^2/8}{(1-\gamma)^2} \quad .$$

The dynamic equilibrium condition (Equation 4.29) for the adsorbed and bulk phases was applied to equations 4.17 and 4.27.

The dipolar contribution to the Helmholtz free energy of the SW bulk fluid can be added in the Equation 4.12 to test possible improvement of the results; using the following relation: [26]

$$a_D = \frac{1}{T^{*2}} \frac{a_2^D}{1 - \frac{a_3^D}{T^* a_2^D}} \quad , \tag{4.28}$$

With

$$a_2^D = \frac{-\rho^* \mu^{*4}}{6} I_6(\rho^*) \quad ,$$

$$a_3^D = \frac{\rho^{*2} \mu^{*6}}{54} I_{DDD}(\rho^*) \quad ,$$

$$I_6 = J_1 + J_2 \rho^* + J_3 \rho^{*2} + J_4 \rho^{*3} + J_5 \rho^{*4} + J_6 \rho^{*5} \quad ,$$

$$I_{DDD} = J_{D1} + J_{D2} \rho^* + J_{D3} \rho^{*2} + J_{D4} \rho^{*3} + J_{D5} \rho^{*4} + J_{D6} \rho^{*5} \quad ,$$

$$\mu^{*2} = \mu^2 \kappa_c / \epsilon \sigma^3 \quad ,$$

where the coefficients are given in Table 4.1.

J_1	J_2	J_3	J_4	J_5	J_6
4.1888	2.8287	0.8331	0.0317	0.0858	-0.0846
J_{D1}	J_{D2}	J_{D3}	J_{D4}	J_{D5}	J_{D6}
16.4493	19.8096	7.4085	-1.0792	-0.9901	-1.0249

Table 4.1: Values of coefficients used in the expression for I_6 and I_{DDD}. [26]

μ represents the electric dipolar moment of the substance (N_2O in this case) and κ_c is the Coulomb's constant, equal to 8.9874 x $10^9 N \cdot m^2/C^2$ [27]; ϵ and σ are the bulk parameters that need to be calculated for the square-well fluid in the SAFT-VR approach.

The general condition for dynamical equilibrium is: [23]

$$\mu_{bulk} = \mu_{ads} \quad , \tag{4.29}$$

where $\mu_{bulk} = \partial A^{3D}/\partial N_{bulk}$ and $\mu_{ads} = \partial A^{2D}/\partial N_{ads}$, where N_b and N_{ads} are the number of molecules of bulk and adsorbed phases, respectively and $N = N_{ads} + N_{bulk}$. In this work, in order to have an easier analitical treatment, it's enough with the expression of the chemical potential for a pure substance:

$$\mu_{bulk} = \frac{G^{3D}}{N} \quad , \quad \mu_{ads} = \frac{G^{ads}}{N}, \tag{4.30}$$

where G^{3D} is the Gibb's free energy of the bulk fluid. Using the definition of G^{3D} in terms of the Helmholtz free energy

$$G^{3D} = A^{3D} + PV \quad , \tag{4.31}$$

and the equilibrium of chemical potentials, results in the bulk pressure for the square-well fluid, p, at low values of n_{bulk} (the number of moles of the bulk) given by: [24]

$$p = \frac{RT\rho_{ads}}{\lambda_w \sigma} e^{[\Delta\mu_{2D} - N_0\epsilon_w]/RT} \quad , \tag{4.32}$$

where $\Delta\mu_{2D}$ is the difference of chemical potentials between the adsorbed fluid and an ideal gas at the same temperature and density, $\rho_{ads} = n_{ads}/S$ is the molar density of the adsorbed phase, considering a surface of area S and N_0 is the Avogadro's number.

The corresponding expression for the isosteric heat obtained from expression 3.61 using 4.32 is given by:

$$Q_{st} = N_0\epsilon_w + RT + RT^2 \frac{\partial}{\partial T} \left(\frac{\Delta\mu_{2D}}{RT} \right) \quad . \tag{4.33}$$

Then, for non-associating fluids, the first order-perturbation SAFT-VR-2D approach for $\Delta\mu_{2D}$ is given by [24]

$$\frac{\Delta\mu_{2D}}{RT} = \frac{25\gamma - 16\gamma^2}{8(1-\gamma)^2} - \frac{7}{8}ln\,(1-\gamma) - 2\alpha_{vdw}\rho_{ads}g_{HD}(\sigma, \gamma_{eff})\Phi(\gamma_{eff})/RT \quad , \tag{4.34}$$

where this comes from the pressure equation (since the free energies and compressibility factors of the bulk can be expressed in terms of $\Delta\mu_{2D}$ in the isosteric heat expression given by Trejos et al.[24] and solve for its value) α_{vdw} is the energy van der Waals constant given by

$$\alpha_{vdw} = \pi\epsilon_{ads}\sigma^2 \left(\lambda_{ads}^2 - 1 \right)/2 \quad . \tag{4.35}$$

γ is the 2D-packing fraction defined by $\gamma = N_0\rho_{ads}\pi\sigma^2/4$, $g_{HD}(\sigma, \gamma_{eff})$ is defined in Eq. 4.26 , and $\Phi(\gamma_{eff})$ is an auxilliary function dependent on g_{HD} and its first density derivative.
The corresponding expression for $\Phi(\gamma_{eff})$ is

$$\Phi = 1 + \frac{(25 - 7\gamma_{eff})(2\gamma_{eff} - d_1\gamma)}{2(1 - \gamma_{eff})(16 - 7\gamma_{eff})} \quad , \tag{4.36}$$

then, according to the previous theory, the SAFT-VR-2D expression for the isosteric heat is:

$$Q_{st} = N_0\epsilon_w + RT + 4\epsilon_{ads}\gamma(\lambda_{ads}^2 - 1)g_{HD}(\sigma, \gamma_{eff})\Phi(\gamma_{eff}) \quad . \tag{4.37}$$

The expressions for the augmented van der Waals equation of state can be obtained from Equation (4.34) assuming $g_{HD}(\sigma, \gamma_{eff}) = 1$, and consequently $\Phi(\gamma_{eff}) = 1$.

With this analysis, the equation for the isosteric heat of adsorption as a function of the adsorbed quantity, using the Langmuir model (Eq. 3.48) for the pressure, is given by:

$$Q_{st} = E - \frac{1}{2}RT + \Omega RT^2 \left(\frac{n_{sat}}{n_{sat} - n} \right) \quad , \tag{4.38}$$

where E represents the total energy of the system and Ω is a measure of the adsorbed phase thermal expansion coefficient defined by:

$$\Omega = -\frac{d\ln n_{sat}}{dT} = -\frac{1}{n_{sat}}\frac{dn_{sat}}{dT} \quad . \tag{4.39}$$

Equation 4.38 is obtained assuming that n_{sat} and b from the Langmuir theory are temperature dependent; then, the temperature dependence of the adsorption affinity is supposed to follow an Arrhenius expression: [34]

$$b = b_0 \exp\left(\frac{E}{RT}\right) \quad . \tag{4.40}$$

For the system studied in this work, the equation 3.63 can be written as:

$$\Gamma_{Gibbs} = \int_0^{\lambda_w \sigma} dz \rho(z) - \rho_b \lambda_w \sigma. \tag{4.41}$$

so, Equations 3.63 and 3.64 are related through the expression: [10] [23]

$$\Gamma_{Gibbs}\sigma^2 = \Gamma_{abs}\sigma^2 - 6\eta\lambda_w/\pi \tag{4.42}$$

where $\Gamma_{abs}\sigma^2 = 4\gamma/\pi$. So, again, this latter quantity represents the number of absolute adsorbed particles over the adsorbent area and is used to obtain the surface area along with the relation given in Eq. 3.66.

Chapter 5

Methodology

5.1 Adsorption isotherms in the Augmented van der Waals approach

With an introductory purpose, the augmented van der Waals equation of state was applied in a programming code using FORTRAN language to calculate the monomeric contribution of the chemical potential of the bulk fluid interacting via square well potential; this equation results setting g_{HS} equal to one in the expression for a_1 in Approach 2 from Eq. (4.21). Using this latter result with (4.16) in equation (4.17) taking just the first perturbation term in energy and compressibility factor, the potential for the bulk fluid in the augmented van der Waals aproach is:

$$\frac{\mu_{bulk}^{AVDW}}{kT} = a_{ideal}^{3D} + a_{HS} + \beta^* a_1^{3D} + \frac{1 + \eta + \eta^2 - \eta^3}{(1 - \eta)^3} + \beta\theta_1 \quad , \tag{5.1}$$

with

$$a_1^{3D} = \theta_1 = -4\eta(\lambda^3 - 1) \quad .$$

The same procedure was applied to express the chemical potential of the adsorbed fluid, using Eq. (4.27),

$$\frac{\mu_{ads}^{AVDW}}{kT} = a_{ideal}^{ads} + a_{HD} + \beta^* a_1^{2D} - \beta^* \epsilon_w^* - ln(\lambda_w) + \Theta_{HD} + \beta^* \theta_1^{2D} \quad , \tag{5.2}$$

and setting g_{HD} equal to one:

$$a_1^{2D} = \theta_1^{2D} = -2\gamma(\lambda_{ads}^2 - 1) \quad .$$

The condition of dynamical equilibrium [Eq. (4.29)] was applied and it allowed to give a first approximation of the equilibrium values for the bulk (η) and adsorbed (γ) packing fractions to plot the corresponding adsorption isotherms.

The program consist of two loops; one is for setting the variable η, from 0 to 0.5 with increments of 0.0001, and the other is for setting γ, between an interval from 0 to 0.8 with increments of 0.0001, until the equilibrium condition is reached when the difference

of chemical potentials in adsorbed and bulk phases is less than a chosen tolerance (10^{-4}); values for the other parameters ($\lambda, \lambda_{ads}, \lambda_w, \epsilon_{ads}, \epsilon_w, T$) were fixed according to Trejos et al. (2014) [24] to compare the obtained results.

5.2 Adsorption isotherms for a SW fluid in SAFT-VR

To evaluate the difference in the adsorption isotherms in SAFT-VR approach with and without the residual contribution (a_{res}), a new program was elaborated to calculate equilibrium values for η and γ; this time, the perturbation terms were added to the previous code using the second approach for the free energy (Equations 4.21 to 4.23). The results were plotted and compared in order to observe the effect of the residual term and how its incorporation affects the results obtained.

5.3 Bulk's critical parameters for a SW fluid in the Augmented van der Waals approach

After the adsorption isotherms, the dependence of critical thermodynamic variables of the bulk SW fluid with λ was evaluated using the vapor-liquid equilibrium information on the AVDW equation of state for the pressure (See Equation 5.1). The conditions that must be satisfied in the critical point in a P-V diagram for a pure substance are:

$$\left(\frac{\partial P}{\partial V}\right)_{T,N} = 0, \quad \left(\frac{\partial^2 P}{\partial V^2}\right)_{T,N} = 0 \quad . \tag{5.3}$$

These conditions where evaluated using reduced variables (Eq. 4.24) to change the representation to

$$\left(\frac{\partial P^*}{\partial \eta}\right)_{T} = 0, \quad \left(\frac{\partial^2 P^*}{\partial \eta^2}\right)_{T} = 0 \quad , \tag{5.4}$$

in order to evaluate them for each λ.

This procedure was followed, as matter of practice, using a simple equation state (van der Waals) for the obtention of the critical points as a function of lambda, in order to implement the same idea in the determination of bulk and adsorbed parameters for N_2O in the SAFT-VR approach.

The program was made with three "Do" loops, each one to set values with increments of 1×10^{-3} for the variables lambda (λ), from 1.1 to 2.0, reduced temperature (T^*), from 0.001 to 3.7, and reduced density (ρ^*), from 0.2 to 0.6, to evaluate the derivatives until the two previous conditions (Eq. 5.4) are reached for a given tolerance and then these values were saved in a text file. The condition is satisfied when the error propagation of the derivatives is less than a fixed tolerance, so many points for each lambda were generated; the expression of error propagation (τ) is given by:[44]

$$\tau = \sqrt{\left(\frac{\partial p^*}{\partial \eta}\right)^2 + \left(\frac{\partial^2 p^*}{\partial \eta^2}\right)^2} \quad . \tag{5.5}$$

This task was relatively simple, because the critical point could be chosen easily for each critical parameter at a given lambda; the analytic expressions for the pressure in AVDW and its derivatives allow not many points to be generated for each lambda and also cover the whole range in lambda (1.1 to 2.0). Nevertheless, more complex equations of state were implemented in the Boublik's and SAFT-VR theories so the discrimination of critical point implies more computing time due to the abscence of analytic expressions for the derivatives of the pressure. In this sense, if the tolerance was made smaller, less points were generated for each lambda; but there were points not taking into account over the hole range (1.1 to 2.0); then the tolerance had to be determined by proof and error to obtain enough points to cover the hole range, but also to optimize the computing time. Then, another program had to be made to discriminate only one critical point for each lambda so continous curves could be generated for each thermodynamic variable $(\Theta, T^*, p^*$ and $\rho*)$.

The same ideas were implemented in further codes to obtain critical parameters in the next sections.

5.4 Bulk's critical parameters using the Boublik's theory

The same ideas as in the previous section were applied, this time using the Boublik's equation of state for the compressibility factor (Eq. 4.16) derived by the first approach for the Helmholtz's free energy perturbation terms (Eqs. 4.18 to 4.20).

In this case, the program was made with the same three loops as in van der Waals along with the same increment of 0.001, this time for the variables lambda (from 1.1 to 2.0), reduced temperature (from 0.1 to 4.0) and reduced density (from 0.2 to 0.7); these intervals for this and SAFT-VR loops were stablished using reference [13].

Analytical expressions for the derivatives were not available, so a numerical method to approximate both was implemented. This method is given by the five points method for equally spaced abscissas: [51]

$$
\begin{aligned}
f'_p = f'\left(x_0 + ph\right) = \quad & \frac{1}{h}\Big\{\frac{2p^3-3p^2-p+1}{12}f_{-2} \\
& -\frac{4p^3-3p^2-8p+4}{6}f_{-1} \quad + \quad \frac{2p^3-5p}{2}f_0 \\
& -\frac{4p^3+3p^2-8p-4}{6}f_1 \quad + \quad \frac{2p^3+3p^2-p-1}{12}f_2\Big\} + R'_4 \quad ,
\end{aligned}
\tag{5.6}
$$

where the function f represents the pressure given and x states for the density, x_0 is the point of interest to evaluate the derivative, h is the iteration value around x_0, p is a positive or negative integer number and R'_4 represents the residual terms in p; the notation f'_n indicate the evaluation of the function at $x = x_0 + nh$, like $f'_{-2} = f'(x_0 - 2h)$. For this work, the derivative was evaluated at each iteration of density, that means setting $p = 0$ in Eq. 5.6.

The other approximation is for the second derivative:[51]

$$\frac{\partial^2 f_{0,0}}{\partial x^2} = \frac{1}{12h^2}\{-f_{2,0} + 16f_{1,0} - 30f_{0,0} + 16f_{-1,0} - f_{-2,0}\} + O(h^2), \quad (5.7)$$

where the notation remains equal as that for the first derivative; $f_{2,0} = f(x_0 + 2h)$, etc.

As stated in the previous section, the best tolerance to generate enough points for all the range in lambda was 3×10^{-1} for this case and h was set equal to 5×10^{-5}. Once again, the programming code for the discrimination of the critical point in the previous section was applied to generate the points for all the thermodynamic variables for each lambda over the range $1.1 \leq \lambda \leq 2.0$.

5.5   Bulk's critical parameters using the SAFT-VR approach

Exactly the same idea of the previous section was used but using now the SAFT-VR equation of state (Eq. 4.16) by means of Eqs. 4.21 to 4.23. The increments were 0.001 in the three loops, now for lambda (from 1.1 to 2.0), reduced temperature (from 0.6 to 3.0) and reduced density (from 0.2 to 1.0), and setting the tolerance for discrimination points equal to 3×10^{-1} and for the derivatives (Eqs. 5.6 and 5.7) $h = 5\times10^{-5}$ (same as Boublik).

This time, once the data was collected for each variable, the polinomials of approximation were estimated; this allows to have each variable as an explicit function in lambda. With this and using the relations for reduced variables from Eq. 4.24, related to the density, temperature and pressure it is possible to obtain σ and ϵ/k and λ using the critical parameters for N_2O [53].

Following the same procedure for the adsorbed fluid using the equation of state obtained from Eq. 4.26, λ_{ads} can be also determined by means of the critical temperature dependence with lambda of the adsorbed fluid ($\epsilon_{ads} = 0.8\epsilon$ according to the previous chapter).

Now, there are two more molecular parameters to be estimated for the SAFT-VR model, ϵ_w and λ_w . This parameters can be adjusted to reproduce the experimental adsorption isotherms and be compared with the isosteric heat of adsorption at low bulk densities, described in the next section.

5.6   Isosteric heats of adsorption of N_2O in biochar and adsorption Isotherms

In order to apply the SAFT-VR approach to the N_2O sorption on biochar, it was necessary to look widely for information on the internet related to previous research and experiments; one article from Cornelissen et al. [11], reported experimental results with adsorption isotherms of N_2O at six different temperatures and in four types of biochar,

each one named according to its superficial area estimated from the BET model. Also, in this reference, the Langmuir equation was used to make the data interpretation for the estimation of the maximum sorption capacity of the monolayer and the affinity constants, as well as the isosteric enthalpy of sorption.

The first idea was the use of the software xyscan[12] to capture the reported results in Cornelissen et al. directly from the plots in the paper and save them in a text file, to reproduce the adsorption isotherms for each type of biochar; nevertheless, this was not very acurate so at the end the complementary material, given in the same reference, were reported the exact values of the experimental points to reproduce the adsorption isotherms. With the purpose of testing the range of application of the SAFT-VR model applied to adsorption of N_2O on biochar, a comparison between predictions made from this model and the experimental points was needed.

The equation 4.32 is the one used to generate the adsorption isotherms in the SAFT-VR approach with the equilibrium values for η and γ, and Eq. 3.48 is the one to compare with the adsorption isotherms in the Langmuir model, by using the relations given in the previous chapter relative to the development of the model; nevertheless, to make this, it was necessary to work with the isosteric heat expressions, first with Langmuir and the equate with SAFT-VR at low densities of the bulk ,to estimate the ϵ_w and then find the best value for λ_w to reproduce the experimental data.

So, the first treatment was for the isosteric heat expression at Equation 4.38, where both parameters (E and Ω) were adjusted to reproduce the values of the affinity constants as a function of temperature reported in Cornelissen et al. [11]. The values used for these variables for BC-60 were E $= 18.0$ kJ mol^{-1} and $\Omega = 0.00961$ K^{-1}. Also, the values of b from Eq. 4.40 at the different reported temperatures were obtained using $b_0 = 0.00392$ atm^{-1}, and are presented in Table 5.1.

Temperature ($°C$)	n_{sat} $(cm^3 g^{-1})$	b (atm^{-1})
-10	44.79	8.91
0	40.20	7.09
10	36.56	5.68
20	33.31	4.28
30	30.29	3.37
40	27.59	2.58

Table 5.1: Langmuir parameters for adsorption of N_2O on BC-60 at different temperatures [11]

With this, ϵ_w can be estimated and now the only left parameter, λ_w, can be adjusted to generate the required adsorption isotherms.

To proceed, the surface area for use in Equation 3.66, was fitted using the experimental points reported at Cornelissen et al. and reproduced according to the expression:

$$S = S_0 e^{-\omega(T-23.15)}, \tag{5.8}$$

where S_0 corresponds to the surface area at T = 263.15 K, and ω is a constant for all the isotherms. Equation 5.8 is similar to Equation 4.39, that describes the temperature dependence of the saturation capacity in the Langmuir model.

After the necessary conversions between units required in SAFT-VR from the corresponding data given in Cornelissen et al. [11], the isotherms could be generated and compared with Langmuir and experimental results.

It is important to remark that the dipolar contribution was not included, to make first tests of the obtained molecular parameters for N_2O; its incorporation must take into account the dipolar moment of N_2O, using μ equal to $0.167D$, but it is to small for example compared with the water molecule ($1.8546D$) (D stands for Debye). [52].

Chapter 6

Results

6.1 Adsorption isotherms in the Augmented van der Waals approach

Several curves were obtained for this case, each one corresponding to a fixed value of the reduced well's depth of the wall (ϵ_w^*). Figure 6.1 shows the detailed results of the adsorption isotherms in the augmented van der Waals approach, compared with those obtained with SAFT-VR without the residual term; it is possible to observe that for higher values of pressure (or bulk density η) and wall's energy (ϵ_w^*), the quantity of adsorbed fluid is also higher.
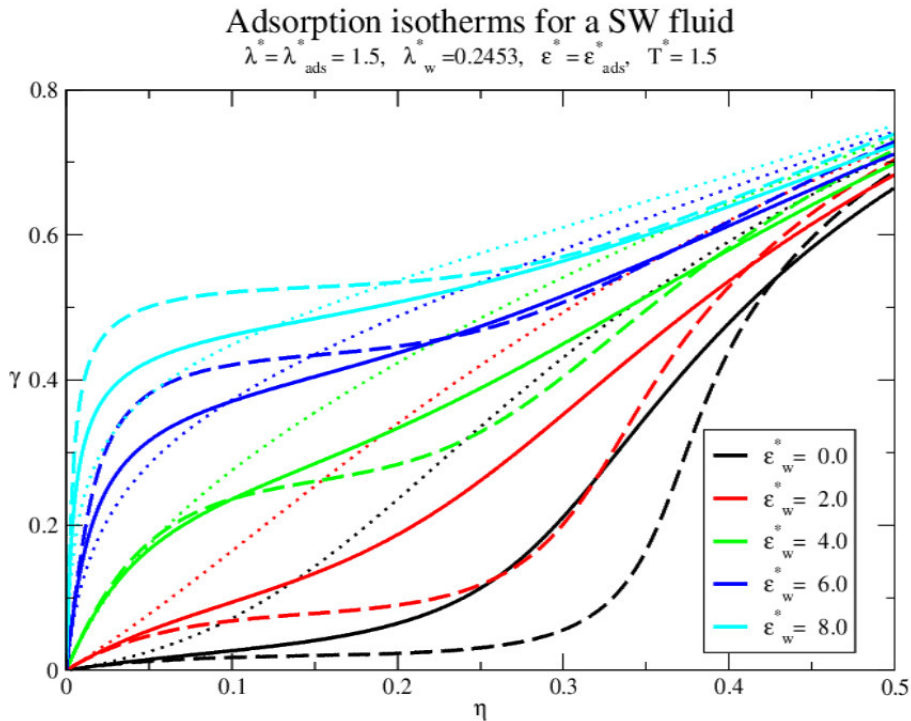
Figure 6.1: *Adsorption isotherms for a monomeric square well fluid obtained with the first program; variables are reduced quantities. Solid and dashed lines correspond to the AVDW and SAFT-VR[13] [10][19] approaches, respectively. The dotted lines represent the HS behavior.*

From Fig. 6.1 and Equations 5.2 and 5.1, one can infer that the attractive contribution (a_1) for both phases plays an important role to control the adsorption rate with respect to a hard sphere fluid (with only repulsive terms); this can be understood when the interactions between particles in the bulk are stronger than those with the wall (for small values of ϵ_w); nevertheless for high values of ϵ_w^*, the rate of adsorption is increased because the interactions with the wall become stronger than those between molecules in the bulk.

6.2 Adsorption isotherms for a SW fluid in SAFT-VR

The results of adsorption isotherms of the SW fluid in SAFT-VR with and without the residual contribution are compared in Fig. 6.2; the difference is practically negligible, so the residual term does not play a determinant role in adsorption, except near the critical point.
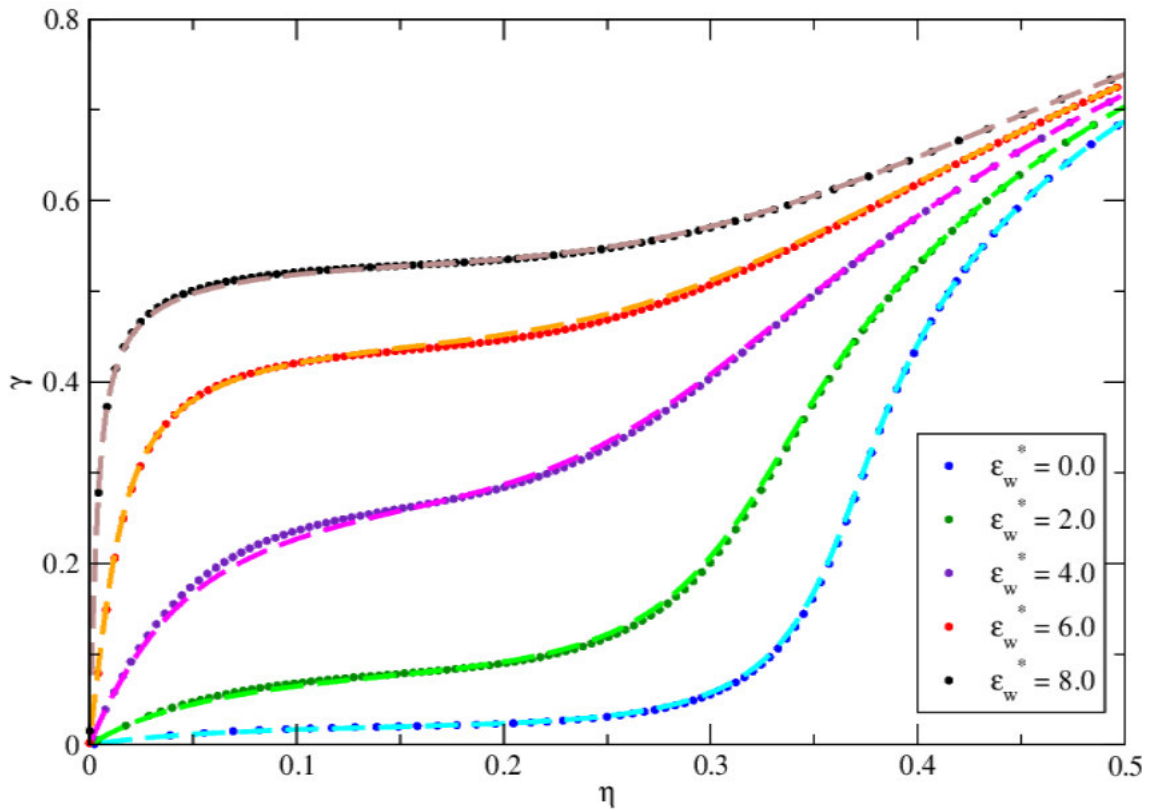

Figure 6.2: Comparisson of SAFT-VR expressions. Dotted lines are the equilibrium values without using the residual term in Helmholtz free energy and dashed lines contain the residual contribution. The parameters are the same as in Figure 6.1

6.3 Bulk's critical parameters using the SAFT-VR approach

In this section are summarized the results from the AVDW and Boublik theories, and are compared graphically with those of SAFT-VR.

The modification of the perturbation terms a_1 and a_2 in this theory, causes variations in the critical parameters; there is a decrement in the critical pressure, density, temperature and compressibility factor. This can be understood because of the strong temperature dependence of a_2 in the Boublik's theory, whereas in SAFT-VR a_2 is temperature independent, so a2 is bigger in the approach of Boublik, changing the compressibility factor and pressure and consequently the other parameters.

If just in this case, as a matter of illustration, is considered the dipolar contribution for adsorption of nitrous oxide in biochar, this causes a reduction of critical density and temperature; this can be interpreted assuming that the fluid interactions become stronger when the fluid is polar. Therefore a non-polar fluid is less sensible to changes and reaches the saturation point at higher values of temperature and density. This reduction is not big for critical density and temperature but it is considerable in the pressure and compressibility factor (Figures 6.7 to 6.10).
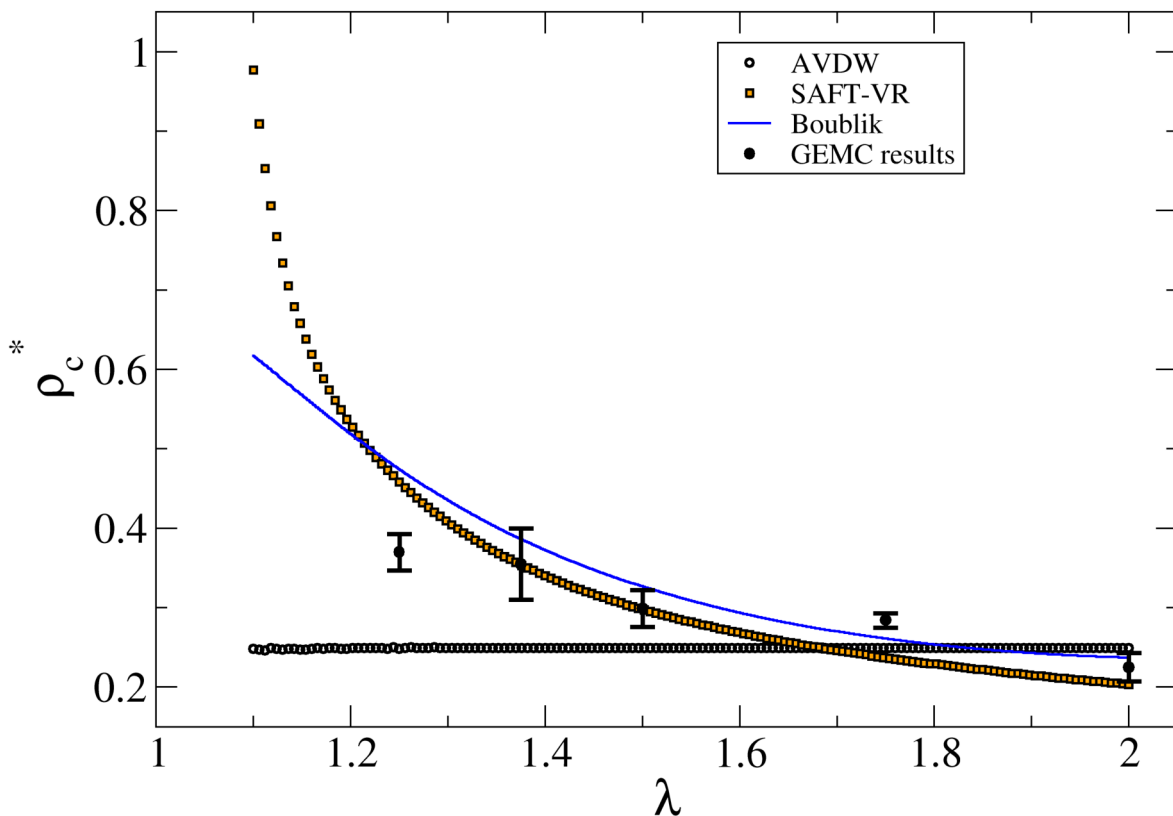

Figure 6.3: Comparison between critical reduced densities obtained from AVDW, Boublik and SAFT-VR theories; points from Gibbs Ensamble Monte Carlo simulation of *Vega et al.* [47] are given.
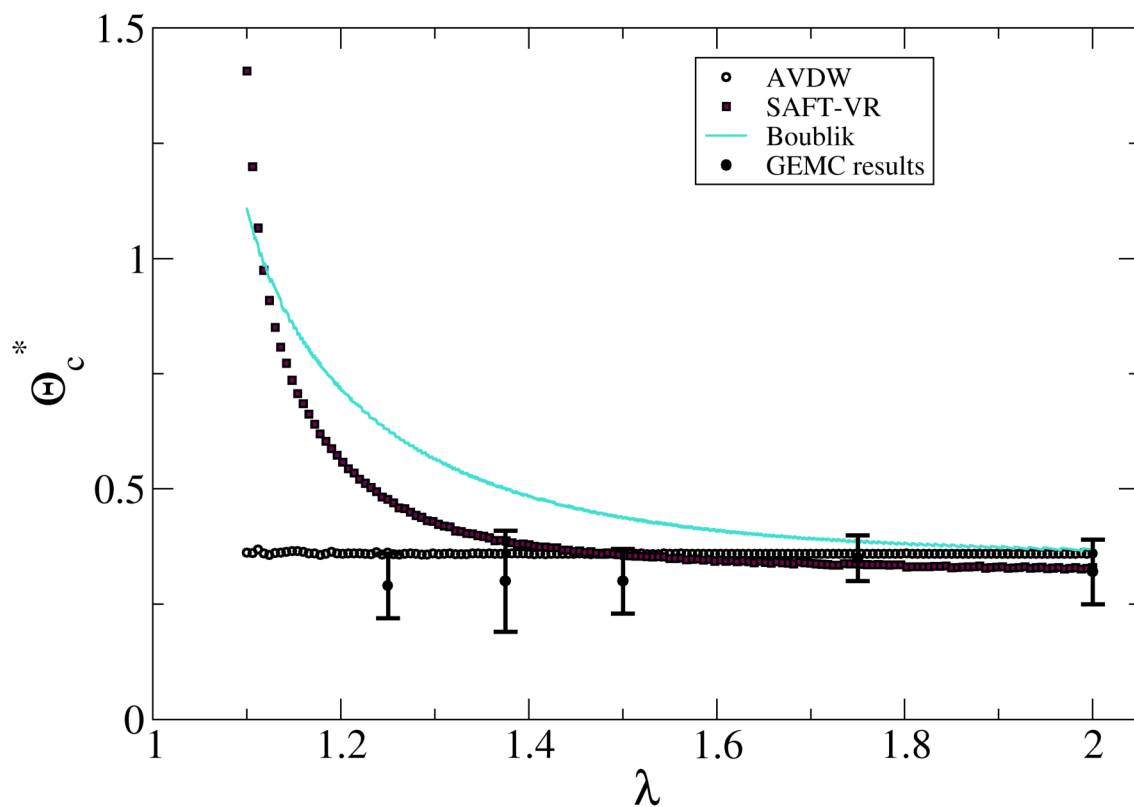
Figure 6.4: Same specifications as in Figure 6.3 for compressibility factor.
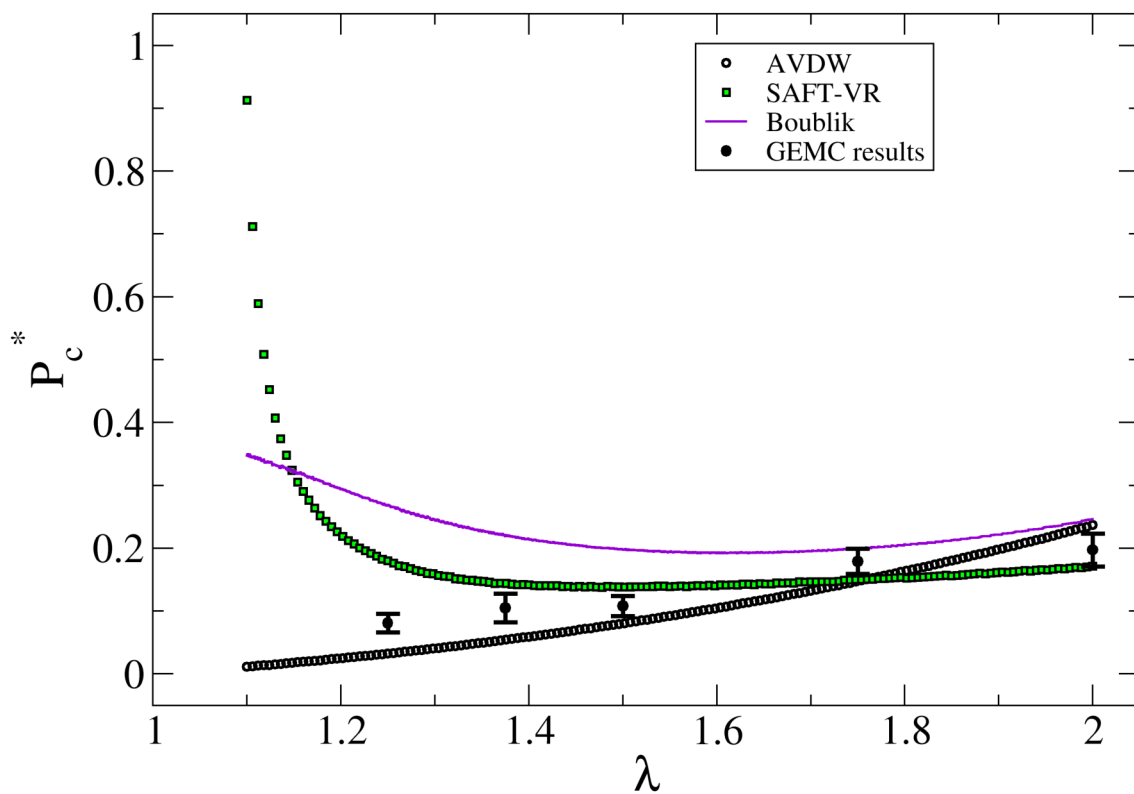

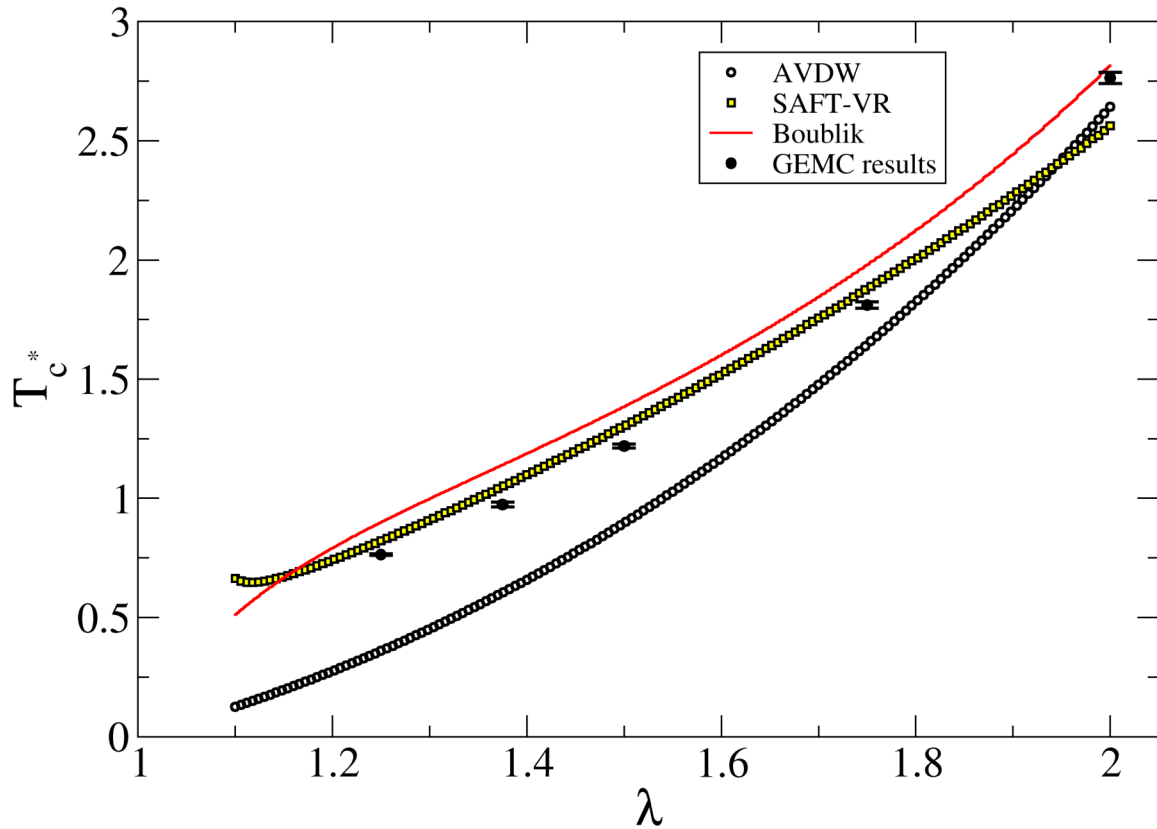Figure 6.5: Same specifications as in Figure 6.3 for reduced pressures.

Figure 6.6: Same specifications as in Figure 6.3 for reduced temperatures.

From the previous plots, can be seen that, in the results for AVDW, the critical density has an approximate value of 0.25 for all lambda, whereas the critical compressibility factor is approximately 0.36. These latter quantities compare well with previous results by Gil-Villegas and del Río[13]. Also, can be seen the beginning of convergence of both SAFT-VR and Boublik with that of AVDW near $\lambda = 2$; it is necessar to remind that AVDW is exact for $\lambda > 3$, but the range used here is $1.1 \leq \lambda < 2$, so several differences should be found. Some points from simulation results are given to make a more objective comparisson.
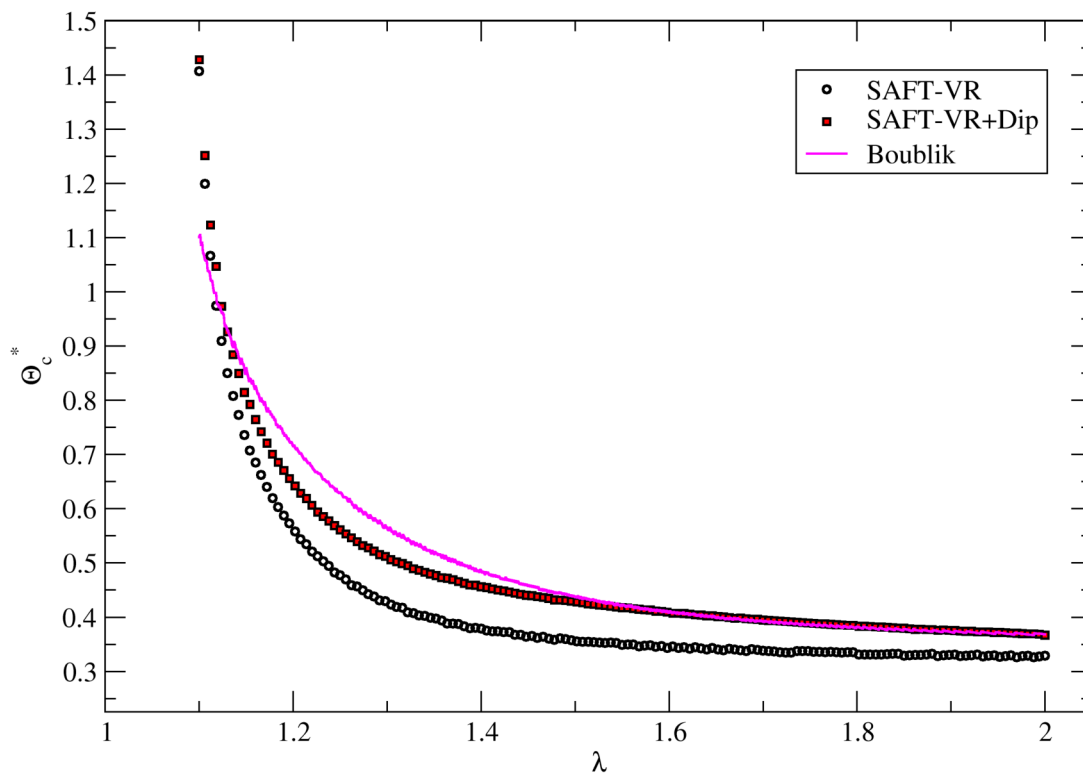
Figure 6.7: Comparison between critical reduced compressibility factors obtained from AVDW, Boublik and SAFT-VR theories
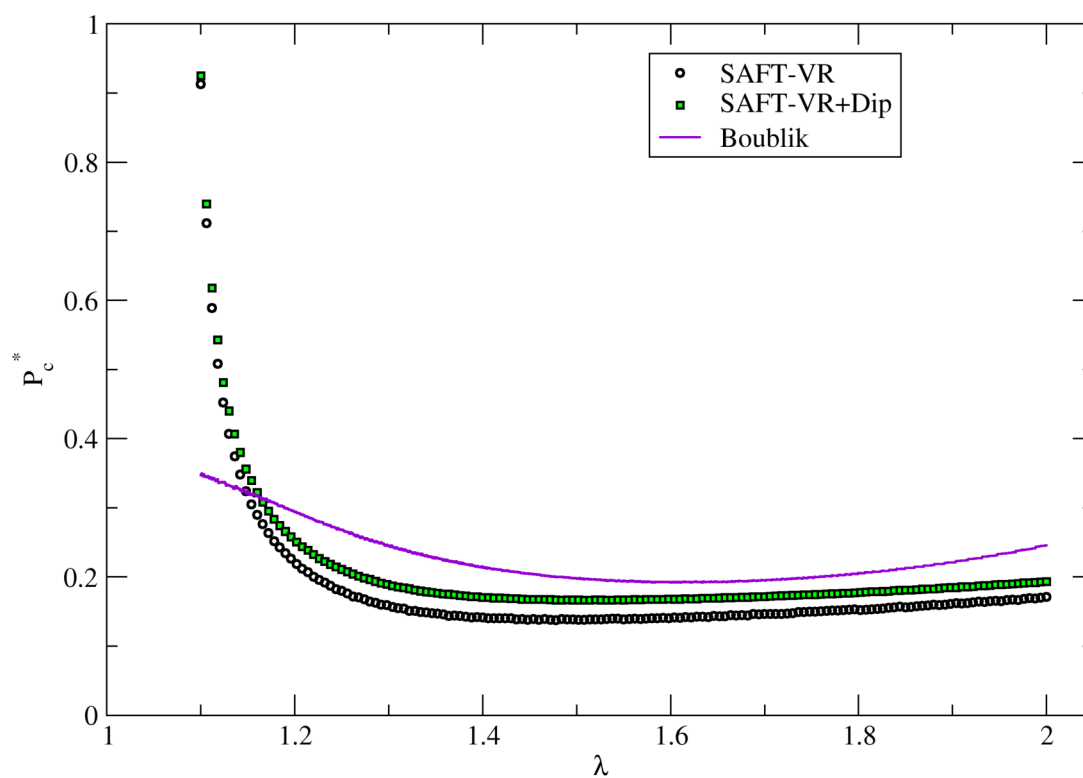

Figure 6.8: Comparison between critical reduced pressures obtained from AVDW, Boublik and SAFT-VR theories
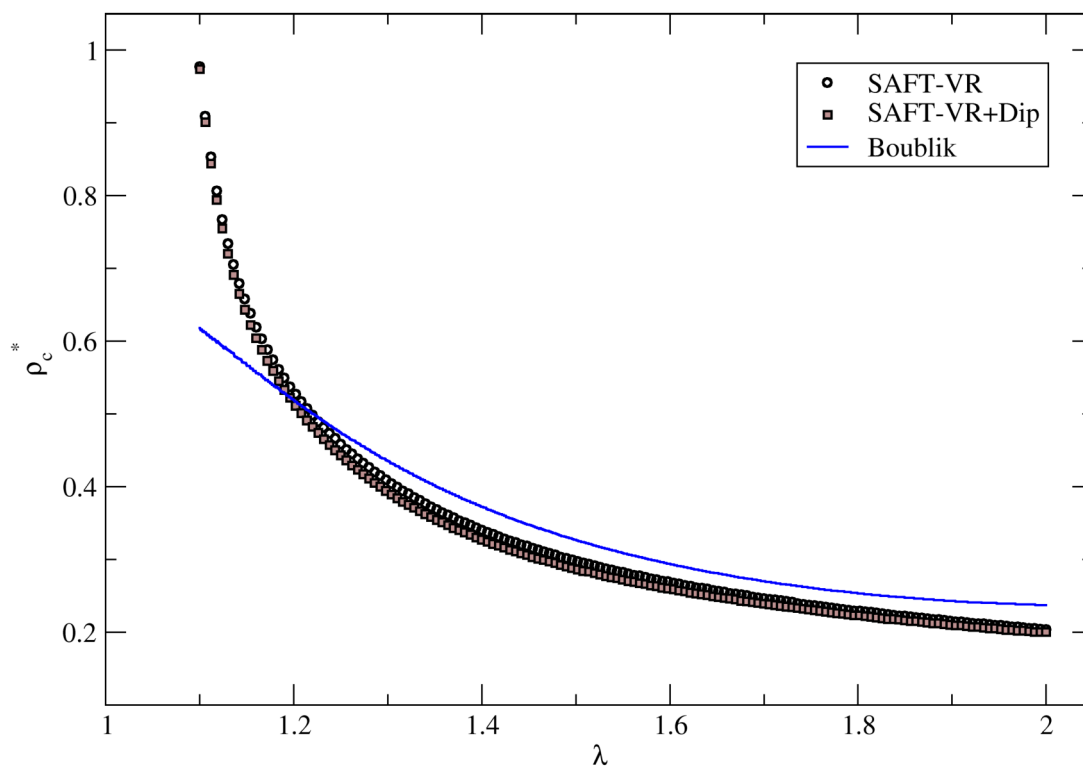
Figure 6.9: Comparison between critical reduced densities obtained from AVDW, Boublik and SAFT-VR theories
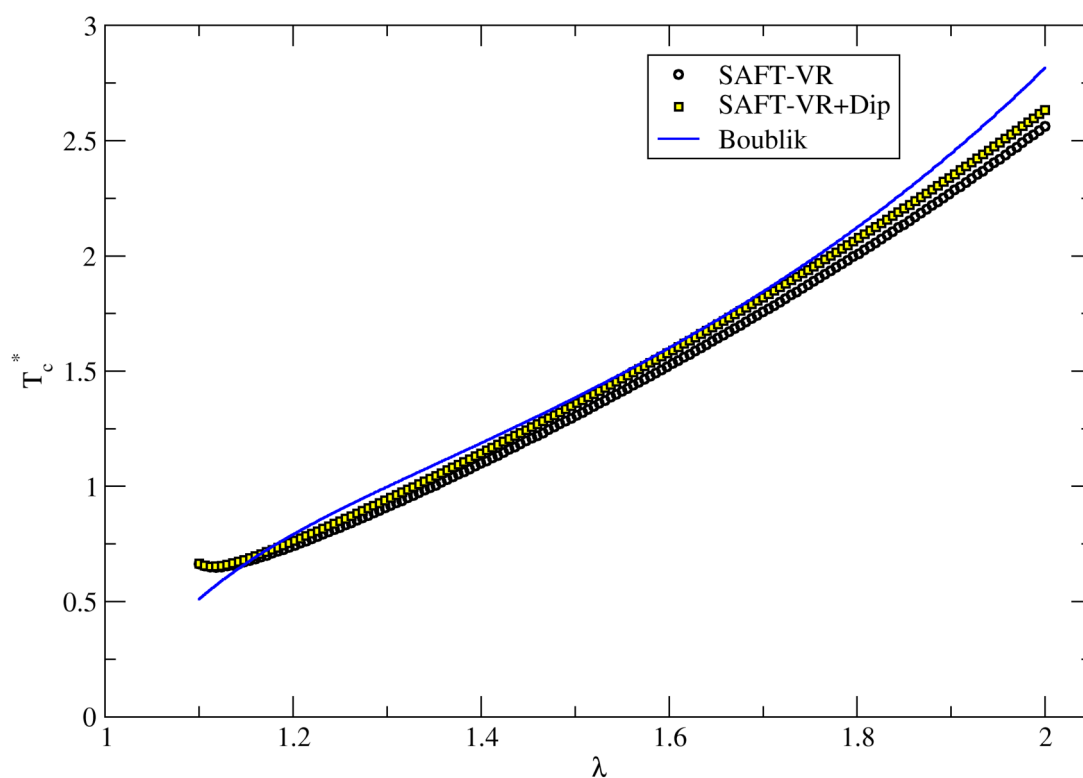

Figure 6.10: Comparison between critical reduced temperatures obtained from AVDW, Boublik and SAFT-VR theories

The dipolar contribution to the free energy does not impact too much the critical density and temperature of the system (the main variables), so deviations are expected to be small with only up to the residual terms. Its inclusion can be incorporated, but it will be seen that even without it, the results adjust very well to the experiments.
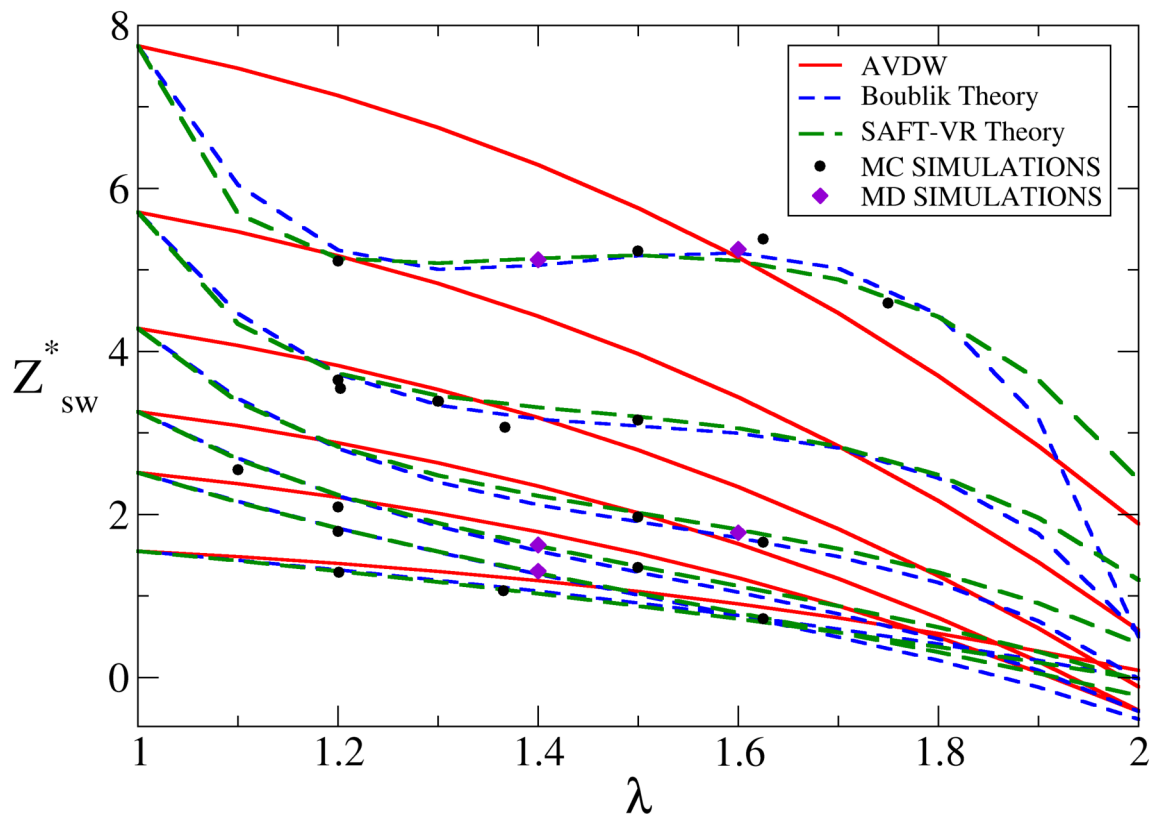

Figure 6.11: *SW Critical Compressibility factor for the bulk fluid as a function of lambda for $T^* = 2.0$; augmented van der Waals (red line), Boublik (blue line) and SAFT-VR (green line) curves are reported. Symbols represent the experimental data from references [28] to [33].*

Figure 6.11 shows multiple values for the compressibility factor of the Square-Well fluid at a reduced temperature of 2.0 and six values of reduced density (0.2, 0.4, 0.5, 0.6, 0.7 and 0.8). This graphic allows a direct comparison of the values of Θ in the Boublik, SAFT and augmented van der Waals approximations; we can see that the adjustment is better for Boublik, but this is because this theory is precisely adjusted in base to this simulation results, so SAFT-VR agrees very well as a predicitive tool.

6.4 Isosteric heats of adsorption of N_2O in biochar and adsorption Isotherms

In the Table 6.1 the resulting parameters used to describe the bulk and adsorbed fluids for N_2O are reported, along with those related to the surface area from Eq. 5.8. The validity of the bulk parameters σ and ϵ/k estimated for nitrous oxide are in the range of values reported by other authors[35]; they found $\sigma = 3.360 \mathring{A}$ and $\epsilon/k = 171K$, so the dipolar contribution does not play a significant role at this stage.

Parameter	Value
λ	1.769
σ /Å	3.3551
(ϵ/k) /K	161.0137
λ_{ads}	1.637
σ_{ads}	3.3551
$(\epsilon_{ads}/k)/K$	128.8111
λ_w	0.4
$(\epsilon_w/k)/K$	15.5464
$S_0/(m^2 \ g^{-1})$	170.72
$\omega/(K^{-1})$	0.00487

Table 6.1: Critical parameters for N_2O obtained with SAFT-VR developed in the previous section of methodology

With the previous information, the results for adsorption isotherms and isosteric heats of adsorption for nitrous oxide (N_2O) on biochar for SAFT-VR and Langmuir models are given in Figures 6.12 and 6.13 with the experimental values; it is possible to say that the SAFT-VR approximation was good enough, but not better than that obtained with Langmuir's approach. This is because the Langmuir model needs 12 parameters, whereas SAFT-VR only uses 3 parameters related to the properties of the bulk fluid and 7 related to the adsorption isotherms (just one of them being free that is λ_w); obviously, a better fit includes more parameters to the analysis, but the important thing to remark is that the results are very good approximated by SAFT-VR, regardless the concept of sites of adsorption concept used in Langmuir model, given a more precise connection with the molecular parameters and variables involved, even to make predictions of isosteric heats.
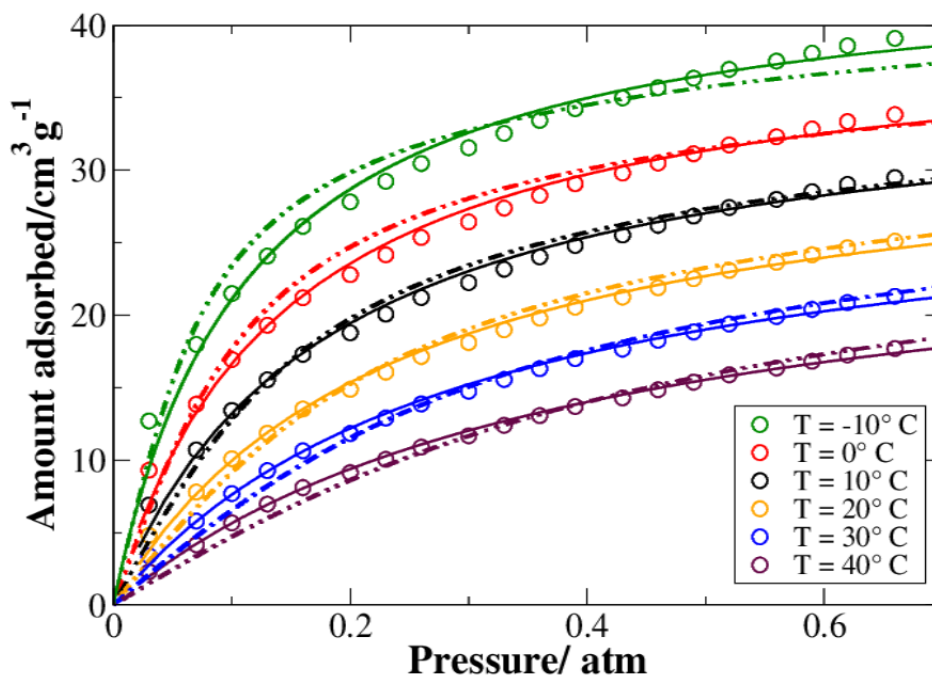
Figure 6.12: *Adsorption isotherms for N_2O on BC-60 for several temperatures; the continous line is the Langmuir model, dotted line is the SAFT-VR model and circles are the experimental data from Cornelissen et al.*
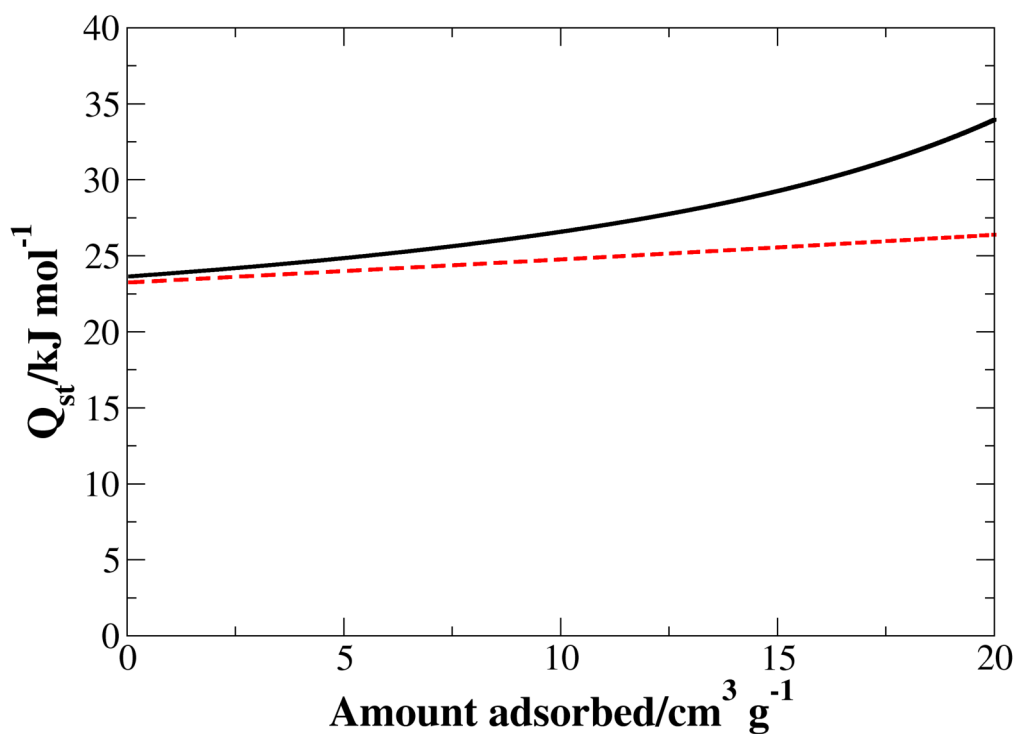

Figure 6.13: *Isosteric heat of adsorption as a function of quantity adorbed; continous line is the Langmuir model and dashed is the SAFT-VR equation. The values were obtained with $E = 18.0$ kJ/mol and $\Omega = 0.00961K^{-1}$*

Chapter 7

Conclusions and perspectives

One of the aims achieved in this work was to prove the effectiveness of SAFT-VR theory when describing and modeling real substances in practical cases of adsorption. Derived from this results, many data can be obtained to model adsorption isotherms for other real substances, like carbon dioxide. The results for nitrous oxide were compared with those derived from other theories (soft-SAFT)[35], showing good agreement even without the use of dipolar contribution.

The obtention of adsorption isotherms of substances in a determined material is not a trivial problem. There are many ways to model this process and it depends on each researcher the choice of one of them, depending on the purposes and objectives of the work. Experimental data are needed to compare the results from simulations and theory. To achieve better results from the theory, new and more complex models are required but this can imply the use of more parameters.

As a first exercise for the first contact and understanding of the model, simple equations of state were implemented (Augmented van der Waals) to obtain properties of the SW bulk and adsorbed fluids; then, the complexity of the equation was growing until reaching the SAFT-VR equations. Possible improvements in this area are the refinement of numerical methods to obtain the critical points faster and with very good precision.

It is expected to include more terms of interaction to the model, to improve it; the first is the dipolar contribution of N_2O, which at this level doesn't play a significant role because its small dipolar moment compared with that of the water, for example at normal temperature and pressure; the associating capacity of the molecules to form chains and chemical interactions (like the hydrogen bond) are the other possible contributions, but neglected in this work. Several new techniques and numerical methods can be included to improve even more the model, and the use of the dual site Langmuir model [37] with the SAFT-VR approach has been proposed to be a good choice to achieve even a better fit of the experimental results.

The results for isosteric heats need to become more precise, so that the plots for Langmuir and SAFT-VR theories have a bigger range of coincidence keeping or improving the corresponding adsorption curves. This can be done in future research during my masters level.

Bibliography

[1] W. Chapman, K. Gubbins, G. Jackson, M. Radosz, Fluid Phase Equil. **52**, 31 (1989).

[2] T. J. Boublík, J. Chem. Phys. **53**, 471 (1970).

[3] "What Is Nitrous Oxide?" Nitrous Oxide FAQ. N.p., n.d. Web. 23 Jan. 2017.
   URL : `http://justsayn2o.com/apple-touch-icon.png`

[4] Index of /wp-content/uploads/2016/11/. N.p., n.d. Web. 15 Feb. 2017.
   URL: `www.arangaktif.com/wp-content/uploads/2016/11/Activated-Carbon-Aplication.jpg`

[5] Roop Chand, Bansal and Goyal Meenakshi. *Activated Carbon Adsorption.* 6000 Broken Sound Parkway NW, Suite 300 Boca Raton, FL 33487-2742: Taylor & Francis Group, 2005, 1-6 & 78-120.

[6] "What Is Biochar?" International Biochar Initiative. N.p., n.d. Web. 15 Nov. 2016.
   URL : `www.biochar-international.org/biochar/faqs`

[7] D. A. McQuarrie. *Statistical Mechanics.* New York, N.Y., Harper & Row, Publishers, Inc., 1976, 254-306.

[8] "Radial distribution function." Wikipedia.
   URL : `https://en.wikipedia.org/wiki/Radial_distribution_function`

[9] N.F. Carnahan and K.E. Starling, J. Chem. Phys. **51**, 635 (1969).

[10] A. Martínez, M. Castro, C. McCabe, and A. Gil-Villegas, J. Chem. Phys. **126**, 074707 (2007).

[11] G. Cornelissen, D.W. Rutherford, H.P.H. Arp, P. Dörsch, C.N. Kelly, and C.E. Rostad, Environ. Sci. Technol. **47**, 7704 (2013).

[12] Xyscan Distribution Page.
   URL :`rhig.physics.yale.edu/ ullrich/software/xyscan/`

[13] A. Gil-Villegas and F. del Río, Rev. Mex. Fís. **39**, 526 (1993).

[14] Atkins, P.W. Physical Chemistry 6 th edition. San Francisco: W. H. Freeman and Company, 1998.

[15] D. Henderson, Mol. Phys. **30**, 971 (1975).

[16] T. Boublík, Mol. Phys. **59**, 775 (1986).

[17] A.L. Benavides and F. del Río, Molec. Phys. **68**, 983 (1989).

[18] A. Gil-Villegas, A. Galindo, P.J. Whitehead, S.J. Mills, G. Jackson, and A.N. Burgess, J. Chem. Phys. **106**, 4168 (1997).

[19] G. Jiménez, S. Santillán, C. Avendaño, M. Castro, and A. Gil-Villegas, Oil Gas Sci. Technol. **63**, 329 (2008).

[20] T. L. Hill, J. Chem. Phys. **17**, 520 (1949).

[21] A. L. Myers, AIChE J. **48(1)**, 145-160 (2002).

[22] W. D. Machin and S. Ross, Proc. R. Soc. Lond. A **265 (1323)**, 455-462 (1962).

[23] F. del Río and A. Gil-Villegas, J. Chem. Phys. **95**, 787 (1991).

[24] V. M. Trejos, S. Figueroa-Gerstenmaier, and A. Gil-Villegas, Mol. Phys. **112 (17)**, 2330-2338 (2014).

[25] O. Sinanoglu and K. S. Pitzer, J. Chem. Phys. **32**, 1279 (1960).

[26] A.L. Benavides, Y. Guevara, and F. del Río, Physica A **202**, 420 (1994).

[27] Base unit definitions: Ampere. N.p., n.d. Web. 04 Aug. 2017.
     URL : https://physics.nist.gov/cuu/Units/ampere.html

[28] D. Henderson, W.G. Madden, and D.D. Fitts, J. Chem. Phys. **64**, 5026 (1976).

[29] Y. Rosenfeld, and R. Thieberger, J. Chem. Phys. **63**, 1875 (1975).

[30] D.A. de Lonngi, P.A. Lonngi and J. Alejandre, Malee. Phys. **71**, 427 (1990).

[31] A. Gil-Villegas, C. Vega, F. del Río, and A. Malijevsky, Mol. Phys. **86**, 857 (1995).

[32] Y. Tang and B. C.-Y. Lu, J. Chem. Phys. **100**, 6665 (1994).

[33] D.M. Heyes and P.J. Aston, J. Chem. Phys. **97**, 5738 (1992).

[34] A.L. Myers, AIChE Journal **48**, 145-160 (2002).
     URL : http://dx.doi.org/10.1002/aic.690480115

[35] L. M. C. Pereira, M. B. Oliverira, F. Llovell, L. F. Vega and J. A. P. Coutinho, J. Supercritical Fluids **92** , 231 (2014).

[36] E. Buenrostro-Gonzalez, C. Lira-Galeana, A. Gil-Villegas and J. Wu, AIChE Journal **50**, 2552-2570 (2014).

[37] P.M. Mathias, R. Kumar, J.D. Moyer, Jr., J.M. Schork, S.R. Srinivasan, S.R. Auvil and O. Talu, Ind. Eng. Chem. Res. **35**, 2477-2483 (1996).

[38] "Overview of Greenhouse Gases." EPA. Environmental Protection Agency, 14 Apr. 2017. Web. 10 July 2017.
     URL : http://www.epa.gov/ghgemissions/overview-greenhouse-gases#CO2
     lifetime

[39] J. Lehmann, Frontiers in Ecology and the Environment, **5**, 381-387 (2007).

[40] A. Gil-Villegas, F. del Río, and A.L. Benavides, Fluid Phase Equilib. **119**, 97 (1996).

[41] "Active Carbon Systems — Begg Cousland - Products." Begg Cousland. Web. 17 July 2017.
URL: `http://beggcousland.co.uk/products/gas-cleaning/active-carbon-systems/`

[42] R. J. Sadus, *Molecular simulation of fluids: theory, algorithms and object-orientation.* Amsterdam: Elsevier, 2002.

[43] D. Woolf, J.E. Amonette, F.A. Street-Perrott, J. Lehmann, and S. Joseph, "Sustainable biochar to mitigate global climate change". Nature Communications **1** (2010).
URL: `http://doi.org/10.1038/ncomms1053`

[44] Bohm, G., & Zech, G., *Introduction to statistics and data analysis for physicists.* Hamburg: Verl. Dt. Elektronen-Synchrotron, 2010.

[45] M.M. Dubinin: "The potential theory of adsorption of gases and vapors for adsorbents with energetically nonuniform surfaces", Chem. Rev., **60** (1960), pp. 235-241.

[46] "Absorption vs Adsorption." Absorption vs Adsorption - Difference and Comparison — Diffen. N.p., n.d. Web. 01 Aug. 2017.
URL: `http://www.diffen.com/difference/Absorption_vs_Adsorption`

[47] L. Vega, E. de Miguel, L.F. Rull, LA. MeLure and G. Jackson, J. Chem. Phys. **96** (1992), 2296.

[48] F. Rouquerol, J. Rouquerol, and K. Sing, *Adsorption by Powders and Porous Solids* (Academic Press, London, 1999).

[49] S. Brunauer, P.H. Emmett, and E. Teller, J. Am. Chem. Soc. **60**, 309 (1938).

[50] S.J. Gregg and K.S.W. Sing, *Adsorption, Surface Area and Porosity*, 2nd ed. (Academic Press, London, 1982).

[51] Abramowitz and Stegun. Page 883-884. N.p., n.d. Web. 07 Aug. 2017.
URL: `http://people.math.sfu.ca/~cbm/aands/page_883.htm`

[52] R. D. Nelson Jr., D. R. Lide, and A. A. Maryott, "Selected Values of electric dipole moments for molecules in the gas phase", NSRDS-NBS10, 1967.
URL: `http://nvlpubs.nist.gov/nistpubs/Legacy/NSRDS/nbsnsrds10.pdf`

[53] "Nitrous oxide." Gas Encyclopedia Air Liquide. N.p., 20 Apr. 2017. Web. 08 Aug. 2017.
URL: `https://encyclopedia.airliquide.com/nitrous-oxide`

DIVISIÓN DE CIENCIAS E INGENIERÍAS
UNIVERSIDAD DE GUANAJUATO

Lomas del Bosque #103, Fracc. Lomas del Campestre. León, Gto.
C.P. 37150, Apdo. Postal E-143
Tel. (477) 788 51 00, Fax (477) 788 51 00 Ext. 8410

León, Guanajuato a 25 de Julio de 2017

Dr. David Delepine
Director de la División de Ciencias e Ingenierías
Universidad de Guanajuato, Campus León
PRESENTE

Estimado Dr. Delepine:

En referencia a la Tesis de Licenciatura titulada "Molecular Thermodynamics of N2O in biochar", desarrollada por el estudiante Jordan de Jesús Villanueva Ortiz y dirigida por el Dr. Alejandro Gil-Villegas Montiel (Asesor) y la Dra. Flor Siperstein (Co-asesora), me permito comunicarle el resultado de mi léctura crítica de la misma.

La tesis que presenta el estudiante Jordan Ortiz reporta un nuevo modelo teórico para describir y determinar las curvas de adsorpción isotermas de oxido de nitrógeno en un tipo de carbón natural llamado biochar. El proceso de adsorción de oxido de nitrógeno en biochar puede contribuir de forma importante a reducir la emisión de este oxido en la atmosfera. El modelo teórico se confronta con simulaciones, con datos experimentales y con otras teorías relevantes.

La tesis está bien organizada y redactada y reporta resultados originales y relevantes. En su elaboración, el estudiante se benefició de una inmersión intensa, seria y sistemática en varios aspectos prácticos y conceptuales del proyecto.

En particular la elaboración del modelo teórico demuestra un conocimiento detallado de los mecanismos físicos que contribuyen al proceso de adsorción de gas en sólidos. Además el método de verificación de las predicciones del modelo es muy riguroso y demuestra claramente los aspectos novedosos del modelo mismo: respecto a modelos anteriores se reducen los parámetros libres a favor de la introducción de términos justificados por procesos físicos. Al mismo tiempo resulta evidente la capacidad del modelo para describir datos de simulación y experimentos.

Por lo anterior, no me cabe duda de que esta tesis cumple sobradamente con los requisitos de calidad necesarios para ser defendida en el proceso de graduación de este estudiante. Así mismo, confirmo mi disposición de participar como parte del jurado de esta tesis. Sin otro particular, reciba un cordial saludo.

Atentamente,
"La Verdad Os Hará Libres"

Dr. Marco Laurati
Profesor Titular
División de Ciencia e Ingenierías

León, Gto., 1 de agosto de 2017

Dr. David Yves Ghislain Delepine

Director División de Ciencias e Ingenierías

Campus León

Estimado Dr. Delepine:

Por medio de la presente le hago saber qué he revisado el trabajo de tesis *Molecular Thermodynamics of N2O in biochar* del Señor **Jordan de Jesús Ortiz Villanueva**, considero que el trabajo puede ser presentado ante el comité sinodal para su defensa. Sin más por el momento me despido extendiéndole un cordial saludo.

ATENTAMENTE

"LA VERDAD OS HARÁ LIBRES"

DR. FRANCISCO SASTRE CARMONA

Director del Depto. de Ingeniería Física

Oficio número: AGV-07-001
Asunto: Carta conformidad
Tesis de Licenciatura de Jordan de Jesús Ortiz Villanueva.
León Gto., julio 24, 2017.

Dr. David Yves Ghislain Delepine,
Director.
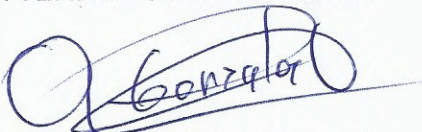División de Ciencias e Ingenierías Campus León

Estimado Dr. Delepine:

Sirva la presente para hacer de su conocimiento que he revisado el trabajo titulado **"Molecular Thermodynamics of N2O in Biochar"** que para obtener el grado de Licenciado en Ingeniería Física pone a consideración el **C. Jordan de Jesús Ortiz Villanueva.**

Le comunico que en mi opinión el trabajo reúne las características de nivel y calidad necesarias para una tesis de licenciatura. Asimismo, he discutido con el **C. Ortiz** algunos aspectos de su trabajo y le he indicado las correcciones que considero pertinentes, las cuales ha incluido en la versión final del documento. De esta manera no tengo objeciones para la presentación del mismo de acuerdo a la reglamentación respectiva.

Agradeciendo la atención prestada a la presente, me despido

A T E N T A M E N T E.
"LA VERDAD OS HARÁ LIBRES"

Dr. Arturo González Vega
Profesor del DIQEB

C.c.p **Jordan de Jesús Ortíz Villanueva**
C.c.p. Archivo AGV.